

# Autonomous Aerial Sensors for Wind Power Meteorology - A Pre-Project



Gregor Giebel (ed.), Uwe Schmidt Paulsen, Jens Bange, Anders la Cour-Harbo, Joachim Reuder, Stephanie Mayer, Aline van der Kroonenberg, John Mølgaard

Risø-R-1798(EN)

January 2012



**Author:** Gregor Giebel (ed.), Uwe Schmidt Paulsen, Jens Bange, Anders la Cour-Harbo, Joachim Reuder, Stephanie Mayer, Aline van der Kroonenberg, John Mølgaard  
**Title:** Autonomous Aerial Sensors for Wind Power Meteorology - A Pre-Project

Risø-R-1798(EN)  
January 2012

**Abstract (max. 2000 char.):**

Autonomous Aerial Sensors, i.e. meteorological sensors mounted on Unmanned Aerial Systems UAS, can characterise the atmospheric flow in and around wind farms. We instrumented three planes, a helicopter and a lighter-than-air LTA system to fly one week together in a well-instrumented wind farm, partly with nano-synchronised sensors (time stamped with about 100 ns global accuracy). Between bankruptcy of a partner, denied overflight rights at the main test location, denied Civil Aviation Authorities permits at the alternative location, stolen planes, and crashed UAS we managed to collect data at a wind farm in Lolland and on an atmospheric campaign in France. Planning of an offshore campaign using the developed techniques is underway.

ISSN 0106-2840  
ISBN 978-87-550-3945-2

**Contract no.:**  
2009-1-10268

**Group's own reg. no.:**  
1130 122-01

**Sponsorship:**  
Energinet.dk, under the Public Service Obligation (PSO) scheme

**Cover :**  
The Lighter-than-Air system of DTU with hangar (left) and some wind turbines in Nøjsomheds Odde. Right: Flyby of a SUMO drone at the Nøjsomheds Odde wind farm in Lolland, Denmark. Picture courtesy of Jesper Hjelme, IWAL.

**Pages:** 90  
**Tables:** 6  
**References:**

Information Service Department  
Risø National Laboratory for  
Sustainable Energy  
Technical University of Denmark  
P.O.Box 49  
DK-4000 Roskilde  
Denmark  
Telephone +45 46774005  
[bibl@risoe.dtu.dk](mailto:bibl@risoe.dtu.dk)  
Fax +45 46774013  
[www.risoe.dtu.dk](http://www.risoe.dtu.dk)

# **Contents**

## **Preface 5**

## **1 Introduction 6**

### **2 Unmanned aerial systems and flow sensors for wind power meteorology 9**

- 2.1 Introduction 9
- 2.2 Platforms for atmospheric wind profiling 10
  - Masts and towers 10
  - Radiosondes 11
  - Tethered balloon systems (TBS) 11
  - Piloted balloons (Pibal) 12
  - Kites 12
  - Manned aircrafts 13
  - Unmanned aircrafts 13
- 2.3 Sensors for atmospheric wind speed measurement: 15
  - Cup anemometers 15
  - Propeller anemometers 15
  - Sonic anemometers 16
  - Hot-wire anemometers 17
  - Pitot-tubes 18
  - Multiple hole probes 18
  - Sphere anemometer 19
  - Laser-Cantilever-Anemometer 20
  - Using aircraft attitude of small UAS for turbulence characterization 21
  - SODAR, LIDAR, RADAR wind profilers 21

### **3 Basic principles of airborne wind measurement for wind-energy research 22**

- 3.1 Introduction 22
- 3.2 Wind measurements using small airborne platforms 23
  - 3.2.1 True airspeed by flight mechanical angles  $\alpha$  and  $\beta$  24
  - 3.2.2 True airspeed by FHP angles  $\alpha$  and  $\beta$  25
  - 3.2.3 Rotation into the MONS 25
- 3.3 Calibration of airborne wind measurements 26
- 3.4 Achievable accuracy 27
- 3.5 New challenges 29

## **4 The Hardware 31**

- 4.1 SUMO 31
  - Airframe 32
  - Autopilot 33
  - SUMO meteorological sensors 33
  - Other uses of the SUMO for wind estimation 35
- 4.2 MASC 35
- 4.3 M<sup>2</sup>AV 36
- Further technical specifications Carolo T200 38
- 4.4 Vario XLC 38
- Helicopter 38
- Onboard computer (OBC) and sensors 39
- Mission sensor 39
- Flight tests 40
- Helicopter for measuring wind 41
- 4.5 SkyDoc 41

Systems design 41  
Modeling 43  
Rigging 46  
Platform canopy 46  
Meteorological instrumentation 48  
4.6 Nanosynchronised data acquisition 52  
Aerial Sensor Node 53  
Front End 54  
Timing System 54  
Possible Applications: 55  
Power supply 55  
Mechanical 55  
Storing GPS data as Waveform Data Type, WDT. 56

## **5 Flight Week(s) and locations 57**

5.1 Høvsøre 57  
5.2 3D sonic anemometer helicopter test flight 59  
Test flight setup 59  
Conclusion 62  
5.3 Nøjsomheds Odde 63  
SUMO 64  
Results 65  
Summary and Conclusions 70  
LTA 70  
Summary on the LTA scientific progress and results 73  
5.4 Risø 73  
5.5 Østerild 74

## **6 Lessons learned 76**

6.1 Permits and legal matters 76  
6.1.1 Danish regulation 76  
Permits for the present project 76  
Dispensation for Vario XLC 79  
Dispensation for above 100 meters 79  
6.2 Practical considerations for future use 79  
Selection of campaign sites 79  
Campaign planning and logistics 79  
Application for permits 79  
Limits and potentials for flight patterns 80  
Safety issues 81  
Aircraft testing and preparations 81  
Data analysis, on-site and off-site 81  
Campaign operation coordination and responsibility 81  
6.3 Design of an offshore campaign 81

## **7 Conclusions 83**

## **8 Glossary 84**

## **9 References 85**

## Preface

This project report is written as a contractual requirement under the PSO (Public Service Obligation) project 2009-1-10268 “*Autonomous Aerial Sensors for Wind Power Meteorology*”, which ran from 1 September 2009 to 31 October 2011.

# 1 Introduction

Large-scale wind farms, especially offshore, need an optimisation between installed wind power density and the losses in the wind farm due to wake effects between the turbines. While the wake structure behind single wind turbines onshore is fairly well understood, there are different problems offshore, thought to be due mainly to the low turbulence. Good measurements of the wake and wake structure are not easy to come by, as the use of a met mast is static and expensive, while the use of remote sensing instruments either needs access to the turbine to mount an instrument, or is complicated to use on a ship due to the ship's own movement. In any case, a good LIDAR or SODAR will cost many tens of thousands of euros, and a fully equipped offshore meteorology mast will easily cost many hundred thousand euros.

Another current problem in wind energy is the coming generation of wind turbines in the 10-12 MW class, with tip heights of over 200 m. Only few measurement masts exist to verify our knowledge of atmospheric boundary layer physics, none of those offshore. Recent research results indicate that the logarithmic wind profile valid for neutral atmospheric conditions, and the stability dependent corrections arising from similarity theory typically used in the surface layer, are only valid up to 50-100 m above ground (e.g Gryning et al., 2007, Pena et al., 2010).



Figure 1: Fog in wind turbine wakes at Horns Rev. Picture UniFly A/S, 2009

Here, automated Unmanned Aerial Vehicles (UAVs) could be used as either an extension of current high masts or to build a network of very high 'masts' in a region of complex terrain or coastal flow conditions. In comparison to a multitude of high masts (a mast of 100m height plus instruments onshore can be about 200.000 euros), UAVs could be quite cost-effective.

In order to test this assumption and to test the limits of UAVs for wind power meteorology, this project's idea was to assemble four different UAVs from four participating groups. Risø built a lighter-than-air kite with a long tether, Bergen University flew the SUMO, a pusher airplane of 580g total weight, the University of

Tübingen in conjunction with TU Braunschweig flew the Carolo, a 2m wide two prop model with a pitot tube on the nose, and Aalborg University used a helicopter equipped with a sonic anemometer. It was intended to fly all those platforms during one week at the Danish National Test Station for Large Wind Turbines at Høvsøre, which is run by Risø DTU. The site is strongly instrumented, with 6 masts above 100m height, one even reaching up to 167m. The comparison of wind speed measurements from planes and fixed masts should give an indication of the accuracy of the measured wind field.

This present project should be seen as the precursor to a larger development effort. At this stage, we needed to map the state-of-the-art and its applicability to wind power meteorology. Valuable lessons especially on the practical aspects of use of the technology have been learned. The next project should then delve into the actual development of dedicated aerial sensor packages for wind power, taking into account the lessons learned from this exercise.

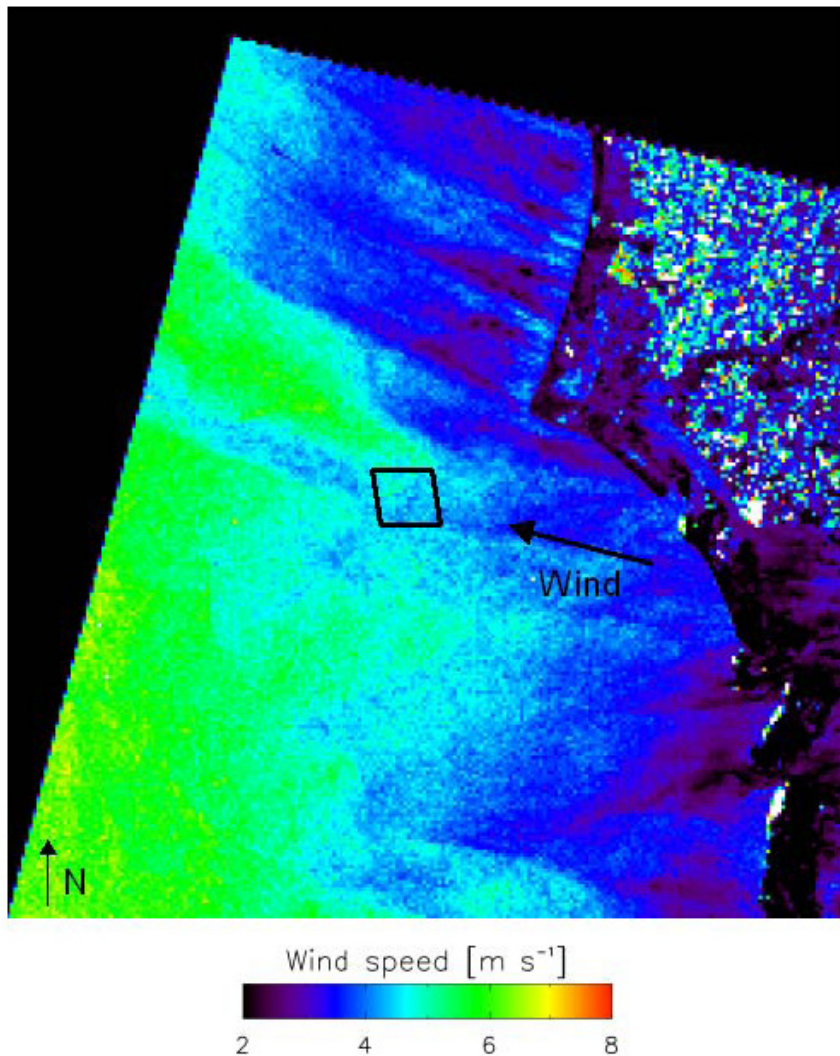


*Figure 2: Wind field at Horns Rev based on ERS-2 SAR image from 25 February 2003. The black trapezoid indicates the wind farm. For scaling, the total wind farm width is ~5 km. The wind direction is 110° from the meteorological mast. A reduction of wind speed is seen downstream of the wind farm. Note also the strong shadowing effects of the land. Source: Christiansen 2007.*

The work was organised in three main work packages. WP1 was strongly based on the similar effort done in the COST action ES0802 “Unmanned aerial systems (UAS) in atmospheric research”, of which Jochen Reuder of Bergen University is the leader. It is the mapping of the state-of-the-art and expected developments in the fields of aerial platforms, including model airplanes, helicopters, quadrocopters, kites, balloons, and any other technology which can transport a sensor package aloft and keep it there for some time. A second part of this WP dealt with the sensors to be mounted on the aerial platforms. The COST Action built a database for airframes and meteorological and chemical sensors to be flown on everything between a SUMO and a Global Hawk. WP2 organised a workshop for wind power meteorology stakeholders. Based on the results of WP2, WP3 was intended to be the experimental measurement campaign at Høvsøre, comparing performance of different aerial sensors directly for the study of the atmospheric boundary layer, and the technological development needed for the campaign. Alas, the campaign at Høvsøre never came to be, just like plans B and D (plan C was eventually executed). The reasons for this will be given in the following.

## **2 Unmanned aerial systems and flow sensors for wind power meteorology**

### **2.1 Introduction**

Wind power is of continuously increasing importance under the aspect of rising global energy demand, the negative effects of anthropogenic CO<sub>2</sub> emission and the corresponding interest in developing renewable energy resources. Most of this development is expected to happen offshore in the future. The characterization of the wind conditions in the lower atmospheric boundary layer (LABL), defined by the rotor area of actual 5 MW turbines (30-150 m) and future wind turbines (up to 300 m for 10-20 MW capacity), is of utmost importance for this purpose. The relevant parameters to be monitored are:

- The wind speed distribution and the turbulence structure in the flow approaching a turbine and in particular the flow over the rotor diameter for the prediction of energy production and the estimation of loads and fatigue.
- The temperature profile required for the understanding of atmospheric stability that is affecting both the wind profile and the turbulence structure in the LABL.

The main issues to be addressed with such measurements are:

- The monitoring and characterisation of the incoming flow. This is in particular important for offshore conditions, where corresponding data availability is sparse to non-existent and the situation is complicated by air-sea interaction and wave effects.
- The investigation of the interaction of the single wind turbines in a wind farm with the LABL, i.e. mainly wake effects caused by the extraction of energy from the incoming mean flow by the turbines while additionally adding turbulence by the turbine towers and in particular the rotating blades. This part is of high relevance for estimation of loads and fatigue of wind turbines inside a wind farm and for the optimization of spacing and siting of the wind turbines in a farm.
- The investigation of the effect of a larger wind farm on the LABL and potentially on the meso-scale flow conditions. Atmospheric stability, and size and density of a wind farm determine the extension of the far field wake downstream that has to be refuelled by downward momentum transfer from higher parts of the ABL. This will be crucial for siting and spacing of the larger wind farms under development now.

Conventional LABL measurement systems, as masts and active remote sensing techniques (Lidar, Sodar) are rather expansive, only of limited flexibility, and demand certain infrastructure, not necessarily available in particular for offshore measurements. In this light unmanned aerial systems are expected to provide the capability of gaining required data sets cost efficient with up to now unknown flexibility.

## 2.2 Platforms for atmospheric wind profiling

Figure 3 gives a schematic overview on the platforms typically used in atmospheric boundary layer research and in particular for LABL profiling relevant for wind energy applications. The different systems will shortly be described with focus on their advantages and drawbacks with respect to wind energy meteorology.

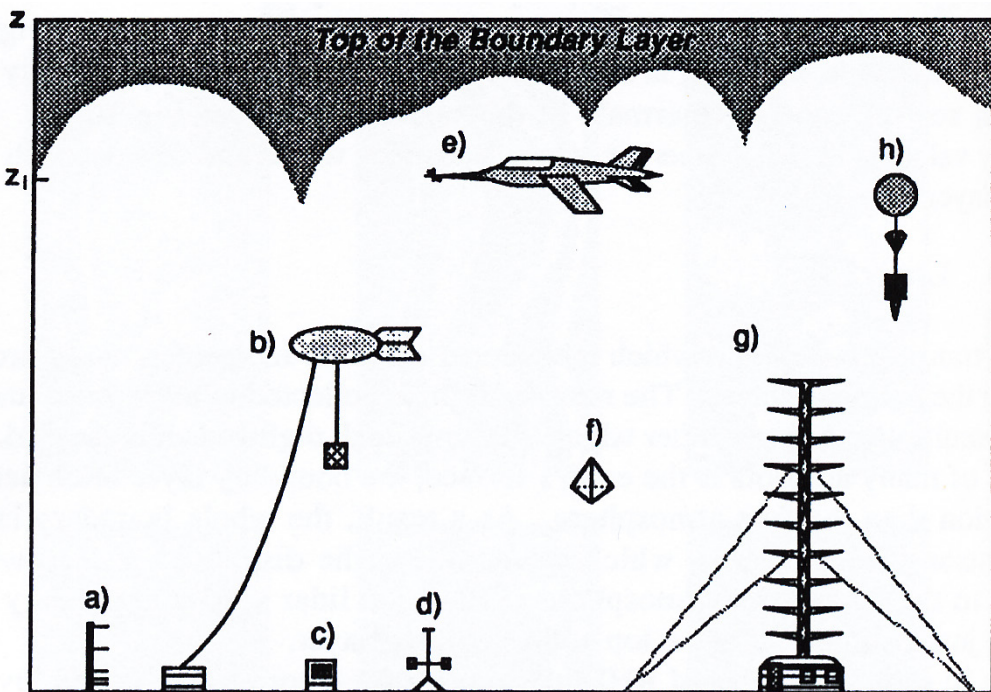


**Fig. 10.2** Sketch of instrument platforms for direct sensors. (a) Mast. (b) Kytoon. (c) Instrument (screen) shelter. (d) Mesonet station. (e) Aircraft. (f) Tetroon. (g) Tower. (h) Radiosonde.

Figure 3: Schematic overview of platforms for atmospheric boundary layer research and LABL profiling (taken from Stull, 1988).

### Masts and towers

Meteorological masts and towers are used as standard instrumentation carriers for wind resource mapping and in atmospheric boundary layer research. Typical masts for wind resource mapping are in the order of 50-100 m, in particular for wind energy research purposes single installations are distinctly higher (e.g. the masts at Risø or Høvsøre, see sections 5.1 and 5.4). Prominent examples for heavily instrumented measurement towers for basic ABL research in Europe are the Cabauw tower in the Netherlands (213 m high, operated by KNMI), the Karlsruhe tower (200 m, operated by KIT) or the Falkenberg tower (99 m, operated by DWD).

Meteorological masts and towers generally provide a solid and stable measurement infrastructure with the potential to mount a large variety of sensors on one structure with adequate accessibility. But they are rather expansive and inflexible with respect to changes in siting. As they represent a solid obstacle for atmospheric boundary layer flow, each wind measurement at a mast or tower will in reality be subject to flow distortion and corresponding measurement uncertainties. For offshore conditions costs and infrastructural requirements for measurement towers are even higher. Examples of

operational facilities are the German FINO 1-3 platforms, but also most operational and planned wind farms have one or more masts deployed. The first floating installations are deployed off the coast of Spain and corresponding plans are on the way to be realized in a Norwegian Infrastructure initiative NOWERI and by the US initiative DeepCWind off the coast of Maine.

## Radiosondes

Radiosonde ascents are one of the well-established standard methods for atmospheric profiling and are important data sources for the initialization of operational numerical weather forecast models. A helium or hydrogen filled balloon carries in the standard version a sensor package for temperature, humidity and pressure. Wind speed and wind direction are derived with the help of a GPS receiver on the sonde. The data are continuously transmitted via radio-signals to the receiver station. Radiosondes reach typically altitudes of more than 25 km and provide therefore information on the state of the whole troposphere and parts of the stratosphere.

For frequent profiling of the lowest few hundred meters of the ABL of interest for most of the wind energy relevant applications, this system is a clear overkill with respect to potential and cost (around 300 € per ascent). In addition it is just measuring the average meteorological values and not able to provide information on the turbulence structure.

## Tethered balloon systems (TBS)

A helium filled balloon with a tether line fixed to a winch at the ground is acting as sensor carrier. Depending on the size of the balloon, payloads up to several kg can be attached to the line. For meteorological purposes mostly two measurement strategies are used. The first one is the use of one sensor package while the atmospheric profiling is done by releasing and retracting the tether line with the winch, typically using vertical velocities in the order of 0.5-2 m/s. The other strategy is to mount several sensor packages on the tether line and with this erecting a kind of temporary meteorological tower.

TBS have typical vertical range of up to 2 km above ground, determined by the length of the tether cable and the prevailing wind conditions that tilt the tether line and reduce the ceiling altitude. TBS operations need a certain amount of infrastructure (power for the winch, helium in bottles). The operation of TBS at levels above ca. 150 m requires permission of the civil aviation authorities. For operation in a wind park, the movement of the balloon by the wind has to be carefully observed to avoid the tether line coming too close to the turbines. In general the operation of TBS is limited to low to moderate wind speeds. The stability of TBS is a design specific variable, as is shown later; a symmetrical shaped balloon will for increasing wind speeds above a characteristic wind speed descend to lower altitudes, due to the increased drag over lift capacity. Uni Bergens own experience with different systems shows that operation gets challenging at around 8 m/s and nearly uncontrollable above 12 m/s. On the other hand the payload is the only limiting factor in the selection of instrumentation for TBS, also allowing direct turbulence measurements, e.g. by sonic anemometers, if they can be motion corrected. Prototypes of corresponding systems have been developed and used for atmospheric measurements. There are at least two systems already in use the authors are aware of. The first one is the Tethersonde, operated by the University of Leeds (Hobby et al.,

2008), the second a corresponding system deployed by the French Meteorological Service METEOFRANCE during the BLLAST field campaign in summer 2011 (BLLAST, 2011).

### **Piloted balloons (Pibal)**

Profiles of wind speed and wind direction can be determined by releasing a small helium filled balloon and tracking it with two theodolites (e.g. Thyer, 1962; Schaefer and Doswell, 1978). The synchronized angular readings of the two theodolites can be combined to calculate a time series of the balloons position and from this the desired profiles of wind speed and wind direction.

The system only can provide mean profiles and is sensible to observation errors as it needs continuous visual contact. It is therefore not well suited for operation inside a wind farm. It requires rather large amount of manpower (2 observers, 1 starter). Observations at higher levels can be difficult and less accurate, in particular in stronger winds where the balloon is blown far away from its starting point and the observing theodolites.

### **Kites**

Historically seen, the first airborne meteorological measurements were performed by kites in the 18th century (Balsley et al., 1998), e.g. reported by Wilson flying a string of paper kites equipped with thermometers or by Franklin 1752 who flew a kite to study atmospheric electricity and lightning. The Golden Age of atmospheric profiling by kites was the decades at the end of the 19<sup>th</sup> and the beginning of the 20<sup>th</sup> century. During that time numerous observatories around the world used kites for tropospheric profiling, partly reaching the tropopause region (i.e., about 10 km height). After that kites have been more and more replaced first by tethered balloons and later by radiosonde systems. However kites are still used sporadically, in particular for boundary layer process studies in areas and situations with limitations by infrastructural constraints (e.g. Guest, 2007).

For operations connected to wind power meteorology similar constraints apply as for tethered balloon systems. It seems that kites can be operated at higher wind speeds; nevertheless the exact control in the vicinity of wind turbines would be a serious issue. In addition a certain minimum wind speed is required for kite operations.

Balsley et al (1998) used a Parafoil kite to lift equipment, together with a ‘windtram’ unit and a measurement platform as shown in Figure 4.

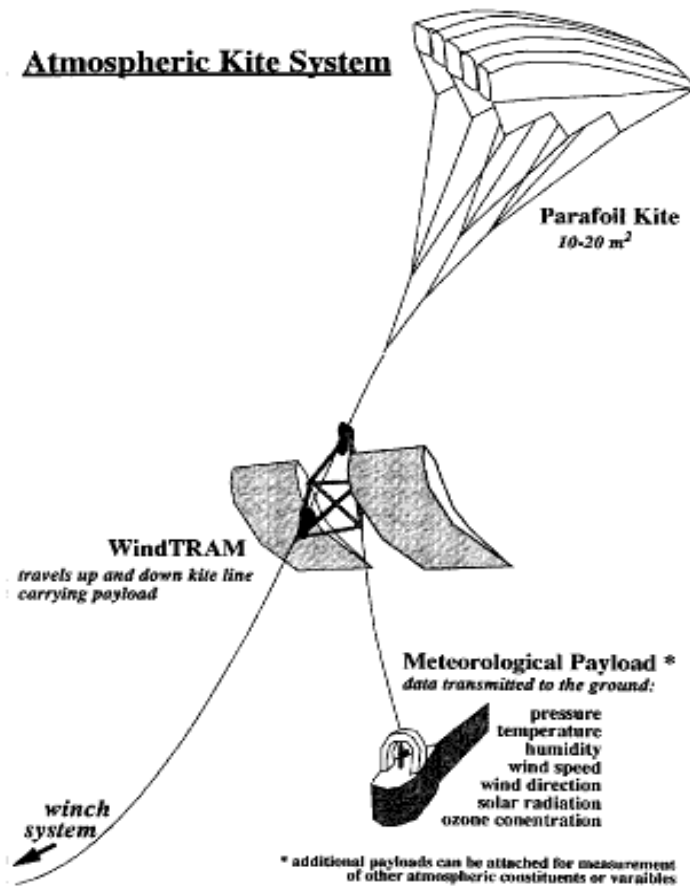


Figure 4: System to lift a measurement platform. Balsley et al 1998.

### Manned aircrafts

Manned aircrafts have been and are widely used for atmospheric research. However the operation of manned aircraft inside a wind farm is out of question due to safety reasons and the legal regulations. Nevertheless the operation of manned aircraft in the vicinity of wind parks has a large potential in investigations on the effect of a whole wind farm on the local to regional scale wind field, e.g. the far wake effect and its dependency of atmospheric stability, and large scale wind speed and wind direction.

### Unmanned aircrafts

During the last decades unmanned aircraft systems (UAS) have been developed and used nearly exclusively for military purposes. A recent survey published by UVS International (UVS, 2011) has listed more than 1200 UAS of different size, weight and complexity, ranging from a few tenths of centimetres in size and weights of a few 100 grams up to full sized aircrafts with take-off weights of several tons, e.g. the Global Hawk. For the operation of such larger systems in and around wind parks and turbines, the same restrictions as for manned aircrafts apply. However smaller and smallest systems will have the potential for safe operation inside and close to wind parks, as the potential damage for a turbine in case of a collision is quite limited.

During the last decade, UAS have also entered atmospheric boundary layer meteorology as flexible and cost-efficient sensor platforms. Starting with the pioneering attempt of

Konrad et al. (1970) there have been sporadic applications of remotely piloted aircrafts in the field of meteorology. In the late 1990s, the profiling system KALI was developed at the University of Munich. It has been operated during nearly one decade for the investigation of orographic effects on atmospheric flow during several field experiments in Nepal, Bolivia, Germany and Iceland at altitudes up to 3 km above the ground (Egger et al. 2002, 2005, Spengler et al. 2009, Reuder et al. 2011). The most significant shortcoming of the KALI system was the need of experienced pilots for continuous remote controlled operation of the aircraft.

With progressing miniaturization, in particular in the field of relevant sensors as e.g. GPS receivers, magnetometers and inertial measurement units (IMU), UAS of gradually decreasing dimensions could be equipped with autopilot systems. As a consequence, corresponding systems became available for scientific purposes. Examples for successful applications in atmospheric research are the Australian Aerosonde (e.g. Holland et al. 2001), the M<sup>2</sup>AV developed in Germany (e.g. Spieß et al. 2007), and the Chinese RPMSS described by Ma et al. (2004). These systems have been used for the investigation of a variety of ABL related phenomena and processes, including polar boundary layer studies (Curry et al. 2004), Arctic sea surface temperatures (Inue and Curry 2004), ABL turbulence (van den Kroonenberg et al. 2008, 2011) and radiative transfer studies (Ramanathan et al. 2007).



*Figure 5: Examples of UAS systems used in atmospheric research. Left: Aerosonde (Image: © Jon Becker, Aerosonde Pty Ltd.), Right: M<sup>2</sup>AV.*

An overview of techniques taken from Balsley 1998 shows the intercomparison of kites, TBS, Radio-sondes, aircraft and met towers.

| A short intercomparison of atmospheric sampling techniques |                           |                           |                                    |                           |                           |
|--|---------------------------|---------------------------|------------------------------------|---------------------------|---------------------------|
| ITEM   | KITES                     | Tethered balloons         | Standard balloon-sondes            | Aircraft                  | Towers                    |
| Maximum altitude coverage*                                 | >5 km                     | ≤ 1-2 km                  | >30 km                             | ≤18 km                    | ≤ 300 m                   |
| Very low-level sampling                                    | yes                       | yes                       | yes                                | no                        | yes                       |
| Constant-height sampling                                   | yes                       | yes                       | no                                 | yes                       | yes                       |
| Eulerian measurements                                      | yes                       | yes                       | no                                 | no                        | yes                       |
| Lagrangian measurements                                    | no                        | no                        | questionable                       | difficult                 | no                        |
| Max payload weight   | ≈10 kg                    | ≈100 kg                   | ≤ 3 kg                             | ≈500 kg                   | large                     |
| FAA clearance needed                                       | yes                       | yes                       | no                                 | no                        | no                        |
| Height resolution  | ≤ 1-10 m                  | ≤ 1-10 m                  | 50 m                               | <10 m                     | < 1 m                     |
| System costs   | \$10-20k                  | \$10-200k                 | \$10k                              | \$50 k-\$6M               | \$1-800k                  |
| Cost/profile   | very low                  | ≈low                      | low-high                           | ≥avg.                     | low                       |
| Wind requirements  | >5-7 (m s <sup>-1</sup> ) | ≤ 12 (m s <sup>-1</sup> ) | ≤ 10 (m s <sup>-1</sup> ) (launch) | minimal                   | none                      |
| All weather?   | no                        | no                        | yes                                | typically                 | yes                       |
| Portable   | yes                       | yes                       | yes                                | yes                       | no                        |
| Payload recovery   | yes                       | yes                       | very difficult                     | yes                       | yes                       |
| Telemetry  | yes                       | yes                       | yes                                | yes                       | yes                       |
| Payload vertical velocity                                  | 0- 5 (m s <sup>-1</sup> ) | 0-5 (m s <sup>-1</sup> )  | ≈4-6 (m s <sup>-1</sup> )          | 0- 5 (m s <sup>-1</sup> ) | 0- 5 (m s <sup>-1</sup> ) |
| Vertical profiling   | yes                       | yes                       | yes                                | expensive**               | possible                  |

\* The highest altitude (9,740 m) achieved by a train of kites occurred in 1919 at Lindenb  rg, Germany (Yolen, 1968).

\*\* Measurements of the spatial turbulent statistics in the vertical direction are difficult with airplanes.

## 2.3 Sensors for atmospheric wind speed measurement:

This section will give a short overview over different in-situ and remote sensing sensors and sensor systems for the determination of boundary layer winds, with special emphasis on their applicability for use on unmanned platforms.

### Cup anemometers

Cup anemometers are rather simple, but robust instruments for wind velocity measurements, consisting of a number of cups mounted with vertical arms on a rotating shaft, see Figure 6. The rotational velocity of the shaft is proportional to the horizontal wind speed. A cup anemometer cannot measure the wind direction, thus e.g. a weather vane must complement it to obtain that information. Cup anemometers are the standard anemometers used for wind assessment prior to onshore wind turbine construction and to the time being the only instruments accepted for “bankable” wind measurements. Under this background all other wind speed measurement methods should be compared to the achievable accuracy of state-of-the-art cup anemometers. Cup anemometers are subject to over-speeding in gusty and turbulent conditions and their measurement accuracy is sensitive to vertical velocity components, e.g. induced by mounting on moving platforms. This makes cup anemometers unusable for faster flying UAS and difficult to apply for kites and tethered balloons.



*Figure 6: Examples for cup anemometers typically used for wind energy applications. First Class from THIES (left), the P2546A from WindSensor (center), and the A100LK from Vector Instruments.*

### Propeller anemometers

A propeller anemometer consists of a propeller mounted on a horizontal axis, often combined with an attached weather vane to keep the propeller plane orthogonal to the incoming wind, see Figure 7. By recording the propeller revolution rate and the anemometer orientation, respectively, the horizontal wind velocity and the wind direction is obtained. The size and weight makes the larger of these systems not applicable for at least faster moving UAs platforms, the orientation issue also difficult to handle on tethered systems.



*Figure 7: Two examples for propeller anemometers. Left: Young Wind Monitor 05103RM; Right: Miniaturized propeller anemometer series Mini Air from Schiltknecht.*

Nevertheless there are miniaturized systems available, e.g. the MiniAir series from Schiltknecht, with rotor head diameters of 11 mm, 22 mm and 85 mm (to the right in Figure 7). The sensors are insensitive to the incoming flow of an opening angle of around 25 degrees. Flow direction information requires mounting together with a wind vane again. These sensors would in principle be feasible for mounting even on small UAS. Corresponding tests at the University of Bergen have shown that there are issues with increased friction at low temperatures and with the stability of the plastic material, in particular when exposed to changing temperatures as for atmospheric profile measurements reaching higher altitudes. Mounting at a tethered system near the ground could be possible.

### Sonic anemometers



*Figure 8: Two examples of sonic anemometers typically used in atmospheric boundary layer research. CSAT3 from Campbell (left) and R100 from Gill (right).*

Sonic anemometers use the travel time difference of ultrasound pulses in opposite directions to measure the turbulent wind vector in a probe volume, typically with a frequency of 10-100 Hz. In addition to the turbulent wind vector, sonic anemometers also can use the density dependency of the speed of sound for the determination of the so-called sonic temperature that is nearly identical with the virtual temperature often used in meteorology to account for the reduced density of moist air. Both 2 and 3 dimensional sonic anemometers are available. The 2-dimensional anemometer measures

the wind in one plane only, typical being mounted such that it measures the horizontal wind vector. No moving parts and the potential of sensor heating make them attractive for long term monitoring even under harsh environmental conditions. Sonic anemometers are not working properly when the probe volume is disturbed by larger particles, e.g. in conditions of moderate to heavy precipitation or sea spray.

Size (probe volume typically 10-20 cm) and weight (typically 1.5 kg for the sensor head) make sonic anemometers inapplicable for smaller UAS, nevertheless there is a clear applicability for larger systems with a total take-off weight above ca. 20 kg. They are for sure applicable on tethered systems (see e.g. Hobby et al., 2008, O'Connor et al., 2010; the authors are also aware of a corresponding test deployment by Meteo France during the BLLAST field campaign in summer 2011, <http://bllast.sedoo.fr/>) and e.g. as slung load under unmanned helicopter systems. In addition there is a miniaturization potential for the corresponding systems in the future.

### **Hot-wire anemometers**

Hot wire anemometers use a very fine wire that is electrically heated up to a temperature above ambient. The air flowing passing has a cooling effect on the wire. As the electrical resistance of most metals is dependent upon the temperature, a relationship between the resistance of the wire and the flow speed can be obtained. Due to their low mass and corresponding low heat capacity, hot wire anemometers are capable of measuring wind speed with high temporal resolution (up to several kHz) and are therefore well-suited for turbulence studies. The use of the extreme thin wires makes those sensors very delicate and sensible to damage, e.g. by insects, pollen, larger aerosol particles or cloud and rain droplets. Therefore the use of unshielded hot-wire anemometers on fast moving UAS is impractical, while measurements on tethered or slow moving platforms could be possible. Shielded versions could be feasible for UAS applications, e.g. the combined temperature /air flow sensor CAFS-220-S5M from Cambridge Accusense. This sensor has dimensions to fit even in very small UAS, unfortunately do the specifications (temperature range 0-100 °C; wind speed 0.1-15 m/s) not meet the environmental requirements for UAs operations.

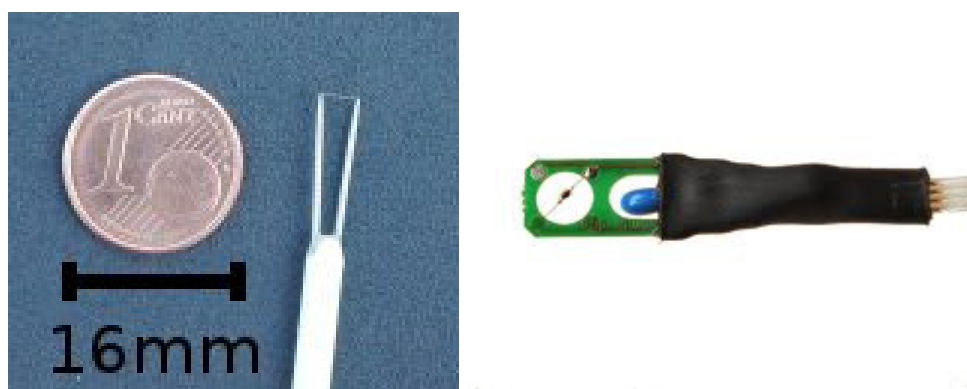


*Figure 9: Two examples for hot wire anemometers. An unshielded sensor to the left and a shielded one to the right (Cambridge Accusense CAFS-220-S5M - Temp/Air Flow Probe).*

## Pitot-tubes

Pitot tubes are the typical measurement device for the determination of airspeed in aviation. The basic pitot tube consists of a tube pointing directly into the fluid flow. As there is no open outlet, the moving fluid is brought to rest (stagnates). This pressure is the stagnation pressure of the fluid, also known as the total pressure or (particularly in aviation) the pitot pressure. From the measured stagnation pressure the fluid velocity or airspeed can be determined by Bernoulli's equation when also the static pressure is known.

Pitot tubes are available in a large variety of sizes and realizations and therefore applicable for all types of relatively fast moving UAS. There are also miniaturized systems available fitting UAS in the SUMO class. One system dedicated to speed measurements of model aircrafts, the Eagle Tree Pitot tube and Airspeed Micro Sensor V3 (see Figure 10 right) has been tested by GFI/UoB and ENAC (L'Ecole Nationale de l'Aviation Civile) in Toulouse, France. It showed the distinct offset and instability of this rather inexpensive (ca. 50 USD) system. Using the pressure transducers of the Airspeed Micro Sensor V3 with a mechanically improved version of the Pitot tube could enable measurements of the 1D incoming flow on an airframe with a temporal resolution of up to 10 Hz, giving at least a raw estimate of the 1 dimensional turbulence structure in the ABL.

Size and weight are in general no limitation for the use on even small UAS systems. The accuracy and reproducibility of these miniaturized systems is still under consideration. As the accuracy decreases towards lower flow speeds, Pitot tubes are mainly applicable for faster flying fixed wing UAS and not for more stationary systems as helicopters, kites and tethered balloons.

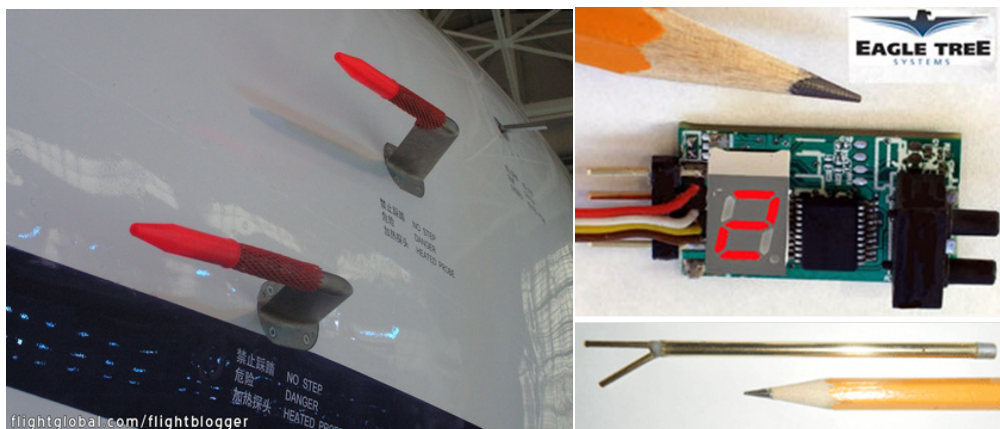


Figure 10: Pitot tubes mounted on the fuselage of an aircraft for airspeed measurements (left) and the miniaturized Pitot tube and Airspeed Micro Sensor V3 from EagleTree, tested on the SUMO system (right).

## Multiple hole probes

As the Pitot tube, multiple hole probes are also based on dynamical pressure measurements. Using several holes at the tip of the probe, e.g. 4 arranged with 90 deg angle distance around the central one for the typically used 5-hole probe, extend the theory of the Pitot tube to 3 dimensional flow measurements. Flow approaching the

sensor off the main axis leads to pressure differences between the holes placed around the central one. When once calibrated, this can be used to determine the velocity and direction of the incoming flow. Corrections for the aircraft movement have to be accounted for to transform the flow data into the coordinate frame relevant for meteorological applications.



*Figure 11: Miniaturised 5 hole probes (left) and the 13 hole Omniprobe (right) from Aeroprobe as examples for multiple hole probes for directional flow measurement useable on UAS.*



*Figure 12: The 5-hole probe from Aeroprobe mounted on the SUMO aircraft. The right picture shows a detailed view of probe, tubing and the air-data computer unit inside the fuselage.*

The straight version of the 5 hole probe and the corresponding pressure transducers and data logger, commercially available from Aeroprobe Corporation in the USA has been integrated into the SUMO system. The system is capable to measure the 3-dimensional turbulence flow vector impinging the aircraft with a temporal resolution of 100 Hz. The mounting of the 5-hole probe and air-data computer is shown in Figure 12.

This type of sensors will for sure be one of the favourable options for wind and turbulence measurements on relatively fast moving UAS with high temporal resolution. However it requires also an accurate and fast determination of the aircrafts attitude for motion correction to calculate the flow vector in the meteorological relevant coordinate frame (see section 3.2).

### Sphere anemometer

The sphere anemometer uses the relationship between the drag force acting on a sphere mounted on the tip of a rod with known bending moment. The amount of deflection is proportional to the square of the wind speed (Hölling et al., 2007). It is capable for measurements of the wind speed up to a temporal resolution corresponding to the

resonance frequency of the rod (in this case 80 Hz, but surely variable by use of different dimensions and/or materials). In its current version it would be feasible for use on larger UAS, a miniaturization down to a future use on SUMO sized UAS seems realistic.

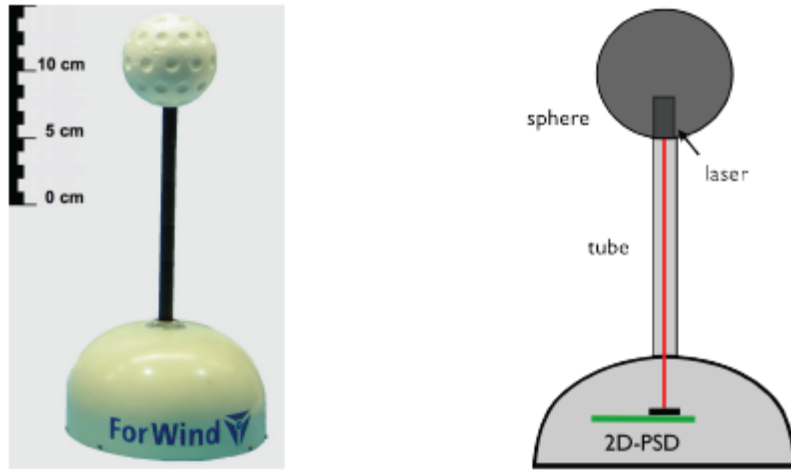


*Figure 13: Principle of operation (right) and picture of a prototype of the sphere anemometer developed at the university of Oldenburg (taken from Heisselmann et al., 2009).*

### Laser-Cantilever-Anemometer

The system described has been developed at the University of Oldenburg (Barth et al, 2005; Puczyłowski et al., 2011). The used measuring method is based on the laser pointer principle. The sensitive component of the sensor is a cantilever made of stainless steel and measuring only 1.5 mm in length and 0.4 mm in width. Its thickness is only about 30  $\mu\text{m}$ . The largest dimension, i.e. the length, gives the limitation for the spatial resolution. When exposed to flow the cantilever experiences a deformation due to the acting force that depends on the square of the flow speed. A laser beam provided by a laser diode is pointed at the tip of the cantilever and causes a reflecting spot, which again is routed on a 2-dimensional position sensitive detector (2d-PSD), similar to the one used for the sphere anemometer described above. The system allows turbulence measurements with a temporal resolution in the range of 1-10 kHz.



*Figure 14: The 2-d Laser Cantilever Anemometer for atmospheric use (2d-ALCA) developed at the University of Oldenburg (taken from Puczyłowski et al., 2011).*

The system is in an advanced prototype stage and now mounted at the German FINO3 platform for environmental testing. Size and weight make it at the moment not applicable for smaller unmanned systems. In addition it is not clear how vibrations in-flight would affect the measurement principle.

### **Using aircraft attitude of small UAS for turbulence characterization**

While flying, UAS interact with the atmospheric flow and are therefore exposed to all kinds of turbulent motions that have to be handled by the attitude control of the UAS autopilot system to keep it flying stably. The smaller a UAS, the smaller the turbulent eddies that causes the corresponding disturbances. Continuous registration of the aircraft's attitude and accelerations by an IMU and of the control commands to correct for that, it should be possible to retrieve qualitative, and in case of thorough intercomparison, e.g. by flights around high masts with direct eddy correlation measurements or by parallel flights with an UAS carrying turbulence probes, even quantitative information on the turbulence structure of the ABL without having a flow sensor on board.

At the moment a new upgrade for the Paparazzi autopilot system used on SUMO is under development. With this it will be possible to monitor and store all relevant parameters during the flight with a temporal resolution of at least 100 Hz on a SD card. Those data can then be post-processed with respect to the ABL turbulence structure.

### **SODAR, LIDAR, RADAR wind profilers**

These active remote sensing methods are based on the Doppler shift of emitted sound waves (SODAR) or electromagnetic waves (RADAR and LIDAR), reflected by density inhomogeneities (SODAR and RADAR) or aerosol particles (LIDAR) that are moving with the wind. All 3 methods are in use for ground based determination of wind profiles, in particular LIDAR systems are already playing an important role in wind power meteorology. All existing systems are by far too large to be integrated on UAS systems with a total take-off weight below 150 kg. The largest potential of miniaturization and application on fast moving platforms have for sure lidar systems, that are already in use for more than one decade for airborne wind measurements by larger manned aircrafts. (e.g. Koch et al., 2010; Reiterbuch et al., 2001). The applicability of LIDAR systems on UAS in the class below 150 kg take-off weight during the next years is seen as very unlikely.

### **3 Basic principles of airborne wind measurement for wind-energy research**

#### **3.1 Introduction**

The purpose of measuring the wind vector up-, down-stream and within a wind park using aircraft is usually not to determine the meso-scale wind field all over the troposphere, continuously during the entire diurnal cycle and every day of the year. For this ground-based remote-sensing technologies like wind profilers are much better suited than aircraft that can probe the lower atmosphere only along a one-dimensional path during a quite limited flight endurance of e.g. one hour. The advantages and the unique features that come with the application of airborne meteorological measurement systems are

- *in situ* measurements that do not rely on further and complex physical models,
- high spatial and temporal resolution,
- very flexible applicability (as long as no runway is required or is close enough to the area of interest, no ground installations are needed),
- a high translatory speed compared to the mean wind speed, which allows for 'snap shots' of the turbulent wind field, when Taylor's hypotheses can be assumed to be fulfilled,
- the additional measurement of further thermodynamic quantities like humidity and temperature.

Thus, meteorological research aircraft focus the medium and small scale wind fluctuations and structures for instance in the order of a few wind turbine rotor diameters, e.g. 500 m or 1 min (assuming a mean wind of 10 m/s). These include the vertical wind profile that interacts with the individual wind turbines, smaller turbulent eddies that cause a heterogeneous load on the rotor blade, and wakes behind individual converters that travel to 'second-row' turbines downstream.

Among research aircraft, small UAV (unmanned aerial vehicles) with size and mass in the order of a large seabird have large advantages compared to manned aircraft for wind-farm research:

- UAV can be controlled by auto-pilot systems that are usually able to maintain track and altitude more precisely than human pilots,
- these UAV are small and agile enough to fly close and between wind converters,
- the application of small UAV is much cheaper,
- small UAV do not require runways,
- in case of an accident,
  - wind converters are usually designed to endure a collision with such mass and speed,
  - no human pilot is jeopardised.

In the following sections the principles of wind measurements using small UAV are presented (see also Bange, 2009), as well as a recently developed calibration strategy. Finally the achievable accuracy of wind measurements with small UAV is assessed.

### 3.2 Wind measurements using small airborne platforms

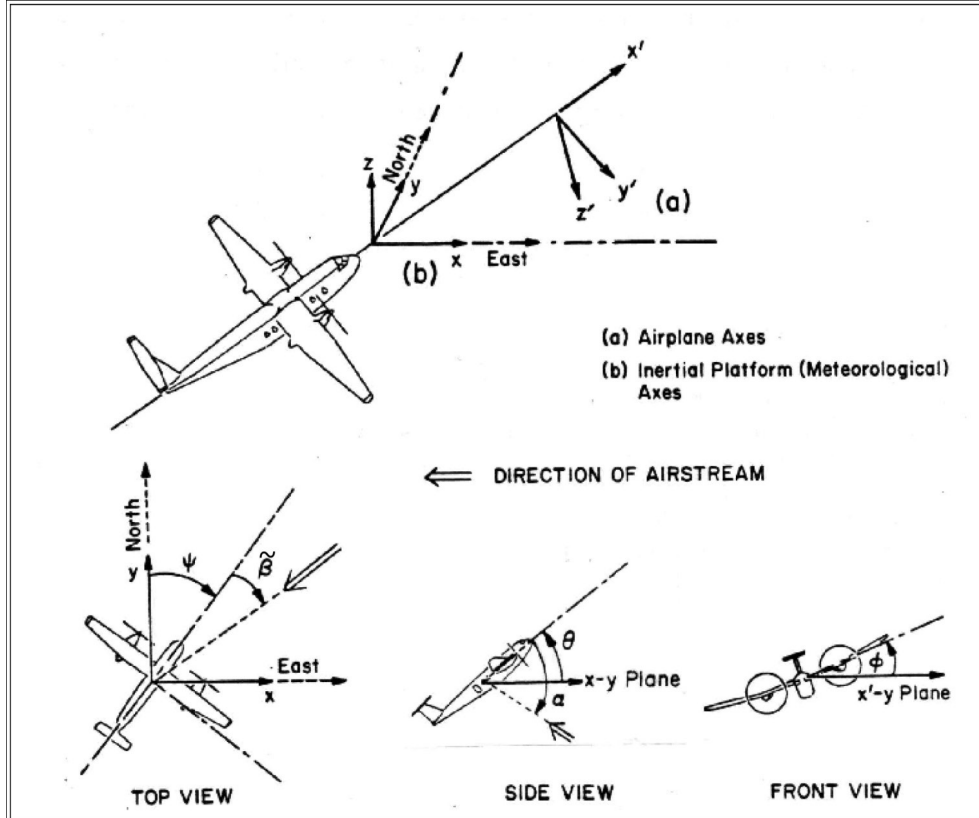


Figure 15: Aircraft attitude angles  $\Theta$ ,  $\Phi$ ,  $\Psi$  in the MONS and air flow angles  $\alpha$ ,  $\beta$  in the ACONS (Lenschow, 1986, with minor modifications).

The meteorological wind vector  $\vec{v}$  (i.e. the wind vector in the earth's coordinate system MONS – Meteorological OrthoNormal System, index  $m$ ) can be calculated from navigation, flow and attitude measurement using

$$\vec{v} = \vec{v}_{gs} + M_{mf}(\vec{v}_{tas} + \vec{\Omega} \times \vec{s}_p) \quad (1)$$

(Williams and Marcotte, 2000). The ground-speed vector  $\vec{v}_{gs}$  describes the movement of the origin of the aircraft-fixed coordinate system ACONS (AirCraft-fixed OrthoNormal System, index  $f$ ) with respect to the earth's surface and is determined using the on-board navigation system, aboard small UAV usually an Inertia Measurement Unit (IMU) combined with GPS data via a Kálmán filter. The true-airspeed vector  $\vec{v}_{tas}$  is the flow vector measured by the *in situ* wind or gust probe, usually a Five-Hole Probe (FHP), and is therefore defined with respect to the FHP. Thus, for a fast-flying aircraft with  $|\vec{v}| \ll |\vec{v}_{tas}|$ , the true airspeed is orientated more or less towards the ground speed. The location of the FHP related to the origin of the ACONS is described by the lever-arm vector  $\vec{s}_p = (x_p, y_p, z_p)$ . The vector of angular body rates  $\vec{\Omega} = (\Omega_p, \Omega_q, \Omega_r)$  contains the

angular velocities of the aircraft system ACONS related to the MONS and is among the primary output data of the IMU. The lever-arm correction in (1) using primary measurements in the ACONS is therefore:

$$\vec{\Omega} \times \vec{s}_p = \begin{pmatrix} \Omega_p \\ \Omega_q \\ \Omega_r \end{pmatrix} \times \begin{pmatrix} x_p \\ y_p \\ z_p \end{pmatrix} = \begin{pmatrix} \Omega_q z_p - \Omega_r y_p \\ \Omega_r x_p - \Omega_p z_p \\ \Omega_p y_p - \Omega_q x_p \end{pmatrix} \quad (2)$$

Often the transverse components  $y_p$  and  $z_p$  are much smaller than  $x_p$  (especially if the sensor is installed at the tip of the UAV) and are neglected (Lenschow, 1972). The vector sum  $(\vec{v}_{tas} + \vec{\Omega} \times \vec{s}_p)$  describes the measured airflow vector with respect to the ACONS and is transformed into the MONS via the operator  $\mathbf{M}_{mf}$ . Since the (relatively small) meteorological wind vector is obtained by combining two large vectors in (1), the challenging task is to determine  $\vec{v}_{tas}$  and  $\vec{v}_{gs}$  with very high precision. While the ground speed  $\vec{v}_{gs}$  is already measured in an earth-fixed coordinate system, the second term in (1) requires some more attention.

### 3.2.1 True airspeed by flight mechanical angles $\alpha$ and $\beta$

To obtain a proper solution of (1) we have to start in the aerodynamic coordinate system ADONS (index  $a$ ) of the flight. The ADONS is defined as the system in which the airspeed vector has the components  $\vec{v}_{tas,a} = (-|\vec{v}_{tas}|, 0, 0)$  and is therefore called the airspeed-fixed coordinate system, (Luftfahrtnorm, 1970). A rotation of the ADONS about the vertical (lift) axis  $z_a$  by the angle  $-\beta$

$$\mathbf{T}_{ea}(-\beta) = \begin{pmatrix} \cos \beta & -\sin \beta & 0 \\ \sin \beta & \cos \beta & 0 \\ 0 & 0 & 1 \end{pmatrix} \quad (3)$$

and then about the transverse axis (cross-force) axis  $y_a$  by the angle  $\alpha$

$$\mathbf{T}_{fe}(-\alpha) = \begin{pmatrix} \cos \alpha & 0 & -\sin \alpha \\ 0 & 1 & 0 \\ \sin \alpha & 0 & \cos \alpha \end{pmatrix} \quad (4)$$

results in the description of the airspeed vector in the ACONS:

$$\vec{v}_{tas} = \begin{pmatrix} u_{tas} \\ v_{tas} \\ w_{tas} \end{pmatrix} = \mathbf{T}_{fe}(\alpha) \mathbf{T}_{ea}(-\beta) \vec{v}_{tas,a} = -|\vec{v}_{tas}| \begin{pmatrix} \cos \alpha \cdot \cos \beta \\ \sin \beta \\ \sin \alpha \cdot \cos \beta \end{pmatrix} \quad (5)$$

with

$$\mathbf{T}_{fe}(\alpha) \mathbf{T}_{ea}(-\beta) = \begin{pmatrix} \cos \alpha \cdot \cos \beta & -\cos \alpha \cdot \sin \beta & -\sin \alpha \\ \sin \beta & \cos \beta & 0 \\ \sin \alpha \cdot \cos \beta & -\sin \alpha \cdot \sin \beta & \cos \alpha \end{pmatrix} \quad (6)$$

(Luftfahrtnorm, 1970; Boiffier, 1998). The angles  $\alpha$  and  $\beta$  are named angle of attack and sideslip, respectively,  $\alpha$  is positive for nose-lifting rotations,  $\beta$  is positive for rotations to the port side. Both the angles and the order of rotation might have their origin in wind-tunnel experiments. The components of the true-airspeed vector  $\vec{v}_{tas}$  in the ACONS are

- $u_{tas}$ , orientated along the roll axis of the aircraft, positive in flight direction,
- $v_{tas}$ , orientated along the pitch axis of the aircraft, positive in starboard direction,
- $w_{tas}$ , orientated along the normal (or yaw) axis, positive downwards.

### 3.2.2 True airspeed by FHP angles $\alpha$ and $\beta$

The components of  $\vec{v}_{\text{tas}}$  cannot directly be measured during flight. The output of the FHP are pressure differences that are used to calculate  $\vec{v}_{\text{tas}}$  in spheric coordinates in the ACONS (Figure 15):

- angle of attack  $\alpha$ , air flow from below gives positive  $\alpha$ ,
- sideslip  $\beta$ , air flow from starboard gives positive  $\beta$ ,
- $|\vec{v}_{\text{tas}}|$ , the norm of the true-airspeed vector.

Using these in-flow measured quantities, the expression for the true-airspeed vector is

$$\vec{v}_{\text{tas}} = -|\vec{v}_{\text{tas}}| \cos \alpha \cdot \cos [\arctan(\cos \alpha \cdot \tan \beta)] \begin{pmatrix} 1 \\ \tan \beta \\ \tan \alpha \end{pmatrix}. \quad (7)$$

Apart from the preceding scalar function, the resulting true-airspeed vector equals the well-known definition of Lenschow (1986)

$$\vec{v}_{\text{tas}} = \frac{-|\vec{v}_{\text{tas}}|}{D} \begin{pmatrix} 1 \\ \tan \beta \\ \tan \alpha \end{pmatrix}, \quad (8)$$

with normalisation factor

$$D = \sqrt{1 + \tan^2 \alpha + \tan^2 \beta} \quad (9)$$

(see also Leise and Masters, 1993; Williams and Marcotte, 2000). Numerically it can be shown that  $D = 1 / \cos \alpha \cdot \cos(\arctan(\cos \alpha \cdot \tan \beta))$  for  $\alpha, \beta < \pi/2$ .

### 3.2.3 Rotation into the MONS

The attitude of the aircraft can be described by the Eulerian angles  $\Theta$  (pitch),  $\Phi$  (bank or roll) and  $\Psi$  (yaw, heading or azimuth, Figure 15). The transformation from the ACONS to the MONS is performed by three sequential turnings (Luftfahrtnorm, 1970; Haering, 1990; Leise and Masters, 1993; Boiffier, 1998), rolling about the  $x_f$  axis:

$$\mathbf{T}_1(\Phi) = \begin{pmatrix} 1 & 0 & 0 \\ 0 & \cos \Phi & -\sin \Phi \\ 0 & \sin \Phi & \cos \Phi \end{pmatrix}, \quad (10)$$

pitching about the  $y_f$  axis:

$$\mathbf{T}_2(\Theta) = \begin{pmatrix} \cos \Theta & 0 & \sin \Theta \\ 0 & 1 & 0 \\ \sin \Theta & 0 & \cos \Theta \end{pmatrix}, \quad (11)$$

and yawing about the  $z_f$  axis:

$$\mathbf{T}_3(\Psi) = \begin{pmatrix} \cos \Psi & -\sin \Psi & 0 \\ \sin \Psi & \cos \Psi & 0 \\ 0 & 0 & 1 \end{pmatrix}. \quad (12)$$

The three transformations are often merged into one matrix  $\mathbf{T}_3(\Psi) \mathbf{T}_2(\Theta) \mathbf{T}_1(\Phi)$ :

$$\begin{pmatrix} \cos \Theta \cos \Psi & \sin \Phi \sin \Theta \cos \Psi - \cos \Phi \sin \Psi & \cos \Phi \sin \Theta \cos \Psi + \sin \Phi \sin \Psi \\ \cos \Theta \sin \Psi & \sin \Phi \sin \Theta \sin \Psi - \cos \Phi \cos \Psi & \cos \Phi \sin \Theta \sin \Psi - \sin \Phi \cos \Psi \\ -\sin \Theta & \sin \Phi \cos \Theta & \cos \Phi \cos \Theta \end{pmatrix} \quad (13)$$

(Luftfahrtnorm, 1970; Lenschow, 1972). The result is the airspeed vector in the geodetic coordinate system (usual index  $g$ ) with the x-axis pointing north, the y-axis pointing east and the z-axis pointing down (Luftfahrtnorm, 1970; Leise and Masters, 1993). The permutation

$$\mathbf{T}_4 = \begin{pmatrix} 0 & 1 & 0 \\ 1 & 0 & 0 \\ 0 & 0 & -1 \end{pmatrix} \quad (14)$$

is necessary to transform into the MONS which is defined by the meteorological wind vector components

- $u$ , positive eastwards,
- $v$ , positive northwards,
- $w$ , positive upwards.

Finally,  $\mathbf{M}_{mf} = \mathbf{T}4 \mathbf{T}3 \mathbf{T}2 \mathbf{T}1$  is inserted into (1), and the components of the meteorological wind  $\vec{\nu}$  can be written as  $\mathbf{M}_{mf} \vec{\nu}_{tas} =$

$$\frac{-|\vec{\nu}_{tas}|}{D} \begin{pmatrix} \cos\Theta\sin\Psi + \tan\alpha(\cos\Phi\sin\Psi\sin\Theta - \cos\Psi\sin\Phi) + \tan\beta(\cos\Phi\cos\Psi + \sin\Phi\sin\Psi\sin\Theta) \\ \cos\Psi\cos\Theta + \tan\alpha(\sin\Phi\sin\Psi + \cos\Phi\cos\Psi\sin\Theta) + \tan\beta(\cos\Psi\sin\Phi\sin\Theta - \cos\Phi\sin\Psi) \\ \sin\Theta - \cos\Phi\cos\Theta\tan\alpha - \cos\Theta\sin\Phi\tan\beta \end{pmatrix} \quad (15)$$

(identical with Lenschow, 1986) and  $\mathbf{M}_{mf}(\vec{\Omega} \times \vec{s}_p) =$

$$\begin{pmatrix} (\cos\Phi\sin\Psi\sin\Theta - \cos\Psi\sin\Phi)(\Omega_p y_p - \Omega_q x_p) + (\cos\Phi\cos\Psi + \sin\Phi\sin\Psi\sin\Theta)(\Omega_p x_p - \Omega_p z_p) + \cos\Theta\sin\Psi(\Omega_q z_p - \Omega_q y_p) \\ (\sin\Phi\sin\Psi + \cos\Phi\cos\Psi\sin\Theta)(\Omega_p y_p - \Omega_q x_p) + (\cos\Psi\sin\Phi\sin\Theta - \cos\Phi\sin\Psi)(\Omega_p x_p - \Omega_p z_p) + \cos\Psi\cos\Theta(\Omega_q z_p - \Omega_q y_p) \\ \sin\Theta(\Omega_q z_p - \Omega_q y_p) - \cos\Phi\cos\Theta(\Omega_p y_p - \Omega_q x_p) - \cos\Theta\sin\Phi(\Omega_p x_p - \Omega_p z_p) \end{pmatrix} \quad (16)$$

### 3.3 Calibration of airborne wind measurements

The calibration of wind sensing systems is a complex task that includes the laboratory calibration of the individual sensors (pressure, temperature, humidity), the wind-tunnel calibration of the flow angles and the total pressure ( $|\vec{\nu}_{tas}|$ ), preferable including the entire UAV, and finally the in-flight calibration of the whole system. Two different ways of performing in-flight calibration are common, the Lenschow and the Rodi maneuvers (see also Lenschow *et al.*, 2007).

A quite simple method that only requires repeated straight and level flights in two perpendicular directions (e.g. on a cross-or square-shaped flight pattern) was published by van den Kroonenberg *et al.* (2008) and can be used for in-flight calibration of any FHP. The method presumes that the following airborne measurements are performed under identical aerodynamic conditions, especially regarding the true airspeed.

Also presented by van den Kroonenberg *et al.* (2008) is a very useful method to calibrate a FHP mounted on a small UAV like the MASC and the M<sup>2</sup>AV (Section 4.3) that can be used at wind farms. The method is based on five pressure difference measurements (this presumes that the FHP was tubed accordingly): the difference between the central hole and each of the four remaining total pressure ports ( $\Delta P_{01}, \Delta P_{02}, \Delta P_{03}, \Delta P_{04}$ ), and the difference between the static pressure and the central hole ( $\Delta P_{0s}$ ). These measurements are used to determine a total pressure difference

$$\Delta p = \left[ \frac{1}{5} \sum_{i=1}^4 \left( p_i - \frac{1}{5} \right)^2 \right]^{1/2} + \left[ p_0 - \frac{1}{4} \sum_{i=1}^4 p_i \right] \quad (17)$$

which uses the absolute pressures. Since the measurement of the absolute pressures  $P_i$  is often not feasible, (17) can also be expressed by the pressure differences:

$$\Delta p = \sqrt{\frac{1}{125} \left[ \begin{array}{l} (\Delta p_{01} + \Delta p_{02} + \Delta p_{03} + \Delta p_{04})^2 \\ + (-4\Delta p_{01} + \Delta p_{02} + \Delta p_{03} + \Delta p_{04})^2 \\ + (\Delta p_{01} - 4\Delta p_{02} + \Delta p_{03} + \Delta p_{04})^2 \\ + (\Delta p_{01} + \Delta p_{02} - 4\Delta p_{03} + \Delta p_{04})^2 \\ + (\Delta p_{01} + \Delta p_{02} + \Delta p_{03} - 4\Delta p_{04})^2 \end{array} \right] + \frac{1}{4} (\Delta p_{01} + \Delta p_{02} + \Delta p_{03} + \Delta p_{04})} \quad (18)$$

Next step is to calculate the dimensionless pressure coefficients

$$k_\alpha = \frac{\Delta p_{01} - \Delta p_{03}}{\Delta p} \quad \text{and} \quad k_\beta = \frac{\Delta p_{02} - \Delta p_{04}}{\Delta p} \quad . \quad (19)$$

Then, three functions are defined to calculate the airflow angles and the dimensionless coefficient  $k_q$  (later needed for the dynamic pressure)

$$\alpha = f_1(k_\alpha, k_\beta), \beta = f_2(k_\alpha, k_\beta), k_q = f_3(k_\alpha, k_\beta), \quad (20)$$

with the general calibration polynomial form

$$f_x(k_\alpha, k_\beta) = \sum_{i=0}^m (k_\alpha)^i \left[ \sum_{j=0}^n X_{ij} (k_\beta)^j \right], \quad (21)$$

with  $x = \alpha, \beta, q$  and typically  $m = n = 10$ . Here,  $X_{ij}$  represents the individual calibration tensors for the angle of attack  $a_{ij}(f_\alpha)$ , sideslip  $b_{ij}(f_\beta)$ , and dynamic pressure  $q_{ij}(f_q)$ . Thus, the function (21) contains  $m \times n$  unknown coefficients  $X_{ij}$  that have to be determined via a system of  $m \times n$  independent equations (e.g., using a least-square method). The most accurate method to obtain these equations are measurements in a calibrated wind tunnel. Combinations of differential pressures with adjusted  $x = \alpha, \beta, q$  can be achieved by varying the air speed and flow angles by turning the FHP in the wind tunnel. Preferably, the FHP is mounted on the aircraft (and not be removed between calibration and measurement flight). Of course, this is only feasible for very small aircraft like UAV and large wind tunnels. Finally the dynamic pressure  $q$  is given by

$$q = \Delta p_s + \Delta p \cdot k_q. \quad (22)$$

where  $p_s$  is the static air pressure.

### 3.4 Achievable accuracy

The quantification of the accuracy of any airborne wind measurement is a difficult task since the calculation of the meteorological wind vector relies on many (and also some quite challenging) measurements of thermodynamic quantities, attitude angles, navigation and additional parameters (see the sections above). In the end, only a direct comparison with e.g. a ground-based *in-situ* instrument like a large tower can help to quantify the resulting accuracy. However, even the wind measurement on a tower is afflicted with measurement errors (e.g. interaction of the turbulent atmospheric flow with the structure of the tower), so that even two measurements with different technologies only show the same to about 1% in the best case. The main difficulty to compare

atmospheric time series measured at a fixed location (e.g. tower) with time-dependent spatial series measured with a quickly moving vehicle (here: UAV) is the assumption that Taylors' hypothesis of frozen turbulence is fulfilled, an assumption not necessarily valid. For example: Turbulent eddies with significant kinetic energy are found at the large-scale end of the turbulent spectrum. To measure e.g. eddies of 200 m diameter with a statistical standard error of about 10 %, about 100 hundred eddies must be sampled. Under high-pressure conditions (convective ABL) with low mean wind speed (e.g. 5 m/s) the tower has to wait 4000 s. During this averaging period the diurnal cycle of the ABL cannot be ignored, i.e. the incoming solar radiation and thus the source for turbulence and wind changes significant. The influence of the short-term changes in the cloud pattern is still neglected in this consideration. Even a slowly operating research UAV (e.g. 22 m/s airspeed like the M<sup>2</sup>AV or MASC) samples these 200 eddies within 15 minutes. To conclude, ground-based and other fixed-position measured atmospheric statistics are very difficult to compare with those measured by fast moving airborne systems.

The spatial resolution of both measurement strategies is mainly defined (besides the sensors inertia time) by the temporal resolution of the data sampler and the speed of the transporting wind or airspeed, respectively. E.g. assuming that the UAV uses a sampling rate of 100 Hz and very fast sensors, its spatial resolution is not better than airspeed divided by a third or quarter of the sampling rate (due to Nyquist theorem) and thus in the range of a metre or half a metre. Ground-based installations can carry much heavier and thus much faster and more accurate equipment, like hot-wire anemometers (CTA), that are able to reach even the dissipation sub-range of turbulence, which will not be resolved by airborne systems in the following ten years, probably.

The research UAV of type M<sup>2</sup>AV (Section 2.1) was intensely tested and its measured data compared to instruments of the German Meteorological Service (DWD) in Lindenberg (near Berlin) during the LITFASS-2009 (LIndenberg-To-Falkenberg: Aircraft, Scintillometer and large-eddy Simulation) experiment (Martin *et al.*, 2011). For comparison, the 99 m tower, a sodar, and a wind profiler RASS system was available. Since the research UAV of type MASC (Section 4.2) are very similarly equipped with thermodynamic sensors and are of similar size and weight, the results and the achievable measurement accuracy are valid for both systems. As explained in Section 3.1, the research UAV is able to measure with much higher spatial and temporal resolution compared to the ground-based systems, so only temporally and spatially averaged data was available for comparison. However, the analysis of vertical profiles clearly demonstrated that both wind direction and wind speed measured by the UAV were in remarkable agreement with the ground-based measurements. Deviations between airborne and ground-based data were in general in the range of 5° and 0.5 m/s, respectively. Of course it is not possible to decide whether these deviations were caused by the UAV or by the ground-based systems.

An analytical analysis of the systematic error of airborne wind measurements was performed by van den Kroonenberg (2009). Typical calibration and measurement errors of all parameters in (16) were added up to 0.5 m/s for the velocities and 1° for the flow and the Eulerian angles. Under common research flight conditions and using a 6 kg, 2 m wingspan research UAV like the M<sup>2</sup>AV or the MASC at 20 m/s airspeed, the resulting error of the meteorological wind components was not larger than 0.5 m/s.

### 3.5 New challenges

In the summer of 2010, we organised a workshop as preparation for the flights later this year. We intended to get input on three main topics: wind speed measurements, wind power meteorological questions and flight related issues.

The first topic is mainly the question of how to derive good wind speed measurements from the devices, and to what accuracy those can be measured. With a Pitot tube, turbulence can be measured up to 100 or 200Hz, so spectra of turbulence up to the inertial sub-range are an option. What the sonic can do on the helicopter, and how contaminated the measurements are from the helicopter movements is another point for investigation. Scientifically quite interesting is the question of how to compare measurements along a flight path with measurements from a fixed mast. This leads to the limits or extensions to Taylors hypothesis, which relates spatial wind patterns to time-based measurements. Essentially, Taylors Frozen Eddy hypothesis claims that eddies in the atmosphere are advected past a fixed sensor without structural change. This is strictly only true for instantaneous snapshot measurements. However, the cornerstone of wind power meteorology is the 10-min mean wind speed. How this can be achieved reliably, is an open question for a moving platform. In this sense, even the movements of the tethered LTA system needs to be verified.

Secondly, once the tools are available, which questions would we like to find answers to? Details of the wake structure, including multiple wakes offshore, are a logical candidate. The fine structure of vortex near the tip of the blade is another logical field. For a more generic meteorology investigation, the development of internal boundary layers both from offshore to onshore flow and the night-time stable layer are good candidates. Also the wind speeds in heights greater than typical meteorology masts or even lidars allow (above 200m) could be investigated.

Another interesting investigation could be the variation of wind profile/wind shear with atmospheric stability, as the UAS also provide temperature and humidity information.

Finally, how to best employ the technology at hand is a final point of discussion. Which flight patterns are best for which investigation? For the wakes, a logical idea is to do “race tracks” in front and behind the turbine row in various heights. However, for the Pitot tube, the angle of attack where it measures reliably is limited to some 20 degrees off the main axis. Can the plane be flown across the wake structure, i.e. perpendicular to the incident wind, and still measure reliably? Can the plane do loopings in the wakes (*probably, though maybe not under computer control*), and if yes, can the data be interpreted (*no, only data from straight line tracks is reliable*)? How can a flight pattern be found to measure a 10-min average wind speed with the same accuracy as a fixed sensor on a mast, e.g. by flying circles around the anemometer? What is the advantage of being able to hover – can this be used for the 10-min average, or does it have other advantages? Can the Funjet be made to fly so slow into the wind as to also hover (*no, since the autopilot needs movement to work*), or will it have to stand so much on its tail that gusts cannot be handled any more? Is the “standing on its tail” too battery consuming? A further complex of questions relates to safety. How close can the planes get to the turbines while staying safely in the air? The tip speed vortices are quite violent, so it should not be too close, but which distance is safe? How far away can the wake structure actually be resolved? Is loitering time an issue? Can the small tip vortices of the single blades be actually resolved, as in Figure 16 below? Note that the tip vortices

would only stay so well defined in fully laminar inflow – in realistic wind onshore, they would be mixed out after about 1 rotor diameter.

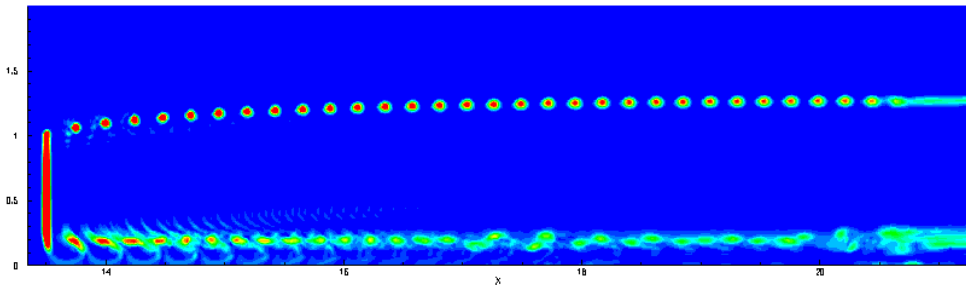


*Figure 16: Visualisation of the tip vortex in laminar inflow calculated by CFD. Image courtesy Jens Nørkær Sørensen, DTU.*

The full workshop minutes and talk slides are available from [http://www.risoe.dtu.dk/Research/sustainable\\_energy/wind\\_energy/projects/VEA\\_AerialWindSensors/Workshop.aspx](http://www.risoe.dtu.dk/Research/sustainable_energy/wind_energy/projects/VEA_AerialWindSensors/Workshop.aspx). After a round of introductions, the first session went underway with a talk of Arnulf Knittel, of wind power developer hrfnakel. His emphasis was on a better Power Production Estimate during the wind resource assessment phase including uncertainty. To cover all relevant wind classes for a wind resource assessment, one has to get about 300 hours of measurements, which costs between 25.000 and 50.000 euro. If this time could be shortened with a better knowledge of the total wind field in the whole wind farm, clear savings would ensue, and the margin of error would be decreased, which would mean that the difference between the P50 (the most probable Annual Energy Production from a new wind farm) and the P90 (the value with only 10% probability to not be reached, i.e. the value the banks look at when lending money) would be smaller. This additional knowledge could encompass certain meteorological phenomena such as cold air outbreaks in valleys in the south or zones of flow detachment behind hills. During the discussion it was made clear that manned vehicles are not an option, as they are too expensive (order of magnitude 2000 euro per flight hour). The use case would be to have the planes on standby, and use them if there is some significant meteorological event.

Sven Erik Gryning of Risø DTU then discussed the use of tethersondes. The Civil Aviation Authorities (CAA) allow them up to 500m, provided that the line can be cut through by a plane. They work fine in no wind conditions, but have a hard time withstanding stronger winds. For a full Boundary Layer (BL) assessment, one would have to go beyond 1 km. For the aircraft, he proposed to use them for energy budgets. One difficulty in his opinion was the footprint problem: the higher the aircraft gets, the more surface on the ground is influencing the measured wind speeds. And it is not quite clear now to deal with it. One possibility would be to measure in the blended layer, where the very local influences already have been washed out - in about 2-300 m.

Ed Bervoets of Vestas R&D had some ideas for the use of such a technology, especially deep wakes behind large wind farms (especially offshore), a study in loads and the related winds, and a full wind farm optimisation for lifetime and power production.

## 4 The Hardware

Since the project's aim was to get a good overview of the possibilities for a autonomously operating field tool for wind power meteorology, we also tried to get several different flying platforms within the project. While the project directly funded the development and acquisition of the SkyDoc system (section 4.5) including the nano-synchronised sensors (section 4.6), it also paid for the integration of the measurement system of the Vario XLC with the sonic anemometer (section 4.4) and some further development of the measurement techniques used on the SUMO (section 4.1) and MASC (section 4.2).

*Table 1: Overview of the UAS.*

|                        | <b>SUMO</b>           | <b>MASC</b>    | <b>M<sup>2</sup>AV</b> | <b>VarioXLC</b>           |
|------------------------|-----------------------|----------------|------------------------|---------------------------|
| vehicle type           | fixed wing UAS        | Fixed wing UAS | Fixed wing UAS         | Helicopter UAS            |
| <b>DIMENSIONS</b>      |                       |                |                        |                           |
| wingspan               | 80 cm                 | 210 cm         | 200 cm                 |                           |
| length                 | 75 cm                 |                |                        |                           |
| height                 | 23 cm                 |                |                        |                           |
| propeller diameter     | 227 mm (9x6)          |                |                        |                           |
| Max. take off weight   | 580 g                 | 4 kg           | 5.6 kg                 | 40 kg                     |
| Payload                | 140 g                 | 1 kg           | 1.5 kg                 |                           |
| <b>PROPELLSION</b>     |                       |                |                        |                           |
| motor                  | electric<br>brushless |                |                        | Jakadofsky Gas<br>turbine |
| motor type             | AXI2212/26            |                |                        |                           |
| motor power            | 120 W                 |                |                        |                           |
| battery type / tank    | Lithium-<br>Polymer   | LiPo           | LiPo                   |                           |
| battery capacity       | 2.1 Ah / 11.1 V       |                |                        |                           |
| <b>SPEED</b>           |                       |                |                        |                           |
| minimum speed          | 29 km/h (8 m/s)       | ~15 m/s        |                        |                           |
| maximum speed          | 151 km/h (42<br>m/s)  | ~30 m/s        |                        |                           |
| cruise speed           | 54 km/h (15<br>m/s)   | 22 m/s         | 22 m/s                 |                           |
| Climb rate             |                       | 3 m/s          |                        |                           |
| <b>RANGE/ENDURANCE</b> |                       |                |                        |                           |
| horizontal             | < 5 km                | 120 km         | 30 km                  | 40 km                     |
| vertical               | > 4 km                |                | 2.5 km                 |                           |
| duration               | < 30 min              | 1.5 hours      | > 45 min               | 30 min                    |
| Autopilot              | Paparazzi             | Paparazzi      | MINC                   |                           |

### 4.1 SUMO

The Small Unmanned Meteorological Observer SUMO is a micro-UAS (unmanned aerial system) developed and operated as controllable and recoverable boundary layer measurement system. For the application within this project, an extension of the system for flow measurement, additionally equipped with either a rather cheap and simple pitot tube or an advanced 5-hole probe, have been in operation. Part of the sensor system and the adaptation to the SUMO airframe was funded by the project.

## Airframe

SUMO is based on the commercially available model construction kit FunJet by Multiplex, a delta-wing structure composed from EPP (expanded propylene) foam material. With its wingspan and length of around 80 cm and a total take-off weight of around 600 g it falls into the category of micro-UAS. The aircraft has electric propulsion by a 120 W brushless motor driving a pusher-propeller in the rear. SUMO has been developed in cooperation between the Geophysical Institute, University of Bergen, Norway and Martin Müller Engineering, Hildesheim, Germany. A detailed description of the system can be found in Reuder et al. (2009). Figure 17 shows the 3 SUMO systems operated during the project, the key technical specifications are summarized in Table 2.

*Table 2 Technical specifications of the SUMO system*

| SUMO technical specifications  |  |
|--------------------------------|--|
| <b>SENSORS</b>                 |  |
| altitude control               | IMU and infrared thermopiles                 |
| navigation                     | GPS  |
| basic meteorology              | pressure, temperature, humidity              |
| <b>SUMO operation</b>          |  |
| mode of control, mode 1        | autopilot (AUTO2)                            |
| mode of control, mode 2        | stabilized manual (AUTO1)                    |
| mode of control, mode 3        | manual (MAN)                                 |
| launch method                  | hand launch                                  |
| landing method 1               | belly landing, manual                        |
| landing method 2               | belly landing automatic                      |
| personell during start/landing | 2, operator and pilot                        |
| personell in flight            | 2, GCS operator and safety pilot in stand-by |
| ground station                 | PC with 2.4 GHz radio modem                  |



*Figure 17: The 3 SUMO airframes used during the flight week. The system in the foreground is equipped with the 5-hole probe, the two in the background with the simple Pitot tubes (photo: J. Reuder).*

## Autopilot

SUMO is equipped with the open source autopilot system Paparazzi, mainly developed and maintained by the École Nationale de l'Aviation Civile (ENAC), Toulouse, France. This freely available autopilot is used by several hundreds of educational and scientific users all over the world. It enables the aircraft to be flown autonomously under the supervision of an experienced RC pilot and a ground control station (GCS) operator. The system enables automatic flights following predefined mission plans that can be modified at any time in-flight using the 2.4 GHz bidirectional data link.

Until 2010, the attitude control of the SUMO aircraft by the Paparazzi autopilot system, i.e., the in-flight regulation of the aircraft's pitch and roll angle, has been realized by an array of 6 IR thermopiles measuring the radiation temperature in different directions (e.g. Brisset et al. 2006). This method limited the operation of SUMO as it required an IR temperature difference of at least 8 K between sky and ground. Therefore SUMO could not be operated e.g. below low clouds or within clouds. With progress in miniaturization, progressively smaller inertial measurement units (IMU) entered the market and could finally be adapted to the SUMO system. In the SUMO version operated during the campaign, the ArduIMU from Diydrone has been used. By the adaptation of the IMU, the range of meteorological conditions suitable for save operation of the system has been extensively increased.

## SUMO meteorological sensors

In its current version, the SUMO system is equipped with the following sensors for basic meteorological parameters. Temperature and humidity are measured by the combined sensor SHT 25 from Sensirion. This sensor is mounted inside a radiation protection tube on the upper side of the wing (see Figure 17). Atmospheric pressure is monitored by a SCP1000 sensor from VTI inside the fuselage. The surface temperature below the aircraft can be estimated with the help of an IR sensor (MLX90247).

*Table 3: Specifications of the meteorological sensors currently carried by the SUMO airframe. The acquisition frequency is defined by the sampling rate of the data logger.*

| Parameter                         | Sensor                  | Range        | Accuracy    | Acquisition frequency |
|-----------------------------------|-------------------------|--------------|-------------|-----------------------|
| Temperature                       | Sensirion SHT 75        | -40/+124 °C  | +/-0.3 K    | 2 Hz                  |
| Humidity                          | Sensirion SHT 75        | 0-100 %      | +/-2 %      | 2 Hz                  |
| Pressure                          | VTI SCP1000             | 300-1200 hPa | +/-1.5 hPa  | 2 HZ                  |
| surface temperature (IR emission) | MLX90247                | n/a          | n/a         | 2 Hz                  |
| 1 D flow vector                   | Pitot tube Eagle Tree   | 1-156 m/s    | n/a         | 7 Hz                  |
| 3D flow vector                    | 5 hole probe, Aeroprobe | 11-35 m/s    | +/- 0.1 m/s | 100 Hz                |



*Figure 18: The 5-hole probe and its data logging system as mounted on the SUMO airframe (photo: J. Reuder).*

For flow measurements the SUMO system has been equipped with 2 different sensors. The first one is a rather simple and cheap pitot tube (Airspeed Sensor v3 from Eagle Tree Systems), typically used for air speed measurements by model aircraft enthusiasts. This sensor has been directly connected to the data system of the Paparazzi autopilot and was configured for maximum measurement rate of around 7 Hz. The mounting of these sensors can be seen on the 2 SUMOS in the background of Figure 17 and on the cover. The second flow measurement system consists of a miniaturized a 5-hole probe and the corresponding pressure transducers and data logger, commercially available from Aeroprobe Corporation in the USA. The system is capable to measure the 3-dimensional turbulence flow vector impinging the aircraft with a temporal resolution of 100 Hz. The mounting of the 5-hole probe is shown on the airplane in front of Figure 17 and in more detail in Figure 18. The technical details and characteristics of the adapted sensors are summarized in Table 3.

During the deployments in the flight week, the data logger of the turbulence probe had to be operated stand-alone without synchronization with the autopilot continuously logging the attitude of the aircraft, i.e., the Eulerian angles pitch, roll and yaw. These are essential to apply the correction for the movement of the aircraft to transform the in-flight measured turbulent flow into the meteorologically relevant components  $u$  (east-west),  $v$  (north-south), and  $w$  (in the vertical). Due to limitations in the bandwidth of the data transmission between SUMO and the GCS and a lack of corresponding on-board storage capacity, the attitude information during the turbulence flights has in addition been limited to 10 Hz sampling rate. For the turbulence flight missions performed during the flight week at Nøsjomhed this leaves us with the challenging task of motion correction based on two unsynchronized data sets with different temporal resolution. In addition there were certain issues with the fine tuning of the newly integrated IMU during the flight week, causing unsatisfactory behavior of the SUMO aircraft in keeping the predefined altitude, in particular in turns. These difficulties are now solved and

SUMO showed excellent leveling characteristics during the BLLAST campaign in France in June/July.

The main pitfall in atmospheric turbulence determination was the lack of a common data acquisition system for the turbulent flow vector impinging the aircraft and the attitude of the airframe. The synchronization of the data acquisition of the 5-hole turbulence probe and the Paparazzi autopilot system is currently ongoing. From the beginning of 2012 both data streams will be commonly collected and stored on-board using the same temporal resolution of 100 Hz.

### **Other uses of the SUMO for wind estimation**

There are two other groups working with the SUMO to do wind estimation. The group at the Swiss Federal Institute of Technology ETH had instrumented a SUMO with their own seven sensor fast-response probe based on miniature silicon piezo-resistive chips embedded within a 20 mm hemispherical head (Mansour et al, 2011). The SUMO was flying straight into the wake of a turbine, from a distance of about 3 rotor diameters to about half a rotor diameter, and then turned off quickly to avoid crash with the turbine (Kocer et al, 2011a,b).

The Institute for Meteorological Research, Iceland, uses a SUMO to improve the weather forecast for Search And Rescue operations, for the SARWeather project (Rögnvaldsson 2011). The intention is to come with timely and updated information as input to a weather forecasting model (the Weather Research and Forecasting model WRF) by assimilating a flight of the SUMO in the area of interest. A system like this could for example help during the erection of offshore wind turbines, when the installation ship needs a time window of 2-3 hours without too strong gusts to be able to install the rotor.

## **4.2 MASC**



*Figure 19: Research UAV of type M<sup>2</sup>AV (left) and MASC (right).*

At the University of Tübingen (EKUT) the study of the lower atmosphere using small research UAV is continued using an aircraft that was developed in 2010 on the base of the M<sup>2</sup>AV. The research UAV of type MASC (Multi-purpose Automatic Sensor Carrier, Figure 2) weighs about 4 kg including batteries for about 1.5 hour flight and is able to carry 1 kg of scientific payload. The aircraft has 2.1 m wingspan and is electrically powered by two propeller engines. The cruising speed for scientific operation is 22 m/s, and the climbing rate for vertical profiles is typically 3 m/s. The range is 120 km. It is

controlled by the free and open-source Paparazzi autopilot ([paparazzi.enac.fr](http://paparazzi.enac.fr)) combining GPS with a IMU. The meteorological sensor equipment (very similar to the M<sup>2</sup>AV) is installed in a removable sensor container in the centre of the wind, assuring that the sensors are in front of the propellers and the fuselage.

The human safety pilot at the ground (as required by civil aviation authorities) controls the aircraft only during take-off and landing using a digital remote-control unit at 2.4 GHz. The latter allows the operation of several UAV at the same time. During measurement flights the MASC communicates via a radio link with the mission control ground station (a common laptop computer) sending flight data and position, receiving new commands e.g. way point updates.

### 4.3 M<sup>2</sup>AV

The automatically operating meteorological mini aerial vehicle (M<sup>2</sup>AV, Spieß et al., 2007; van den Kroonenberg et al., 2008) was developed at the Institute for Aerospace Systems ILR, Technical University of Braunschweig. The development required several specialists from the fields of aerodynamics, navigation, light-weight aircraft design, autopilots, electronics and meteorological measurement technology. It is based on the unmanned “Carolo T200” aircraft as carrier system with a wingspan of 2 m. The maximum take-off weight is 6 kg, including payload of 1.5 kg (Spieß et al., 2007). The aircraft is hand-launched and operates then under the control of a board computer. The MINC autopilot was developed at ILR. It is programmed prior to the flight, and the waypoints in three dimensions can be updated during the mission by a telemetry link within a distance of 5 km from the ground-based station (the remote control operates at 2.4 GHz). The M<sup>2</sup>AV can also perform longer flight segments (up to about 30 km) with automatic flight at a cruising speed of 22 m/s, limited by the endurance of the batteries (about 1 h). It covers the entire ABL height and can fly as low as few 10 m above ground.



*MINC Autopilot System (single board option)*

*Figure 20: The MINC autopilot system.*

The meteorological, navigation and attitude data are stored on board at 100 Hz resolution. Flight information can be transmitted to the ground station to allow monitoring of the state of the mission. The turbulence payload of the M<sup>2</sup>AV was developed by the Airborne Geoscience group of the ILR under the supervision of Jens Bange, now EKUT, Tübingen.



*Figure 21: The meteorological package of the M2AV: 5-hole probe, thermocouple and Humicap sensor.*

The instrumentation for temperature measurement comprises two sensors with different characteristics. One is a Vaisala HMP 50 resistance thermometer sensor with high accuracy but slow response time (in flight about 1 s). The second sensor is a thermocouple (type K) with a poor long-term stability but fast response time (30 Hz) for turbulence measurements. The signals of the two sensors are joint using a complementary filter with an overall temporal resolution of 30 Hz, a temperature resolution of about 0.01 K and an absolute accuracy of better than 0.5 K. The same HMP 50 provides air humidity measurements (Vaisala HMP50). The sensor is a rather slow sensor but achieves a good accuracy (1-2 % relative humidity) over the temperature range of interest for the airborne missions.

The wind vector in the airframe coordinate system is measured by a five-hole probe (FHP) with a mass of only 22 g and a diameter of 6 mm. The FHP was developed and manufactured by the Institute of Fluid Dynamics, TU Braunschweig. It provides the angle of attack and sideslip in the range of -20° to +20° with 0.1° resolution due to calibration. The static pressure is measured via four extra holes at the side of the probe. For the calculation of the wind vector, the attitude of the aircraft is needed in high precision. This is achieved by a 3D GPS attitude measurement system. Additionally to the implemented autopilot hardware including an inertial measurement unit (IMU) with accelerometers and gyros, an extra IMU and GPS system are integrated in the meteorological data acquisition unit. During data post processing, the GPS and IMU data are merged using a complementary Kalman filter. With its overall sampling rate of 100 Hz (except humidity) and effective anti-aliasing filtering at 33 Hz the spatial resolution of M<sup>2</sup>AV turbulence measurements (at typical 22 m/s airspeed) is in the sub-meter range. During vertical profiles (at a typical climb rate of 3 m/s) a vertical resolution of 10 cm can be achieved. All sensors are sampled at 100 Hz, but the resolutions differ due to the different response time of the instruments. In 2005, the first scientific mission of the automatically operating unmanned turbulence probe M<sup>2</sup>AV (Spieß et al., 2007; van den Kroonenberg et al., 2008) was performed during the LAUNCH campaign near Lindenberg, followed by the first application of scientific UAV in Antarctica (during a 14 month stay at British Antarctic Survey station Halley). Latest UAV missions focused on the in situ measurement of the turbulent structure parameter (DFG project BA-1988/9-1), the vertical probing of the convective ABL and morning transition (Martin et al., 2011), and the first measurement of turbulent fluxes with small UAV.



*Figure 22: The M<sup>2</sup>AV flying next to the meteorological tower of the German Meteorological Service near Lindenberg in 2009.*

#### **Further technical specifications Carolo T200**

- operational altitude 0 .. 7 km (with adjusted propeller/motor)
- standard telemetry system 868 MHz ISM band
- remote control system Graupner MC-19, 35 MHz
- operational ambient temperature -20 ... +45 °C

#### **4.4 Vario XLC**

##### **Helicopter**

The helicopter platform chosen for this project is a fairly large model helicopter from the German company Vario. The helicopter is originally designed for carrying camera equipment, and is thus specialized for commercial/industrial applications, and is therefore 1) capable of flying a reasonable big payload and 2) features sufficient space for mounting onboard computer and sensors for autonomous flight. The helicopter is originally powered by a JetCat two-stage turbine that allows for a maximum take-off weight (MTOW) of 32 kg. Of these 4 kg are available for mission payload (which in this project is an ultrasonic wind sensor). The flight time is approximately 30 minutes, the range about 40 km, and the helicopter is capable of sustaining flight in rather rough wind conditions, while take-off and landing conditions have to be carried out in not too strong wind conditions (< 15 m/s peaks). This is ideal for the present project where we expect the wind conditions behind the turbines to be quite turbulent, while the ground wind might be fairly benign. Recently, the helicopter has been upgraded with a prototype kit from the manufacturer. This increases the MTOW to 40 kg, and includes a new turbine (a somewhat bigger one stage Jakadofsky turbine), bigger rotor blades, and a longer and stiffer tail boom. This upgrade also improves the handling characteristics without reducing the flight time significantly.



Figure 23: Vario XLC.

### Onboard computer (OBC) and sensors

To fly the helicopter autonomously the Vario XLC is equipped with a Mini-ITX single board computer (basically a core of a regular PC) and servo board developed at Aalborg University. The latter is the electronics and software interface between the computer and all actuators and sensors on the helicopter. The software running on the OBC is entirely developed at AAU, and includes memory server, controller and planner, state estimator, telemetry server, command interpreter, and data logging. The OBC communicates to a ground station (also developed at AAU) that has graphical user interface for control of the helicopter.

The avionics sensors include a Crossbow NAV400 medium grade INS that provides attitude states, and a Ashtech MB100 RTK GPS (1-2 centimeter accuracy) for positions states. Further, the jet turbine and the wind sensor are also interfacing to the OBC. All sensor input is recorded and time stamped for continuous logging.

### Mission sensor

Since the purpose of the project is to record wind measurements behind wind turbine the helicopter is equipped with a standard off-the-shelf 3D ultrasonic wind sensor. To avoid disturbances from the down draft of the rotor the sensor is suspended as a slung load in a 4-5 meter wire hanging below the helicopter. This provides an almost vibration and disturbance free environment for the sensor, but obviously also complicates the actual flight, since both take-off, landing, and stability of the platform becomes more difficult with a slung load. However, at AAU we have done extensive studies on automated flight with slung load systems, and both hardware and software are initially designed for accommodating a slung load. See e.g. Bisgaard et al 2009, Bisgaard et al 2010 and la Cour-Harbo and Bisgaard 2009.



*Figure 24 Wind sensor as slung load*

The Vario XLC has been flown several times during the project period, but due to technical and regulatory problems (see section 6.1) we have not been able to fly close to a wind turbine to record actual wind turbine flow data.

The conducted flight test was with the AAU Bergen Industrial Twin helicopter on a windy day. A couple of minutes of data were recorded before the helicopter (due to the strong wind) became partially unstable, and the backup pilot had to make a safety landing which damaged the helicopter. Subsequently, it was determined that the tail rotor lacked sufficient actuation to keep the helicopter flying with the side against the wind. This is easily corrected and helicopter was fairly quickly ready for flying again. Figure 24 shows the helicopter carrying the wind sensor in a 4 meter wire. The helicopter is not flying forward, but rather leaning into the wind to stay stationary. The INS recorded the wind sensor swinging motions and it was possible to correct the rotation and swing of the wind sensor to acquire useful wind velocity data.

The wind sensor is a RM Young 81000 capable of measuring with an accuracy of 0.01 m/s at 20 Hz, and produces a 3D direction for each measurement. Temperature and the speed of sound are also recorded continuously. An Xsens MTiG INS is mounted on the wind sensor and records the attitude and approximate position (within the accuracy of a standalone GPS) of the wind sensor during flight. This is necessary since the sensor will be swinging and rotating (around the vertical axis) during flight, and therefore the helicopter position and attitude is not directly useful as reference for the wind sensor state. However, since the swing of the slung load is fairly predictable (at least short term) it is possible to get a more accurate position of the slung load by combining the MTiG position measurements with the much more accurate position measurements of the helicopter, thus getting a 10 cm accuracy of the wind sensor during flight. The OBC records all data from all onboard sensors at 50 Hz (or whatever lower refresh rate is available from each sensor) and time stamps it so that it is easy to process post flight.

### Flight tests

Unfortunately, it has not been possible to flight the test system behind an actual wind turbine during the project period. However, the wind sensor has been flight tested on another AAU helicopter. Also,

The test flights of the Vario XLC has shown good resistance to wind and it is expected that the helicopter will be able to complete test flights in quite strong wind conditions. We have not yet flown the Vario XLC with the wind sensor as slung load. The picture shows the Vario XLC during a test flight.

### **Helicopter for measuring wind**

The project has contributed to a better understanding of the challenges and benefits of using a model helicopter for measuring wind turbine wakes. Although no helicopter has actually flown round a turbine, we can conclude based on the preliminary tests that it is very likely that it is possible to acquire useful wind velocity data using a (fairly large) model helicopter, and that the helicopter is capable of sustained flight with a slung load in the rather turbulent and strong wind conditions found in the vicinity of wind turbines. Since the initial obstacles have to a large degree been overcome in the present project AAU would be able to - in a subsequently project - be airborne and making measurements reasonably quickly.

## **4.5 SkyDoc**

### **Systems design**

The objective is to provide a low cost met mast like system to measure the wind characteristics with vector  $\mathbf{U}$  ( $x,y,z,t$ ) $(u,v,w)$  at different heights  $z$ . Of primary interest is the wind direction and –speed, turbulence, air temperature  $T$  and air barometric pressure  $B$ . In order to be able to measure these parameters at different heights, the intent was to build a system, which could be able to carry the instrumentation, operate at almost all conditions, and that measurements should be insensitive to flow distortion from the carrier. Some feasibility criteria for this carrier emerged:

- Easy access to instrumentation
- Low-cost
- Easy operation of whole system(one-two persons)
- Possibility for long operation periods(hours, days, months)
- Possibilities for adding on light markers and other technologies for controls
- Ability to operate at wind speeds 0-20 m/s(or even higher), temperatures -10.+30 DegC

We did not include lightning issues in this phase (i.e. we simply would avoid this during testing), and with rain as well (i.e. we want to avoid water-proof issues with the instrumentation).

At this stage the literature survey demonstrated a vast amount of research and efforts put in areas for using kites (de Bort and The Franco 1903, Hobbs 1986, Balsley et al 1998) or balloon, or a hybrid (Bamler 1908, Meisner and LeRoy) to accomplish payload or systems requirements. The advantage to use the technology is the high pay load (proportional to balloon volume). The disadvantages are:

- Buoyancy at a loss of gas (Helium)
- High drag at the cost of height  $h/L$
- Dynamic loads with dynamic wind force

The challenges concerned with proper analysis of the technology are:

1. A precise description of the tether line subjected to gravity and wind force in equilibrium and dynamic equilibrium in 2-D or 3-D
2. A precise description of the lifting body in equilibrium and in dynamic equilibrium in 2-D or 3-D
3. A precise description of the interaction of the tether line and the lifting body and unified description in 2-D or 3-D

The mathematical analysis of tethered systems and applications are described in Hoerner 1965, Glauert 1930, Glauert 1934, Bryant, Brown and Sweeting 1942, Landwebber and Proter 1944, Neumark 1963 with different levels of complexity in the analysis approach. The number of articles at the stage of survey was at least 2347. An overview of the different techniques for atmospheric measurements was provided by Balsley et al 1998, and shown here:

In the final design we saw these possibilities consistent with the mentioned systems requirements, where the measurement platform is connected to a lifting device able to keep the payload positioned. The measurement instrumentation was decided to be built into a streamlined canopy looking like a zeppelin or a fish shape. A photo of the complete system is shown in Figure 26. The SkyDoc LTA is a lenticular shaped balloon with a sort of skirt hanging from the leeward side and extending half-way around the perimeter. This device is intended to provide lift over drag capacity, preventing the balloon to be blown down as wind speed increases. The manufacturer provided characteristic for the SkyDoc is shown in Figure 25 and compared to other generic LTA. Within the limits shown, SkyDoc should be stable at 98 m height at 4.5 m/s and stay at this height until wind speeds of 44 m/s.

However, the operators experienced in this project difficulties with this skirt in how to adjust the stability of the LTA when launched in winds above 8-10 m/s.

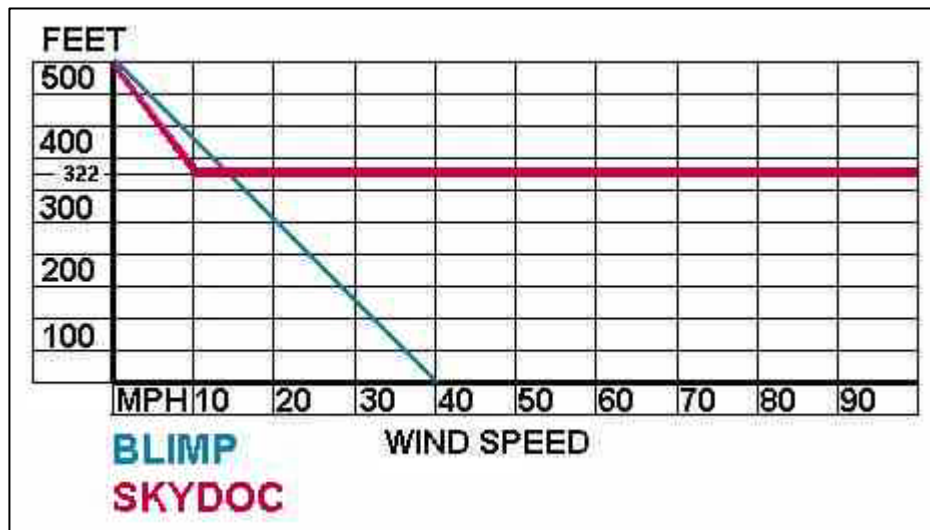


Figure 25: Height performance of SkyDoc and generic LTAs. Source: Floatograph.



Figure 26: Skydoc fotograph with measurement platform during operation.

The tasks to comply were to ensure following issues in the project, and to satisfy technical qualities of the measurement system:

- Description of the dynamics of the measurement platform and the LTA
  - Prediction model with turbulent wind
- Measurement system requirements
  - Satisfactory resolution of the variables(angles <1 deg, speed < 0.1 m/s)
  - Satisfactory uncertainty of variables (approx 0.1-0.3 m/s)
  - High band width with sampling of 50 kHz, with potentially digital low pass filter (chapter 4.6)
  - System for data capture of several GByte (chapter 4.6)

## Modeling

A student project was initiated to deal with the prediction model (Piperas 2010), which follows the work of kites (Hobbs 1986) and the study of a tethered aerodynamic body (DeLaurier 1972) with inclusion of buoyancy and dynamics. The analysis of the system is difficult because of:

- The aerodynamics of the cable is known to first order assumptions (Hoerner 1965, Glauert 1930, Poulin and Larsen 2007, Melbourne 1997, Peters 2000)
- The inclusion of body forces, and surface forces (Glauert 1934, Bryant, Brown and Sweeting 1942, Landwebber and Protter 1944, Neumark 1963) of lenticular shapes are not studied in details/at low speed operation (Demele et al 1961, Keyes 1965)
- The dynamics of warps/cables (MacLennan, Ferro et al) is complex and not studied for winds in ABL.

In parallel a simplified model was made to show the basic characteristics of a lenticular shaped balloon (more elliptic than circular in both dimensions). The basic model is shown in the sketch.

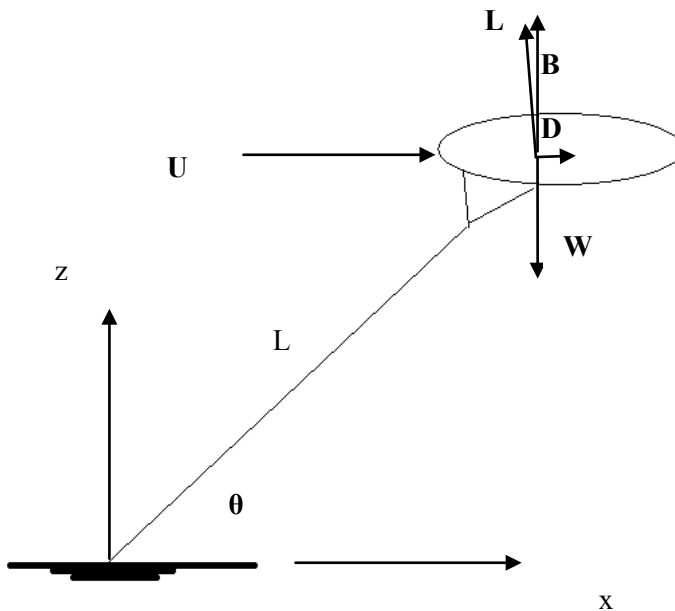


*Figure 27: The factors of influence on the lighter-than-air tethered platform.*

The cable weight and drag is neglected, and lift and drag on the carrier are determined on the basis of a characteristic area  $A$ , dynamic pressure  $q = \frac{1}{2} \rho U_{00}^2$  and a coefficient  $C_L$ , and  $C_D$ , respectively. Buoyancy  $B$  and weight  $W$  are assumed constant, opposite and their centres are assumed to be coincident with the aerodynamic centre. Temperature and pressure are constant with height.

The projections of the force equilibrium in horizontal and in vertical directions allows after some algebra to isolate the angle  $\theta$  as  $\theta = A \tan\left(\frac{C_D}{C_L + \frac{B-W}{qA}}\right)$ . The geometry of

the structural ideal cable is  $h(z)=L \cos\theta$ . The limiting value of  $\theta$  is determined as  $\cos^{-1}(A \tan(C_D/C_L))$ . The balloon is fitted with values from Table 4, air temperature at 15 °C. The aerodynamic coefficients are collected from a wind tunnel study on lenticular shapes (DeLaurier 1972, Piperas 2010) for  $t/2c=0.65$ .

Table 4: Balloon characteristics.

| Variable           | Number  | SI Unit      |
|--------------------|---------|--------------|
| breaking strength  | 450     | kg           |
| tether             | 610     | m            |
| CD                 | 0.8     |              |
| $\epsilon = CL/CD$ | 0.6     |              |
| CL                 | 0.5     |              |
| $dCN/d\alpha$      | 0.03    |              |
| $\emptyset$        | 3.61188 | m            |
| H                  | 2.34696 | m            |
| $t/2c$             | 0.65    |              |
| A                  | 10.25   | $m^{**2}$    |
| V                  | 16      | $m^{**3}$    |
| $\rho_{Air}$       | 1.2     | $kg/m^{**3}$ |
| B/W                | 1.1     |              |
| Weight W           | 10      | kg           |
| g                  | 9.81    | $m/s^{**2}$  |
| Weight W*          | 98.1    | N            |
| Buoyancy B *       | 107.91  | N            |

The variation of tether angle  $\theta$  is shown in Figure 28, and the cable force F is shown in Figure 29.

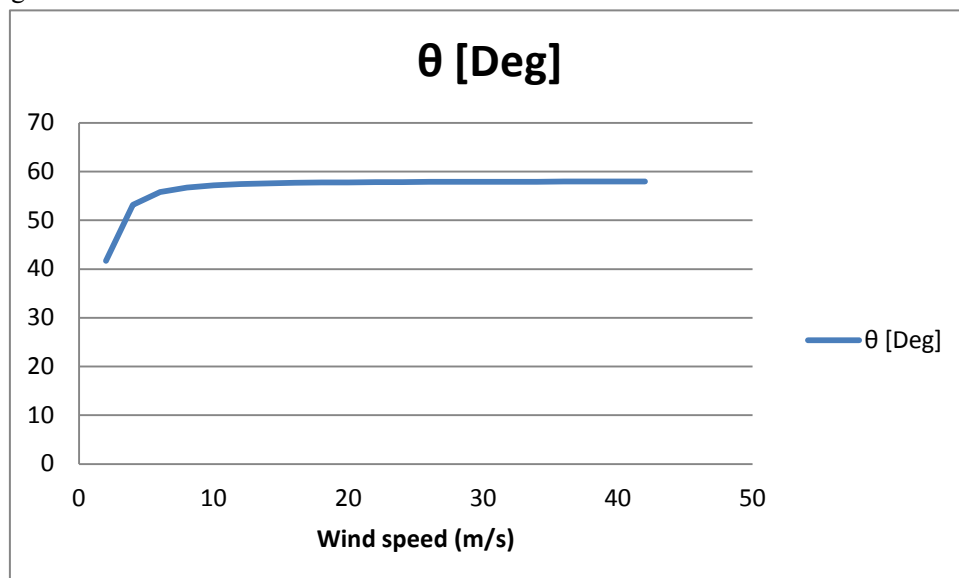


Figure 28: Tether angle of balloon vs wind speed..

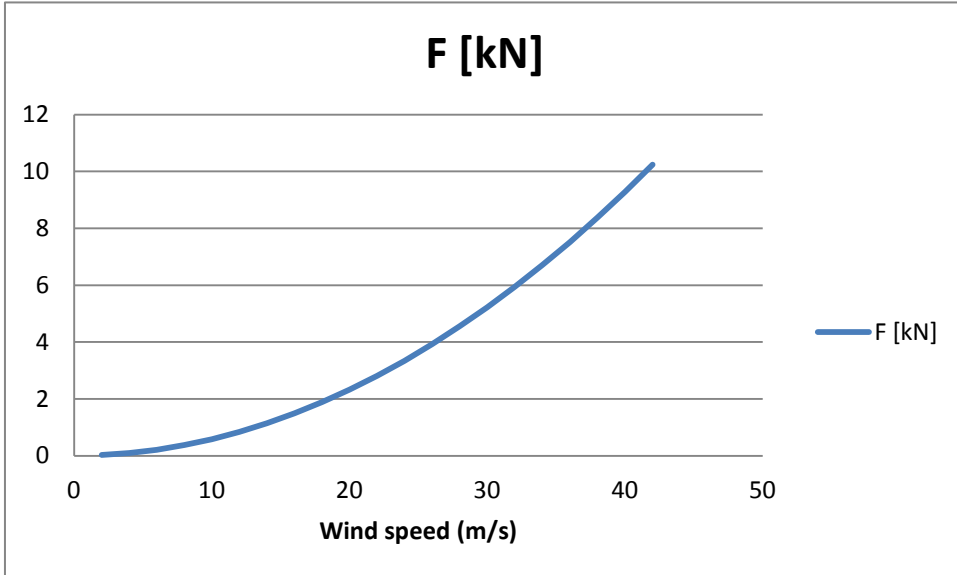


Figure 29: Cable force vs wind speed.

The analysis performed in DeLaurier 1972 shows an identical asymptotic limit value in case of  $B/W=1$ . It is concluded, that ".the response of the balloon LTA has been simulated in MATLAB environment and the static and dynamic cases have been studied. The former assumes that the forces acting on the system are in a constant equilibrium whereas the latter allows the LTA to dynamically change its position in space. A strong correlation was observed between the cable top tension and the fluctuating wind speed for the static case, as well as between the horizontal wind speed and the horizontal displacement for the dynamic case. Furthermore, the measurement of the wind speed was deemed to be possible via the measurement of the cable tension at the tether point". The review of the report showed some undisclosed issued in the physical description of the simulated displacements, and it was concluded not directly to use the results in its present formulation.

### Rigging

The balloon was shipped with rope, and there were made trials of determining the length of the cables from the bridle point to the attachment points of the balloon and the position of the bridle point. The handling of the LTA was not guided by manufacturer's instructions, and trials for flights had to be made by technicians on particular where to place the bridle point and attach the skirt. During flight week experiences the 'tuning' of the bridle point setting did not meet the expectations gained from pre-flight week tests performed at Risø Campus: the SkyDoc LTA showed instability at higher wind speeds which were not experienced prior. The first test flights at Risø Campus showed that the LTA had to be stowed in a hangar or sheltered building during off-flights, and that the man power to operate the LTA was in the order of at least two persons. In high winds as indicated by the predicted cable forces, there is a high force on the cable foundation (200 kg at 20 m/s).

### Platform canopy

The shape is made out of light weight sandwich GRP structure tight together with carbon stringers. In the base an aluminum rod was installed to divide the cable forces into an upper section and a section below the shape. In that way the sonic anemometer was

always behind the lower positioned string, and the inclination was in this way limited. In front of the ‘fish’ is an aero dynamical shaped foam cone, enclosing the Pitot tube.

In Figure 30 the skeleton is shown; Figure 31 shows the position of the main sensory parts. The ballast is also shown in Figure 31 so that the entire platform with a tail fin mounted camera is perfectly in balance with the relatively heavy LIPO battery. Figure 32 shows the position of the pressure board for the Vaisala transducer and the four SensorTechnics transducers; Figure 33 shows the 5-hole pitot integrated in the base of the platform.



Figure 30: Zeppelin shaped canopy of the measurement platform.

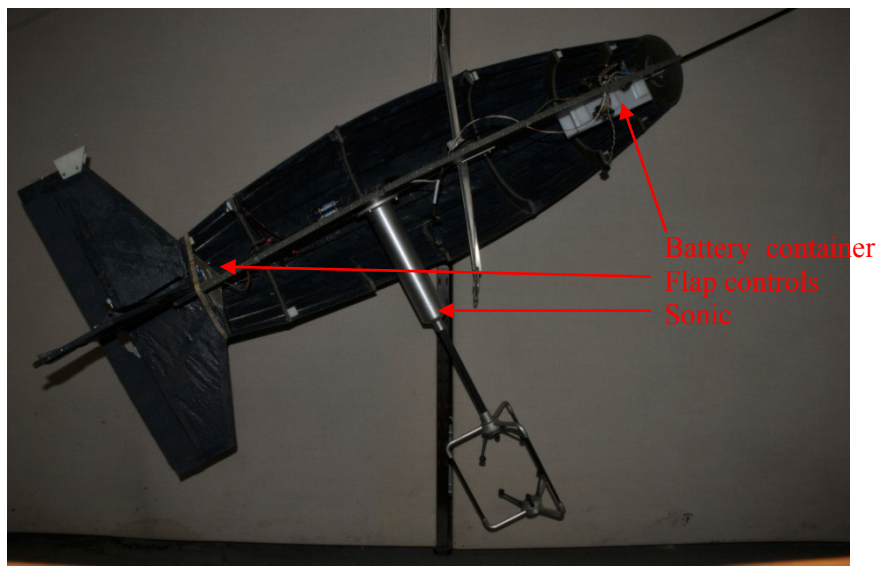


Figure 31: Overall view of interior with sonic, battery container, balancing ballast, pressure transducer board and 5-hole pitot.

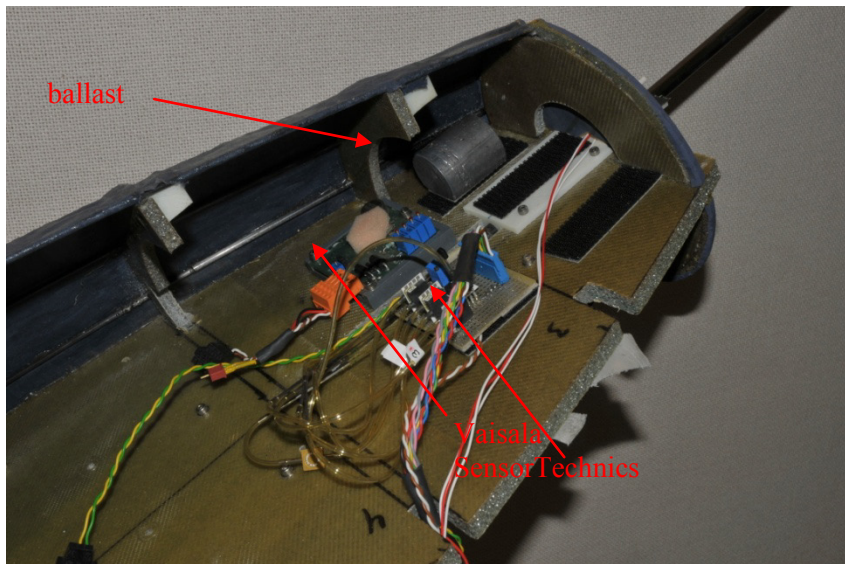


Figure 32: Close up on front part: pressure transducer boards and ballast.

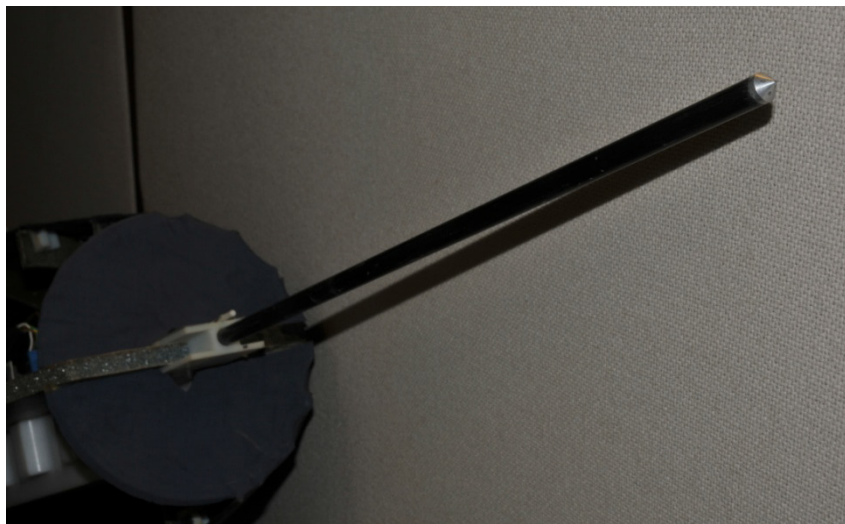


Figure 33: Close up on 5-hole pitot tube with conical head.

### Meteorological instrumentation

The instrumentation consists of a 5-hole pitot tube for measuring the instantaneous wind vector, air temperature and barometric pressure, a 3-D sonic anemometer (Gill) for wind vector measurement and turbulence estimation.

Table 5: Overview of sensors/transducers.

| Name      | Range                    | Manufacture/type             |
|-----------|--------------------------|------------------------------|
| Tair      | -50..120 Deg C           | pt100 system                 |
| Bair      | 600-1200 mBar            | Vaisala                      |
| u,v,w,SoS | +40 m/s, +30 Deg Celsius | Gill                         |
| dP16      | 0...+2.5 hPa             | Sensortechnics HCLA02X5DU    |
| dP23      | -2.5hPa...+2.5hPa        | Sensortechnics HCLA02X5DB    |
| dP45      | -2.5hPa...+2.5 hPa       | Sensortechnics HCLA02X5DB    |
| P6        | 600...1100 mbar          | Sensortechnics HDI0611ARZ8P5 |

Two different sensor heads were manufactured -2 with conical (see Figure 33) and 2 with spherical shapes (see Figure 35) of the sensor head at Risø DTUs workshop. The calibrations of the 5-hole pitot tubes were not carried out. The calibrating facility is shown in Figure 36, and an example of the angle of attack ( $\alpha$ ) and sideslip angle ( $\beta$ ) is shown in Figure 37 as a function of the mechanical preset angle  $\theta$ . The actual range for  $\alpha, \beta$  depend on the actual pitot tube design and is assumed to be less (+-10-12 Deg) than the example.

The rig allows for alignment errors with transverse displacements of +/-0.1 mm at the tip for a pitot tube of 400 mm length.

The ports are connected to pressure transducers as shown to measure (variable in bracket refers to the real measurement, as interpreted with TDMS-see subsequently):

- 1 dynamic pressure  $\Delta p(dP16)$  at the tip for derivation of wind speed
- 2 pressure difference(dP23) providing angle of attack  $\alpha$
- 3 pressure difference(dP45) providing sideslip angle  $\beta$
- 4 static pressure  $p_s(P6)$

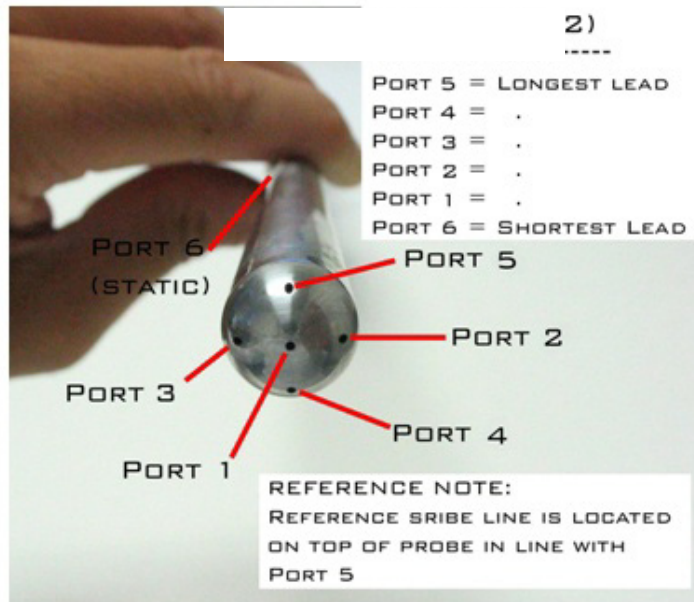


Figure 34: Port identification of the Pitot tube.

$$\text{The wind speed at the tip is calculated as } V_2 = \sqrt{\frac{2 \cdot \Delta p}{\rho}}$$

The air density is calculated from measurements of air barometric pressure and – temperature by using the ideal gas law for dry air.



Figure 35: Five-hole pitot tube with spherical head.

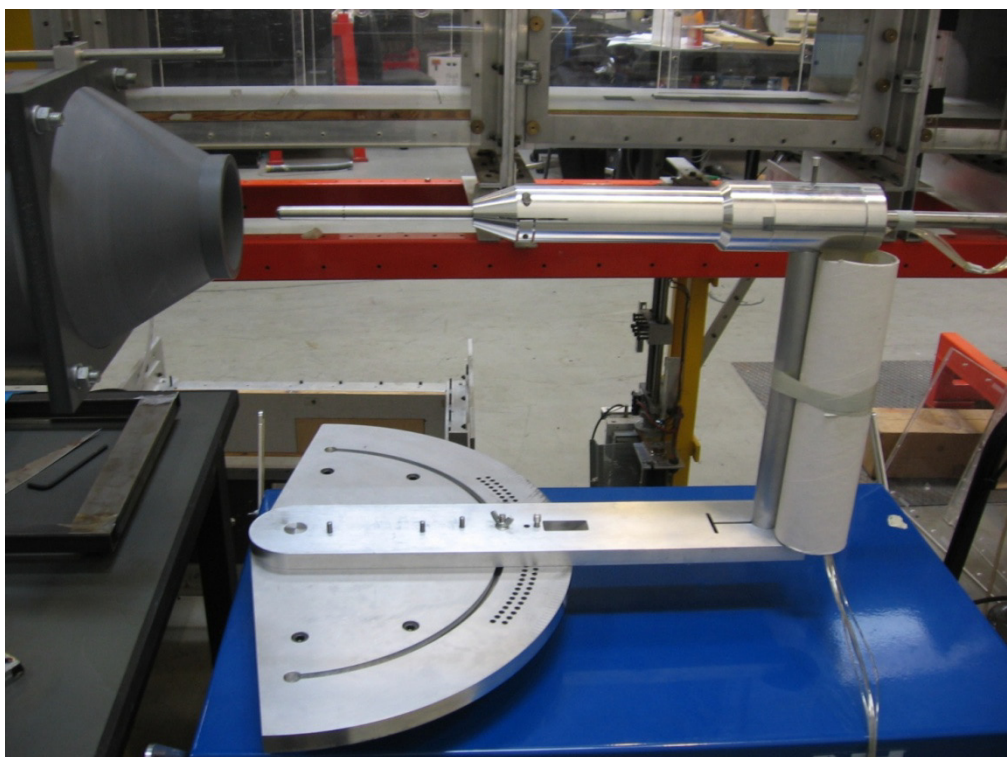


Figure 36: Five-hole pitot calibrating facility. The pitot tube can be turned in plane in line with the vertical and horizontal port holes.

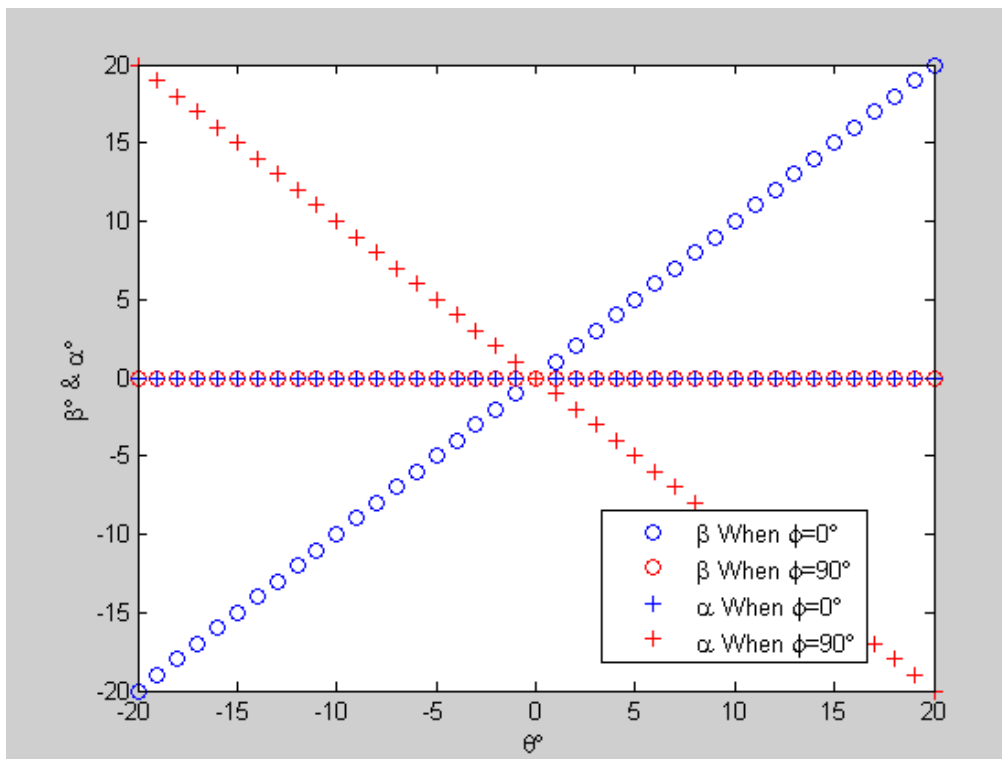


Figure 37: Example of a calibration result.

### Gill:

A photo of the sonic device is shown in Figure 38. The principle of deriving a velocity is shown in Figure 39. Derived signals such as flow angles in horizontal and vertical planes can be carried out. The transducer head is positioned into the wind as shown in Figure 31, with the least exposure of disturbances from the sound emitting support arms.



Figure 38: Photo of Gill sonic anemometer. Left: sensor head with 2x 3 microphones/sound emitter. Right: Sensor head and electronic part.

Path wind speed:

Speed of sound:

$$v_d = \frac{d}{2} \left[ \frac{1}{t_1} - \frac{1}{t_2} \right] \quad c^2 = \left[ \frac{d}{2} \left( \frac{1}{t_1} + \frac{1}{t_2} \right) \right]^2 + v_n^2$$

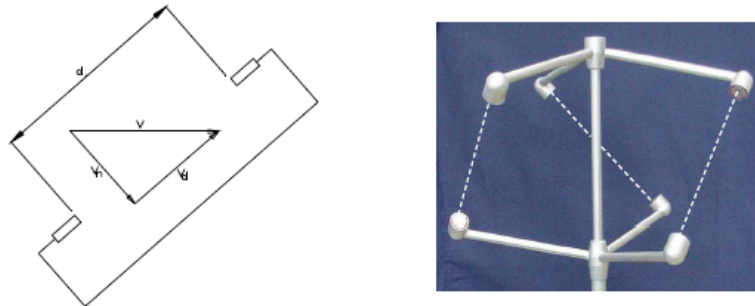


Figure 39: Principle of measurement.

#### 4.6 Nanosynchronised data acquisition

A dedicated measurement system, Aerial Sensor Node, has been developed by DELTA for the measurements to be performed on the airborne sensors in the fish. The measurement system in itself includes several sensors, enabling detailed information on time, position and attitude of the fish.

The measurement system is a further development stage of a nanosynchronised system described for a study of spikes in a wind turbine power plant grid (Christensen et al, 2007). Presently this measurement system in itself includes several sensors, enabling detailed information on time, position and attitude of the fish. A photo of the board with battery package is shown in Figure 40.

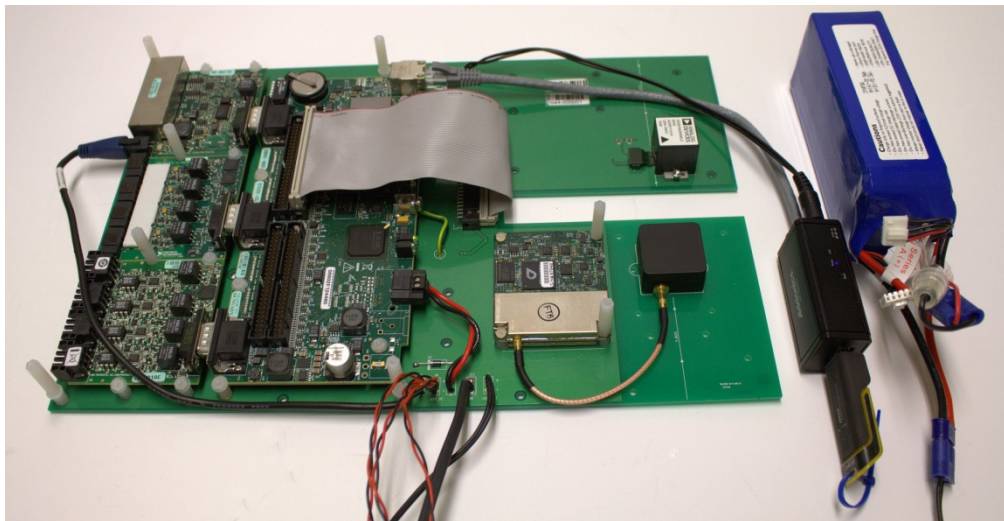


Figure 40: Aerial sensor node with battery package and RAM data storage module. The board portion which is cut away is positioned at the mid part of the fish with the suspension arrangement.

The Aerial Sensor Node is capable of measuring:

- 3D Windspeed, sonic temperature, and speed of sound (sampled 20 times per second) using ultrasonic Doppler shift technology
- 4-channel pitot tube air flow measurements (50k samples/second)
- Temperature and Atmospheric pressure (sampled 2 times per second)
- Differential dual-frequency GPS data sampled at 20 times per second
- Triaxial digital gyroscope (1000 samples/s)
- Triaxial digital accelerometer (1000 samples/s)
- Triaxial digital magnetometer. (1000 samples/s).

An unlimited number of Aerial Sensor Nodes can work together forming a complete distributed measurement system. No provision is made to monitor the operation of the Aerial Sensor Nodes e.g. using WiFi. The measurements are collected in memory sticks, which can subsequently be downloaded to a PC, where the data are time-aligned using the precision time-stamps in the acquired waveforms.

All Aerial Sensor Nodes are equipped with the same sensor modules and use the same measurement SW.

One of the Aerial Sensor Nodes was serving as the Base Station. It was placed on a fixed position and connected to a mast with a Gill Sonic anemometer.



*Figure 41: Picture of the base station, with GPS antenna being on an outrigger. Source: nanosync.wordpress.com*

### Aerial Sensor Node

The Aerial Sensor Node is a compact, battery operated data acquisition system with:

- precision time stamping (100 ns accuracy),
- location determination (<10 cm) and
- A/D conversion (up to 24- bit).

Enabling phase coherent distributed data acquisition using an **unlimited** number of nodes.

## Front End

The system can be configured with a wide range of Commercial-Off-the-Shelf front end modules including

- Low, medium, and high voltage multichannel inputs: isolated or non-isolated.
- Current, Thermocouple, Strain Gauge, RTD,  $\frac{1}{4}$ ,  $\frac{1}{2}$  or full bridge configurations.  
(Changed into general purpose ADC module)
- Microphone or accelerometer (IEPE powered) 50 kS/s 24 bit.
- Analog output
- Digital input/output
- Relay output
- Counter/Timer, Quadrature encoder
- PWM (Pulse Width Modulation Output)
- RS-232\*, 483, CAN bus.

The **Aerial Sensor Node** can be configured with 3 instrumentation modules, each with multiple channels. (Ranging from 4 to 32 channels depending on module type).

**Sensor Types:** the above modules can interface to a broad range of analog and digital sensors, including temperature, strain, pressure, rotation, position acceleration, sound, turbulence (pitot tubes).

## Timing System

**Absolute time precision:** All data acquisition is time stamped with 100 ns global time accuracy. The sampling clock of the A/D and D/A converters are synched to the master clock source (GPS 1 pps).

This means that separate Aerial Sensor Node Systems will be synchronized, independent of the distance between the units.

**Drift Free Timing:** Because all Aerial Sensor Node systems are globally synchronized, their time bases will not drift relative to each other or to absolute time (referenced to atomic clocks driving GPS time).

Typical data acquisition systems with 20 or 50 ppm clocks may drift multiple seconds in a 24 hour day, but this will not occur with the DELTA Aerial Sensor Node.

### Position

The Dual frequency GPS receiver used provides for better than 10 cm location accuracy, sampled up 20 times per second. This is achieved using differential measurements with a stationary reference Ground station receiver, which is just another Aerial Sensor Node.

### Attitude/Inertial data

As a supplement to the GPS data, the on-board Inertial Sensor provides three-axis gyroscope, magnetometer, and accelerometer.

### On board Computing

The on-board computer provides an **FPGA** (Field Programmable Gate Array) for real time signal processing and precision clock distribution synched to the GPS 1 pps clock.

The **FPGA** is programmed to resynchronize and time stamp the data measured to the required sampling times and convert measurements to relevant engineering units.

In addition, a 32-bit real time processor provides for system administration, data logging, and interface to the 64 GByte removable flash memory.

The Aerial Sensor Node is a headless system; it automatically starts the data acquisition, when power is connected.

If no GPS data is available, it will restart, when valid time data becomes available. This typically could happen the first time the Aerial sensor is started in a new location, or if the system has not been in use for some time.

**Data logging:** The measured data as a function of time is streamed to on board solid state disk for subsequent data processing.

Customized FPGA algorithms for the on board FPGA provide for real time data reduction, signal processing and control algorithms.

**Data format:** The measurement data are stored as Waveform Data Type, WDT, including time stamp and meta data, e.g. engineering unit.

(During the measurement campaign data from GPS was stored as NMEA strings and subsequently converted to WDT. In future versions also GPS data will be stored directly as WDT.)

**Storage format:** The storage format is TDMS files.

There is a free plug-in available for importing TDMS files into Excel spread sheets.

The recommended post processing is done using LabVIEW.

A simple TDMS viewer is developed. It can be installed on a PC and does not require LabVIEW to be installed.

### Possible Applications:

- Synchronous data logging using widely separated data acquisition systems.
- Turbulence field mapping using multiple airborne sensors.
- Shock wave/sound source localization using multiple sensors.
- Floating sensor applications for ocean flow/river flow tracking, wave height etc.

### Power supply

- Single 19 to 30 VDC power supply input
- Typ. power consumption, excl. ext. sensors (e.g. Gill anemometer) 10W.
- Battery 22.2 V 5Ah, typical operation time for fully charged batteries, 8 h.

### Mechanical

- Size: 36 x 24 x 4 cm<sup>3</sup>.
- Weight 1150 g, excluding battery, cables, sensors.
- Battery weight 800 g.

The following needs to be improved for future measurement campaigns:

- Better EMC-shielding of the measurement system.
- Automatic updating of Real Time Clock of the Real Time 32 bit microprocessor, from GPS time.
- GPS data to be stored as Waveform Data Type, WDT.

The Aerial Sensor Board was developed using a simple brass shield in order to achieve a light weight construction. The shield was not used due to mechanical complexity of fitting it inside the fish.

EMC issues reduced the sensitivity of the GPS receiver. This was partly remedied during the measurement campaign by moving the GPS antennae away from the Aerials Sensor Board. Subsequent near field EMC analysis revealed radiation in the GPS frequency range from the Real Time 32 bit microprocessor chip. It is unlikely that the brass shield would have solved the problem. The real solution is to provide a shield around the measurement electronics. This will unfortunately add weight and require a rethinking of how to install the Aerial Sensor Node in the Fish.

When connected to the software development system a simple procedure for updating the real time clock from the GPS Coordinated Universal Time, UTC, is available. This needs to be included in an automatic procedure.

### **Storing GPS data as Waveform Data Type, WDT.**

Initially GPS data was stored as NMEA strings, since it provided flexibility to record any GPS data that was needed. Now it is clear which data to use and it is more consequent to store it in the same format as all other measurements, e.g. WDT.

The Aerial Sensor Node improves the quality of state-of-art measurement systems, by resampling the data to a global time source. The use of Dual-Frequency GPS receivers provides 3 digits more of resolution compared to ordinary (single frequency) GPS receivers. When used differentially, with a ground station, resolution in the mm range and accuracy in cm is possible. Having both time and position accurately known enables phase measurement in the whole audio frequency range to be performed. And many other measurements of causality are feasible. Furthermore the 3-D attitude is known with better than 1 degree of accuracy 1000 times per second.

If we just focus on the precise time synchronisation of the Aerial Sensor Node, we call it **Nanosync** due to the 100ns precise time stamping. Nanosynched measurement systems can work together. In the project we had a video camera mounted on the tail of the fish. If each picture frame was properly time stamped, then we would be able to relate the Aerial Sensor Node measurements to the wing position of the wind turbines in view.

The same would be possible, if we had access to housekeeping data of the relevant wind turbines, - provided they were Nanosynched.

## 5 Flight Week(s) and locations

In total, we worked on four different campaigns, of which in the end only one came to work. Our main option was Høvsøre, since it has everything we needed for the campaign – many high-quality measurements up to 176 m, five wind turbines, and nearly no housing or streets in the immediate vicinity which would invoke a safety distance. However, for reasons explained below, this never worked out. The upcoming Risø DTU test station at Østerild in Northern Jutland was ruled out since it would only become instrumented and operational in 2012. Since Risø was not a preferred option due to the vicinity of the main road (one of the most travelled non-motorways in Denmark), we opted for another try to work together with the International Wind Academy Lolland to fly at Nøjsomheds Odde, in north-western Lolland. However, for various reasons only three teams with two flying systems could participate in the trial, so we decided to go for another try at our home base in Risø. There even one additional kite was announced to participate, but it turned out that also here a flight permission was impossible. Some teams resorted to fly in another large campaign (BLLAST) in Lannemezan, France, under the auspices of MeteoFrance, for further instrument development.



Figure 42: Location of Høvsøre test site in Western Jutland.

### 5.1 Høvsøre

When writing the project proposal, the match between the technology of UAS and the test station at Høvsøre was obvious. With 6 high meteorological masts, the site is one of the best instrumented sites in the world. 5 different wind turbines are located there, so wake structures and also differences in wake structures could have been investigated.

The location of Høvsøre test site is shown in Figure 42. The outline of the test site is shown in Figure 43, and a photograph of the test site from west is shown in Figure 44. The sketch shows the location of all test pads, meteorology masts, and 90° measurement

sectors, centred on the direction to the meteorology masts. The distance between the test pads is 300 m and the distance between the meteorology masts and test pads is 245 m.

We envisaged flying along the line of the five smaller met masts (denoted “målemast 1” to 5 in Figure 43, and shown on a line left in Figure 44), to test the methodological differences between line sampling and time sampling, but also to get an impression of the accuracy of the airborne measurement systems.

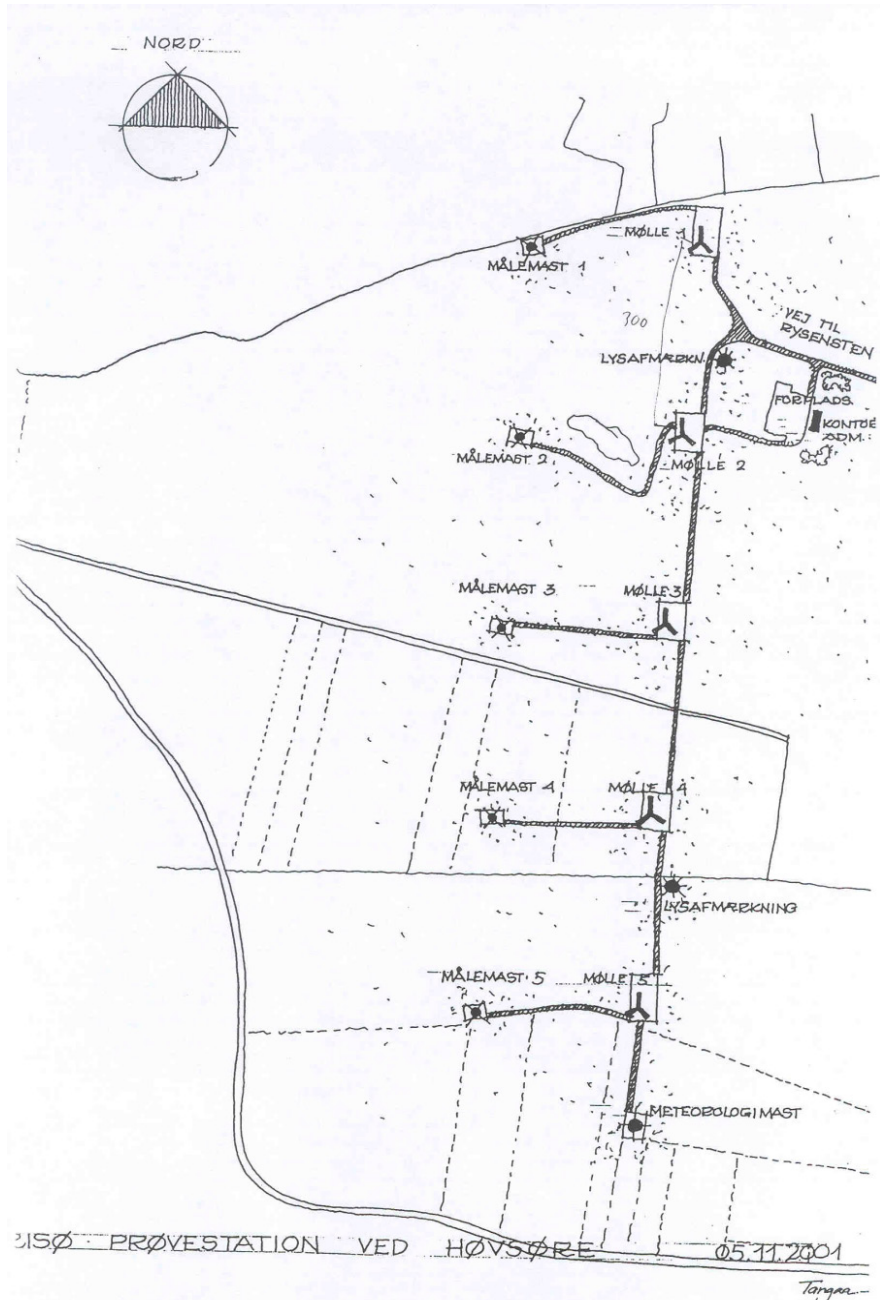


*Figure 43: Sketch of Høvsøre test site, showing the test pads and meteorology masts numbered from one to five from north to south, and with the climatologic mast south of the test pads.*

However, as mentioned later in section 6.1, in order to get a flight permit for an unmanned aerial system from the Danish civil aviation authorities, it is necessary to have

permission from the land owner. Since DTU only owned the land directly around the turbines (essentially the roads and some working areas around the masts and turbines, in black in Figure 43 and the light gravel colour in Figure 44), and the surrounding land is owned by two brothers who were not cooperative due to disputes reaching back to the time of the expropriation of the test station, the overflight permission was not granted under acceptable conditions. This made it necessary to find an alternative solution.



*Figure 44: Photo of Høvsøre test site seen from the meteorology mast.*

## 5.2 3D sonic anemometer helicopter test flight

In preparation for the planned flight week, on September 8<sup>th</sup> 2010 a short test flight was made by Aalborg University at the airfield Aviator in Hesteskøen just east of Aalborg. The flight was with the AAU Bergen Industrial Twin helicopter and a RM Young 81000 ultrasonic anemometer was attached as slung load. An Xsens MTiG INS was fixed to the anemometer to record the attitude during flight. The purpose of the test flight was to 1) demonstrate the feasibility of carrying a relatively heavy anemometer as slung load under a model helicopter for the purpose of recording wind velocity in 3D undisturbed by the helicopter wake, and 2) to use an INS for tracking the sensor attitude (which can vary quite a bit when attached as a slung load) and subsequent corrections of the wind velocity in order to attain the velocity in an Earth fixed frame.

### Test flight setup

The anemometer is attached in a 4 meter long wire directly below the center of gravity of the helicopter. The length of the wire is chosen as a compromise between oscillation frequency, manual flight properties, and the effect of the main rotor downwash (which is negligible at about 3 rotor diameters, i.e. the distance between the rotor of this helicopter and the slung load). The wire is attached to a release mechanism on the helicopter allowing the pilot to perform an immediate release during flight. This can be necessary in situations where the slung load oscillations become too large in amplitude or if the

helicopter has to perform a fast landing due to a critical situation such as low fuel or a faulty sensor. The electrical connection to the anemometer and INS is a separate 6 lead cable connected to the helicopter with an easily detachable connector. The onboard computer records the anemometer output at 32 Hz and the INS output at 50 Hz. The anemometer outputs wind direction (horizontal direction relative to the anemometer) and elevation (elevation from horizontal plane). The INS outputs gyro, accelerometer, and magnetometer measurements. Further, a range of avionic variables (such as helicopter attitude, GPS position, servo motions and so on) was recorded. Some of these were subsequently used to determine the cause of the apparent malfunction during flight. Unfortunately, the INS estimated states were not recorded during flight, but it was easy to do offline computation of these estimates after the flight.

The airfield is an open field next to Limfjorden, and the wind direction that day was from the fjord. The wind was therefore fairly smooth and quite strong. Flight altitude was only around 10 meters, since slung load flights, in particular with a new slung load, is best performed such that if release is necessary, the load will not fall very far. The flight was also performed completely manual, again for safety reasons when flying a slung load for the first time.

### Flight results

The average wind speed during the flight was approximately 12 m/s with wind gust up to 15 m/s. The helicopter took off in a relative safe manner and was able to lift the slung load off the ground and remain stable in a hover position for 80 seconds. During this hover the wind direction was at approximately 45 to 90 degrees relative to the forward direction of the helicopter. This forced the tail rotor of the helicopter to be close to saturation during the entire flight in order to keep the helicopter from turning the nose into the wind. Eventually, after 80 seconds the tail rotor pitch reached saturation and consequently the helicopter started turning into the wind. Since the pilot was not aware of this situation his perception was that the helicopter had lost yaw control and therefore performed an emerging landing during which the helicopter tilted onto the side when impacting the ground with the rotor spinning at full RPM. The helicopter mechanics sustained some damage, but fortunately all electronic components survived, including the onboard computer and thus the flight measurements.

In Figure 45 the raw measurements from the RM Young 81000 during the 80 seconds of flight are shown. Since the wind direction does not change more than 180 degrees in 80 seconds obviously the sensor must have rotated around the vertical axis during flight. This is a common and well-known effect of a single wire slung load. It is also possible to see, although less obvious but still visible in particular during the last 20 seconds, that the sensor is tilting due to wire suspension since the wind elevation is not changing by 60 degrees in a few seconds. This tilting becomes apparent when looking at the frequency spectrum of the anemometer measurements. This can be seen in Figure 46 where the blue graph clearly shows a 1/4 Hz oscillation of the elevation, an effect common to a wind-affect slung load (the oscillation, that is, not the particular frequency).

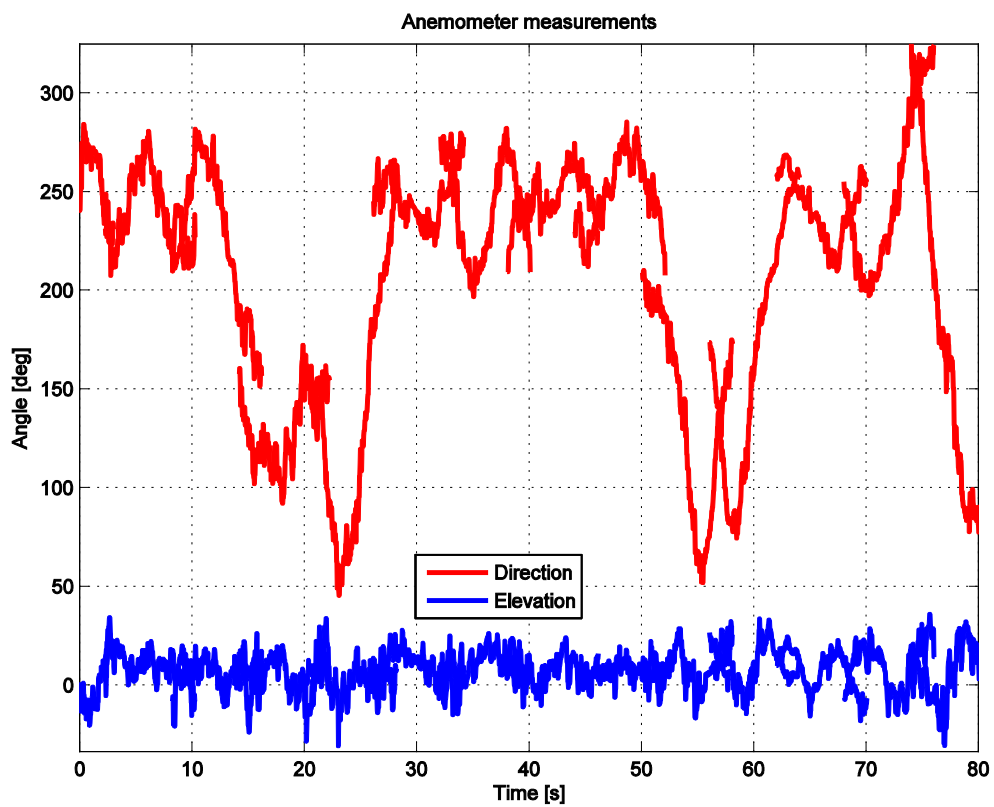


*Figure 45: RM Young 81000 anemometer measurements.*

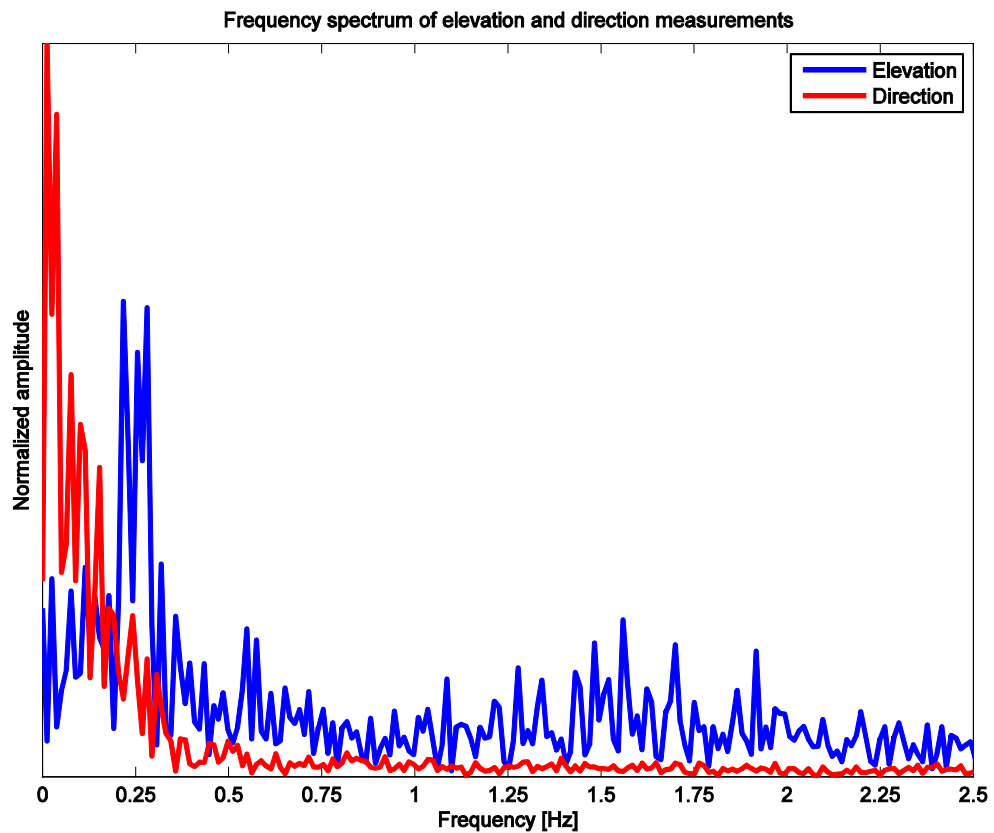


*Figure 46: Frequency spectrum of anemometer measurements. In comparison the direction in red does not show any significant oscillation.*

To determine this motion of the anemometer during flight an INS is fixed to the anemometer and thus the INS attitude estimate is also the estimated attitude of the anemometer. Figure 47 shows the output of the INS which are Euler angles of the anemometer during flight (the angles are in a 3-2-1 configuration). It is obvious that the anemometer is tilting (blue and red graphs) and rotating significantly (black graph). Now the z angle can be used to correct the measured wind direction, and the result is shown in Figure 48. Note that the red line is the estimated true attitude in the Earth fixed frame and therefore this simply is subtracted from the measured wind direction to get the wind direction in the Earth fixed frame (black graph). The elevation can be corrected in a similar fashion (not shown here).

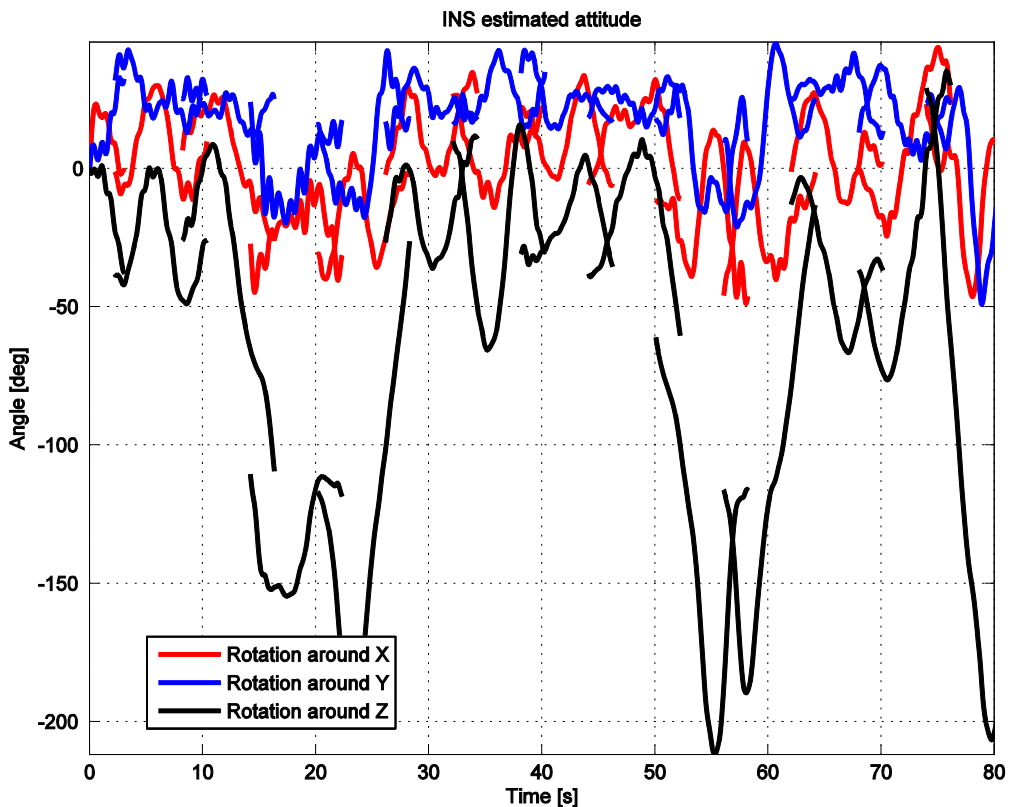
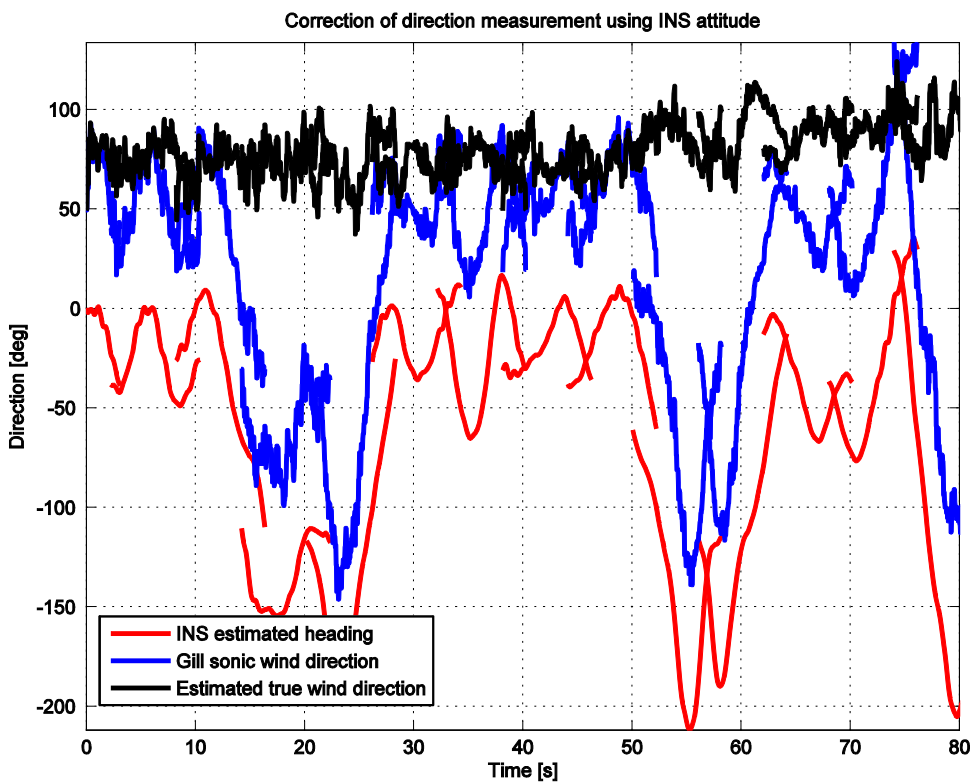


Figure 47: Estimated attitude of INS and anemometer.

## Conclusion

Although the helicopter made an emergency landing and although the reason for this was the strong wind the flight demonstrated that it is feasible to carry a slung load with a helicopter in strong wind conditions. The tail rotor problem can be remedied in a number of ways and is not considered a major issue. The combination on an INS and ultrasonic anemometer seems to be a good approach to accurate 3D wind velocity measurements and is easily attached to the helicopter as a slung load. The weight of this sensor packages is also well within the range for any moderately sized model helicopter. The correction of the measurements is quite easy and can be accomplished online, thus real time wind velocity measurements can be generated and streamed to a ground station and/or used for path generation/corrections during an actual measurement flight.



*Figure 48: Corrected wind direction.*

### 5.3 Nøjsomheds Odde

As an alternative, the test farm used by the International Wind Academy Lolland IWAL was chosen. This was not an ideal situation, since no long-term operating met mast was operating in the wind farm, since the turbines were relatively small and since no university workshop was within the premises. The wind farm is operated and owned by DONG Energy and consists of 21 turbines with a nominal power output of 1 MW (Bonus 1000). The turbines have a hub height of 55 m and a rotor diameter of 52 m. In order to have at least some independent wind measurements, a laser wind profiler or Lidar (a ZephIR from Narural Power) was continuously operated during the campaign at the north eastern corner of the wind farm by Risø DTU. As measurement heights, the lower tip, hub and upper tip of the turbines were taken, plus the levels at 100 and 200 m. During the week, we had to move the Lidar a few metres and up a dyke. As can be seen from the measurements at 98 m (Figure 50), the wind speed during most of the week was quite low. The University of Bergen attended with three new SUMO aircraft, operating the aircraft with a mission pilot operating the computer and a safety pilot also doing start and landing manually. In addition, Risø DTU and DELTA tested a sonic turbulence probe mounted below a LTA (Lighter-than-Air) system from Skydoc. Since wind was envisaged to be a problem during rigging of the Skydoc, a large tent (see Figure 49) was erected as a temporary hangar.

We also got the SCADA data from the wind turbines for the week from the owner, DONG Energy.



*Figure 49: The SkyDoc and hangar. The winch is bolted to a steel frame fitting under the front wheel of the LandCruiser. In the background turbines of the Nøjsomheds Odde wind farm.*

Unfortunately, Aalborg University had damaged the landing gear of their helicopter in a test flight just before the campaign and could not get spare parts in time to participate at the event. Likewise, a few weeks before TU Braunschweig had crashed the only working M<sup>2</sup>AV, and the MASC had not been finished in time, so that flight week only was done with two systems. A later session was envisaged at the time.

Nonetheless, a 5 day measurement campaign was performed in the period May 9 to 13, 2011 at the Nøjsomheds Odde wind farm near Vindeby, on the island of Lolland, Denmark.

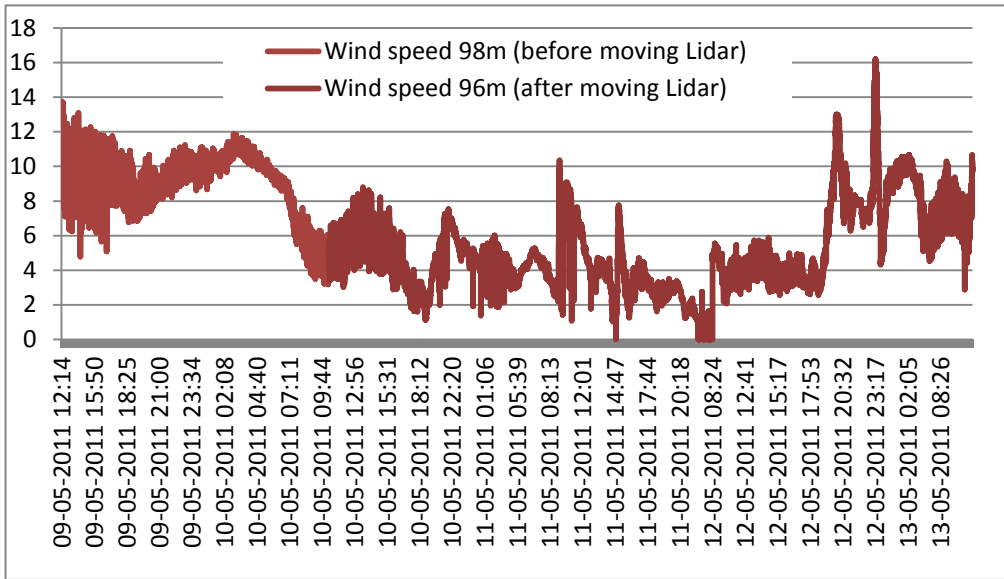


*Figure 50: The wind speed measurements of the ZephIR Lidar during flight week.*

## SUMO

The SUMO system performed a total of 71 flight missions during the campaign, 20 of them carrying the newly adapted 5-hole turbulence probe. The applied flight patterns

were longer horizontal transects of around 1 km in length (e.g. those presented in Figure 51) and race track patterns around groups of turbines, e.g. the three eastern ones. The SUMO results presented in this paper are based on two manuscripts in preparation for publication (Reuder et al., 2012; Reuder and Jonassen, 2012).

## Results

The left panel of Figure 51 shows an example of such a race track pattern. The turbines of the park are denoted as red triangles, the projection of the flight path is given by the white line. Marked in green and red are the straight portions of the flight path selected for the statistical analysis of the turbulence data.

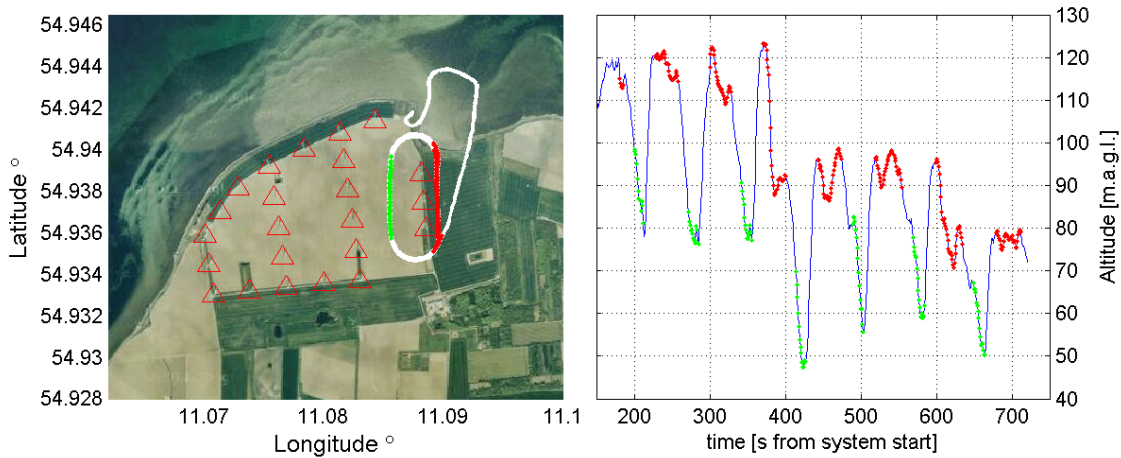


*Figure 51: Race-track pattern flown with the turbulence probe in the Nøjsomhed wind farm (left) on 12.05.2011, 12:09 UTC, and the corresponding time series of the altitude of the SUMO aircraft. The positions of the turbines are indicated with the red triangles. The red and green markers indicate the straight parts of the flight pattern used for further turbulence investigations. The pattern was flown clockwise, the wind coming from SW, i.e. SUMO senses headwind component on the eastern part of the track (red) and tailwind on the western part (green). (Google images © 2011 COWI A/S, DDO, DigitalGlobe, GeoEye, Scankort © Google)*

During the flight, an average wind from SSW was blowing with around 6 m/s. Flying the pattern in clockwise direction this leads to a tailwind component on the western part of the track (green) and headwind on the eastern part (red).

The right panel in Figure 51 shows the corresponding time series of the aircraft's altitude. The straight sections of the flight path are again identified by the color code. The nominal flight levels prescribed to the autopilot were 100 m (150 s-350 s), 75 m (400 s-600 s) and 55 m (> 600 s). In average this value is valid, but during each round on the racetrack the altitude shows an oscillation with an amplitude of around 20 m. The altitude regulation by the autopilot works in this case much better, but far away from optimal, for the headwind conditions, while the aircraft loses altitude nearly continuously in tailwind on the straight westward legs. This unsatisfactory behavior of the SUMO aircraft in keeping the predefined altitude was caused by non-optimal fine tuning of the newly integrated IMU during the flight week. This issue was reworked after the

campaign and the operation of SUMO during a follow-on campaign in June/July 2011 in France showed excellent leveling characteristics, with typical altitude variations below 3 m for arbitrary flight patterns, even in strong wind conditions.

Figure 52 shows exemplary the measured time series of the vertical component of the wind vector with a temporal resolution of 100 Hz. The shaded areas indicate the intervals where the SUMO was flying on the straight legs. The red and green dots and bars indicate the corresponding averages and standard deviations for each leg. The average values of the vertical component in the coordinate system of the aircraft are higher for the headwind legs which can be explained by a change of the average pitch angle of SUMO from headwind (nose up) to tailwind (nose down). A more detailed analysis of the data of this particular flight pattern seems not to be feasible due to the instability of the altitude regulation by the autopilot discussed above.

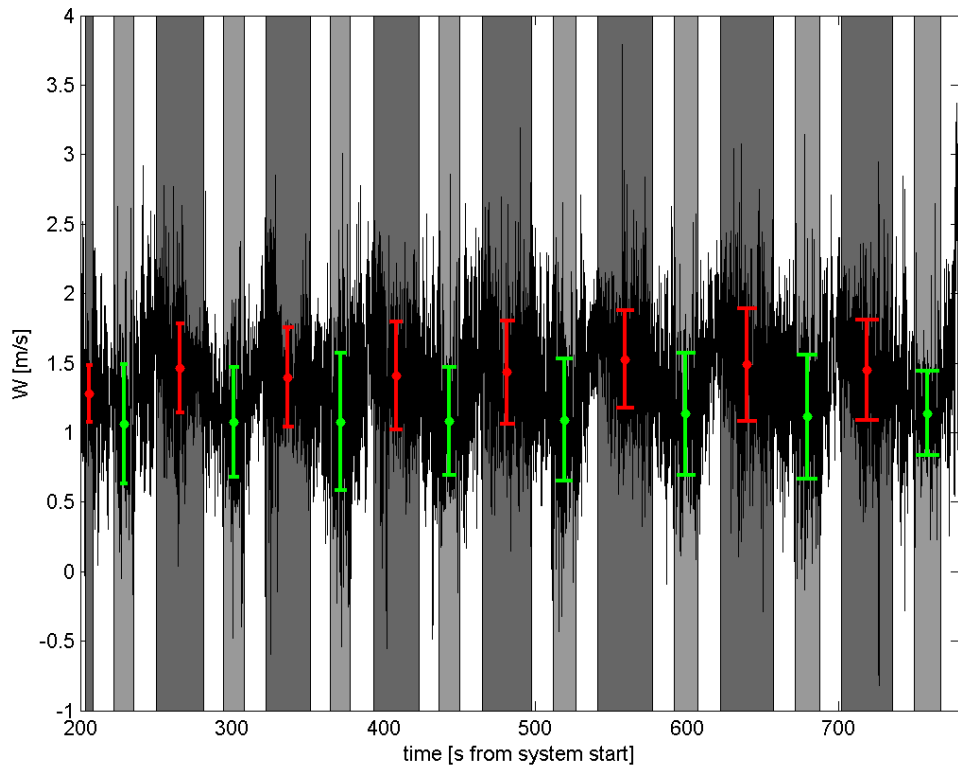


*Figure 52: Time series (100 Hz) of the vertical flow component ( $w$ ) in the aircrafts coordinate system. The grey shaded areas mark the straight parts of the flight legs as also given in Fig. 1. The coloured dots and bars indicate the average and standard deviation for each of those straight legs.*

The following example is based on two flights performed on 12.05.2011 at 13:51 UTC and 14:37 UTC. The flight missions were designed to give an indication on the effect of the wind park on the turbulence structure of the ABL. For this flight with its longer legs terminated by turning circles, the altitude regulation of the autopilot was working much better than in the case described above. The wind at that time was blowing from WSW with wind speeds of around 5 m/s. The projection of the two flights is shown in Figure 53. The western flight path (green), was slightly offshore and parallel to the coastline, and can be considered to represent the undisturbed marine boundary layer. In contrast,

the eastern track (cyan) can be expected to be heavily affected by turbulence induced by the 21 wind turbines. Both missions have been performed at an altitude of 80 m and the straight leg has been repeated 4 times to improve the statistics.

Figure 54 presents the turbulent wind components in the aircraft's coordinate system. The left panels show the data for the undisturbed offshore flow conditions approaching the wind park (green flight path in Fig. 3), the right panels represent the turbulence mainly induced by the presence of the wind turbines. The grey bands in the panels indicate the time intervals where the aircraft was on a stable straight flight path at a certain distance from the turns. Again the standard deviation is expressed by the length of the red bar for each leg. Already the purely visual inspection of the raw data reveals distinct differences in the flow and turbulence structure in front of and behind the wind turbines. All components show a largely increased temporal variability downstream the wind park. The continuous decrease visible in the  $u$  component of the flow vector, in particular visible in the undisturbed case, is a result of the decreasing battery voltage and corresponding loss in motor power with time.



*Figure 53: The flight patterns for two missions on 12.05.2011. During these flights the wind was blowing from WSW with a speed of around 5 m/s. The western flight path (green) thus represents undisturbed offshore inflow conditions, while the eastern path (cyan) is expected to be significantly affected by the wind farm. The red triangles indicate the positions of the wind mills in the park. (Google-bilder © 2011 COWI A/S, DDO, DigitalGlobe, GeoEye, Scankort © Google)*

The results clearly show that the turbulence intensity is increased by around a factor of 3 behind the wind turbines compared to the undisturbed level of the incoming marine boundary layer flow. There is also a clear indication of an increase in the vertical velocity downwind of the park, potentially indicating lifting of part of the incoming air.

These preliminary findings have of course to be validated and endorsed by the evaluation of all the SUMO flights performed during the campaign. These promising results indicate nevertheless the capability of small UAS for turbulence characterization in and around wind farms. A more quantitative evaluation of the turbulence data requires the application of a correction for the movement of the aircraft. As described above this will be a challenge due to synchronization and time resolution issues of the autopilot's data acquisition system.

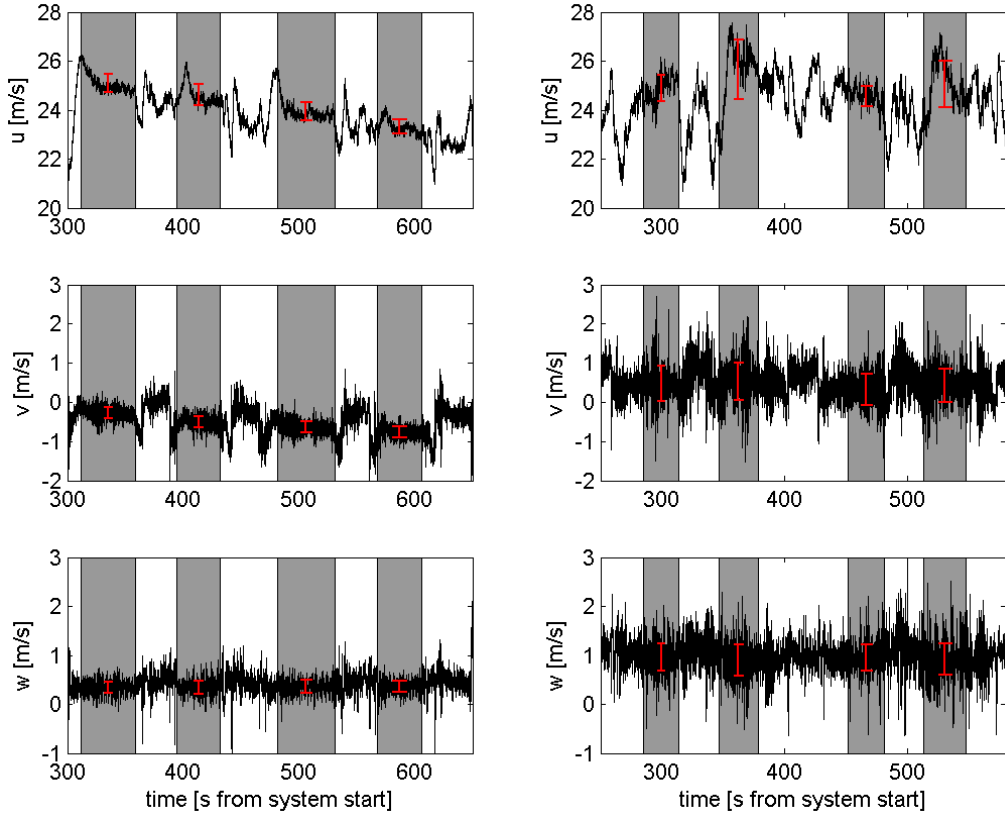


*Figure 54: Turbulent wind components in the aircraft coordinate system (not corrected for aircraft movement and attitude) measured with a frequency of 100 Hz. The left hand side represents the undisturbed, incoming offshore flow (green pattern in Figure 53), the right hand side the boundary layer flow after being affected by the wind farm (blue pattern in Figure 53).*

For a more quantitative evaluation of the turbulence data, the turbulent flow vector in the airframe's coordinate system has been statistically analyzed for the straight legs of the presented flight patterns. For each of the flights, 4 legs at an altitude of around 80 m, corresponding to the uppermost tip height of the rotor blades, are available for the analysis. Desirable measurements at lower levels, e.g. at hub height could not be performed at that time due to safety considerations, i.e., the fact that the tuning of the autopilots control loops was not yet optimized to the newly adapted IMU, leading to distinct variations in flight altitude in the turning circles.

Table 6 summarizes the results from the turbulence measurements. The first 2 columns represent the mean altitude and the orientation of the corresponding straight flight leg, followed by 6 columns with the flow components  $u$ ,  $v$ ,  $w$  (in the aircraft's coordinate

system, not yet transferred to the meteorological reference frame) and the corresponding standard deviations, that represent an estimate of the turbulence intensity.

*Table 6: Basic statistical analysis of the turbulence flights. Note that the wind components are in the coordinate system of the aircraft. (u: along the main axis of the air-craft, v: crosswind component, w: vertical component)*

| avg. alt.<br>[m] | heading<br>[dir] | u<br>[m/s] | v<br>[m/s] | w<br>[m/s] | $\sigma_u$<br>[m/s] | $\sigma_v$<br>[m/s] | $\sigma_w$<br>[m/s] |
|------------------|------------------|------------|------------|------------|---------------------|---------------------|---------------------|
| <b>upwind</b>    |                  |            |            |            | <b>0.35</b>         | <b>0.15</b>         | <b>0.14</b>         |
| 82               | 241              | 25.0       | -0.28      | 0.34       | 0.24                | 0.15                | 0.12                |
| 80               | 62               | 24.5       | -0.52      | 0.35       | 0.42                | 0.17                | 0.17                |
| 79               | 242              | 24.0       | -0.62      | 0.35       | 0.46                | 0.15                | 0.13                |
| 78               | 62               | 23.3       | -0.77      | 0.37       | 0.29                | 0.14                | 0.13                |
| <b>downwind</b>  |                  |            |            |            | <b>1.05</b>         | <b>0.43</b>         | <b>0.31</b>         |
| 80               | 328              | 23.2       | 0.57       | 1.08       | 0.99                | 0.38                | 0.27                |
| 87               | 148              | 24.5       | 0.58       | 1.02       | 1.69                | 0.47                | 0.33                |
| 80               | 328              | 24.7       | 0.49       | 0.98       | 0.85                | 0.40                | 0.25                |
| 85               | 123              | 24.0       | 0.71       | 1.08       | 0.66                | 0.45                | 0.37                |

The mean values of the crosswind (v) and vertical (w) component are slightly but systematically different from zero. This can be explained by different factors, e.g. a slight off-axis mounting of the 5-hole probe, leading to systematic and constant deviations from the neutral values. In case of the v component the values are switching sign, indicating an additional effect of the angle of sideslip of the aircraft in the different wind conditions, with predominant head/tailwind on the western track, and predominant crosswind on the eastern track. For the w component, the pitch angle trimming of the aircraft, e.g. influenced by the exact positioning of the battery, could be another factor explaining small deviations between the two flights. The observed difference here seems however to be too large to be explained by this factor alone, therefore leading to the assumption of a systematic difference in the mean vertical velocity measured during the two flight tracks.

It is obvious that the standard deviation of the u component is distinctly higher than for both of the other components v and w. A look at the rather similar values for v and w, at least for the undisturbed conditions, indicates that the turbulence structure is close to isotropy. We therefore assume that the observed increase in standard deviation by a factor of 2-2.5 in the u component is caused by an instrumental effect due to the high velocity of around 25 m/s in this direction, compared to the values in v and w that are more than one order of magnitude smaller. This issue requires without doubt further attention and investigation, but can in our opinion not be addressed satisfactory until attitude corrected data sets are available after the corresponding technical modifications in the overall data logging system of SUMO.

The results clearly show that the turbulence intensity is increased by around a factor of 3 behind the wind turbines compared to the undisturbed level of the incoming marine boundary layer flow. There is also a clear indication of an increased vertical velocity behind the wind turbine, potentially indicating lifting of part of the incoming air above the wind park. These preliminary findings have of course to be validated and endorsed by the evaluation of all the SUMO flights performed during the campaign. These

promising results indicate nevertheless the capability of small UAS for turbulence characterization in and around wind farms.

One reason for the increased standard deviation in all 3 flow components is for sure the increased turbulence intensity behind the wind park. A part of the observed difference could also be caused by a general difference in the flight behaviour of the SUMO aircraft under varying conditions. The upstream measurements are done in a flight pattern nearly parallel to the mean wind direction, therefore operating SUMO either with head or tailwind, while the flight path behind the turbines is characterized by a large crosswind component. As it is not fully clear how this has affected SUMOs flight characteristics, the data presented here should be interpreted with care. Uncertainties of this kind will hopefully be removed in the future, as soon as the new data acquisition system allowing for the accurate correction of aircraft movement, currently under development, will be available.

## **Summary and Conclusions**

The application of SUMO during a 5 day campaign in and around Nøjsomheds Odde wind farm in Denmark has clearly shown the capability of the system for measurements of atmospheric flow and turbulence in the vicinity of wind turbines. The preliminary results indicate a distinct increase in the turbulence intensity downstream together with evidence of enhanced mean vertical velocity. The main pitfall in atmospheric turbulence determination was the lack of a common data acquisition system for the turbulent flow vector impinging the aircraft and the attitude of the airframe. Therefore a more detailed investigation has to be postponed. The synchronization of the data acquisition of the 5-hole turbulence probe and the Paparazzi autopilot system is currently ongoing. From the beginning of 2012 both data streams will be commonly collected and stored on-board using the same temporal resolution of 100 Hz.

One reason for the increased standard deviation in all 3 flow components is for sure the increased turbulence intensity behind the wind park. However part of the observed difference could also be addressed to general differences in the flight behaviour of the SUMO aircraft under varying conditions. The upstream measurements have been done in a flight pattern nearly parallel to the mean wind direction, therefore operating SUMO either with head or tailwind, while the flight path behind the turbines is characterized by a large crosswind component. As it is not fully clear how this has affected SUMOs flight characteristics, the data presented here should be interpreted with care. Uncertainties of this kind will hopefully be removed in the future, as soon as the new data acquisition system allowing for the accurate correction of aircraft movement, currently under development, will be available.

## **LTA**

First, the LTA was transported from the hangar to the launch spot approximately 50 m left from the stating position indicated in Figure 53. The LTA was launched from this position in order not to interfere with the wind turbines. A ground platform was located as mentioned close to the spot.

The test flights showed different kind of difficulties with the nanosynced devices: poor or no satellite signal because of antenna design, and code fault resulted in no altitude information on the GPS position. In Figure 56 the list of variables which are available

with the aerial node is shown together with the time trace of the barometric signal. The height of the platform changes about 3 hPa or about 30 m gain of altitude. The ADIS component performed well as seen in Figure 57.



Figure 55: Picture from the camera mounted on the tail fin of the fish during a flight.

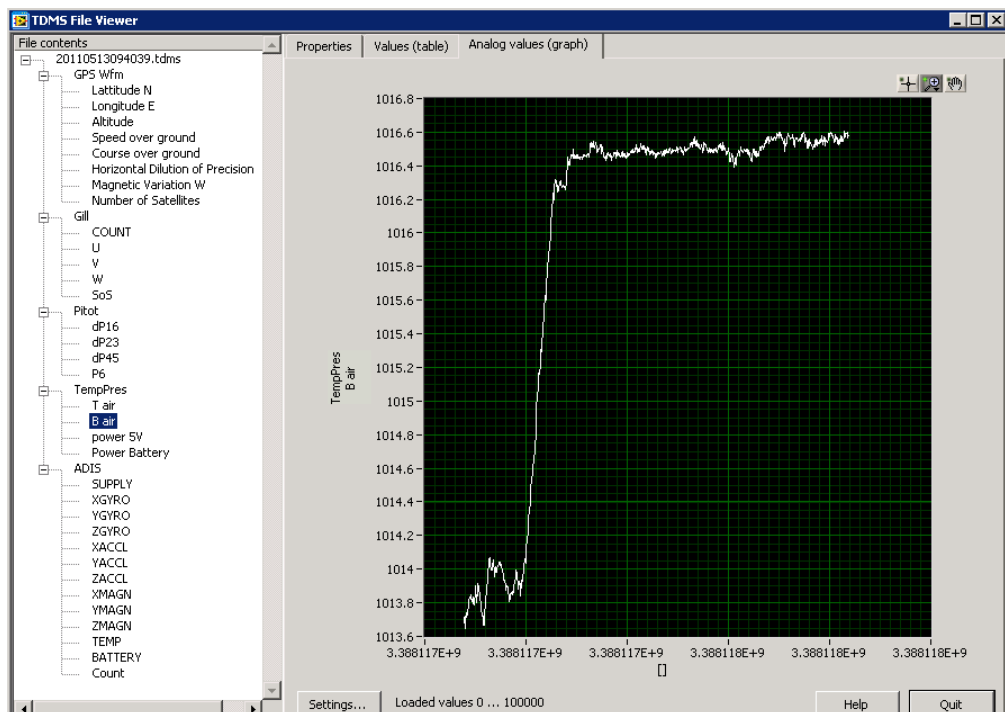


Figure 56: TDMS viewer of aerial node.

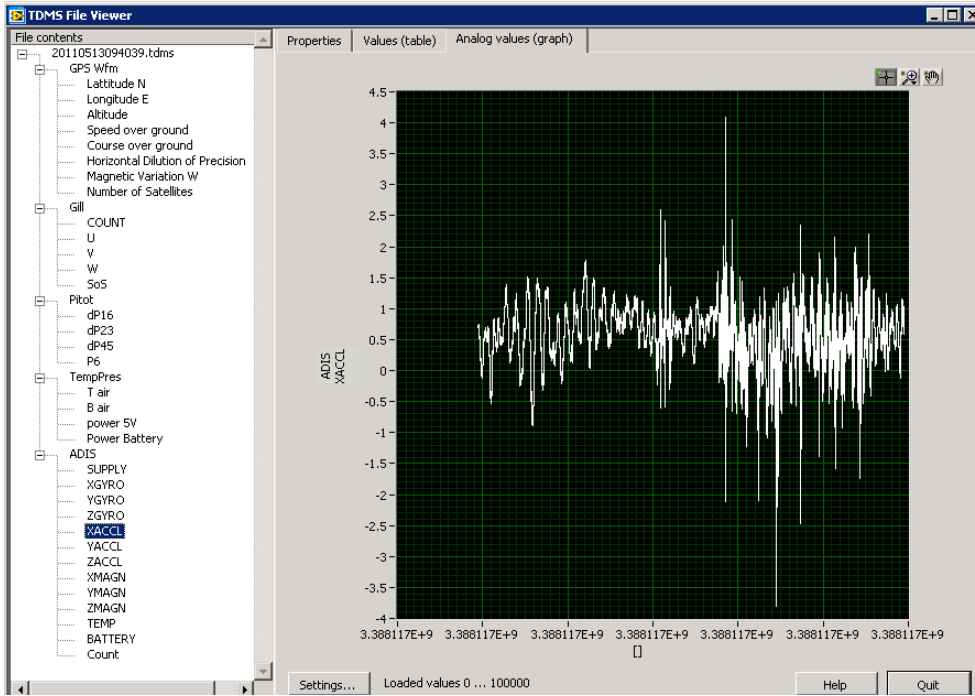


Figure 57: Timetrace of acceleration in platform x-direction.

The ground station node is a copy of the aerial node and positioned at the ground. In Figure 58, the air barometric pressure is shown for comparison. The time is delayed with 5:25 minutes with respect to the aerial node time setting - a consequence of the failing satellite synchronization due to an improperly shielded GPS antenna.

The position and the variables from the ADIS (acceleration terms, Euler angles) are intended to be used in a post processing of the data for the correction of the aerial node in terms of transformations as shown in chapter 3.2. Since it has not been possible to present a fully functioning module, no other post processing analysis tools than the TDMS viewer are available at the moment.

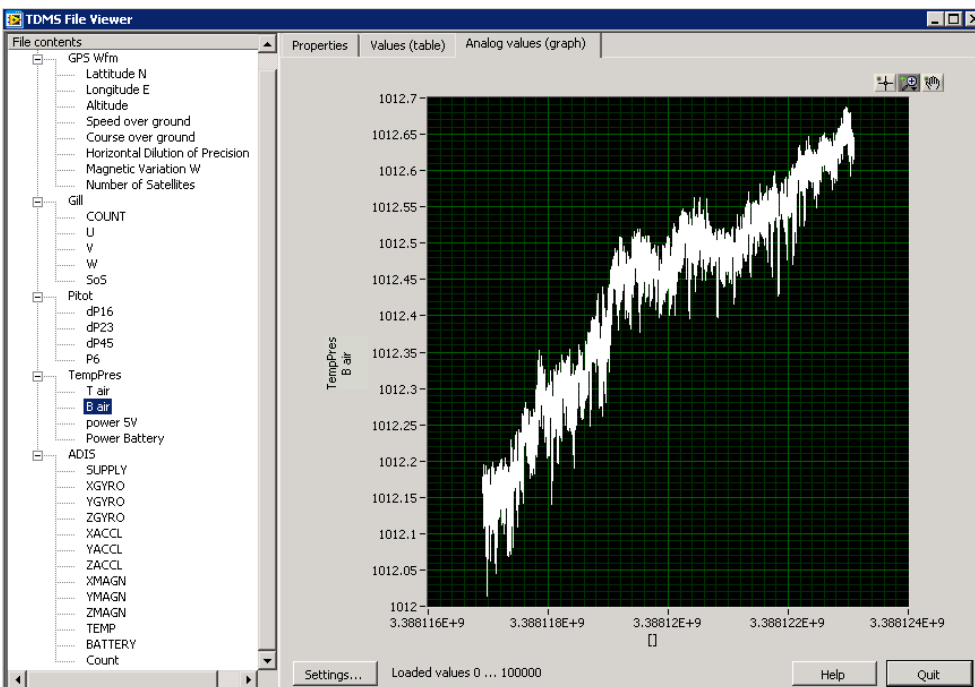


Figure 58: Ground station node air barometric readout.

## **Summary on the LTA scientific progress and results**

The sensing devices (aerial and ground node) are advanced instruments which were not free of prototype faults and need more development in order to function correctly. Due to time delays in finishing the data acquisition system for the flight week, it has not been possible to test the system thoroughly and calibrate the pitot system with the data acquisition system. During the flight week we experienced much of fault finding and troubleshooting, and getting experienced with flying the LTA. We can however conclude that the aerial platform and ground station are very valuable contributions to the topic of characterizing the LABL. The expectations on the systems potential meet the design specifications.

The LTA has the potential to carry the aerial payload over much longer time than powered UAVs. The operation to ground the system was found to be dependent on the wind speed observed. We experienced wind direction shifts as being problematic for safe operation if the equipment was not designed as portable, e.g. foundation (e.g. placed on a car) to be moved away from the wind turbines. The idea to integrate a sensing node as a part of the cable line has introduced an additional variable: dynamic flow separation of the fish. The camera photos have shown that the flow angle increases until stall of the symmetrical profile and a tipping of the fish is started. It stops when the flow again is attached (described under lessons learned). During this cycle the 5-hole pitot system is only applicable in a flow (angle of attack, angle of sideslip) within +/- 10 to +/- 12 Deg; additional rectification of the fish with respect to the angle of the line and horizontal alignment is therefore necessary. Other means, for example to use a feedback loop from the ADIS device, or the autopilot system as in the Paparazzi, could be used to stabilize the fish.

## **5.4 Risø**

After the only partial success at Nøjsomhed, we searched for a second opportunity to convene and testfly the systems against meteorology masts. With the remaining resources it was quite clear that DTU could not support other teams again with a Lidar and the LTA off-campus. For a while, the acquisition of the land at Høvsøre was discussed within DTU (not only connected to this project), but the administrative procedures took far too long to wait for it. In the end, our home base at the DTU Risø Campus was chosen for another flight week (from 15-19 August 2011), since there were turbines, meteorological masts, no interference from the land owner and easy access. In the first instance, we did not choose Risø because the wake is in the prevailing wind conditions east of the small road leading to the turbines (the eastern end of the yellow flight zone indicated in Figure 59). For safety reasons, a distance of 150 m has to be held to the main road 6, which meant that there would be only a 10 m corridor behind the turbines – too little to fly safely.

With a bit of luck, so the reasoning, we would have at least one day with wind from the east, giving us the right conditions to fly in the wakes. In any case it would have been possible to fly along the line of meteorological masts in front of the turbines (more towards the centre of the yellow area). We also had an agreement with Stuttgart University, who had mounted two Lidars on the largest wind turbine looking back from the turbine, in order to use the Lidars in staring mode to scan the flight path.

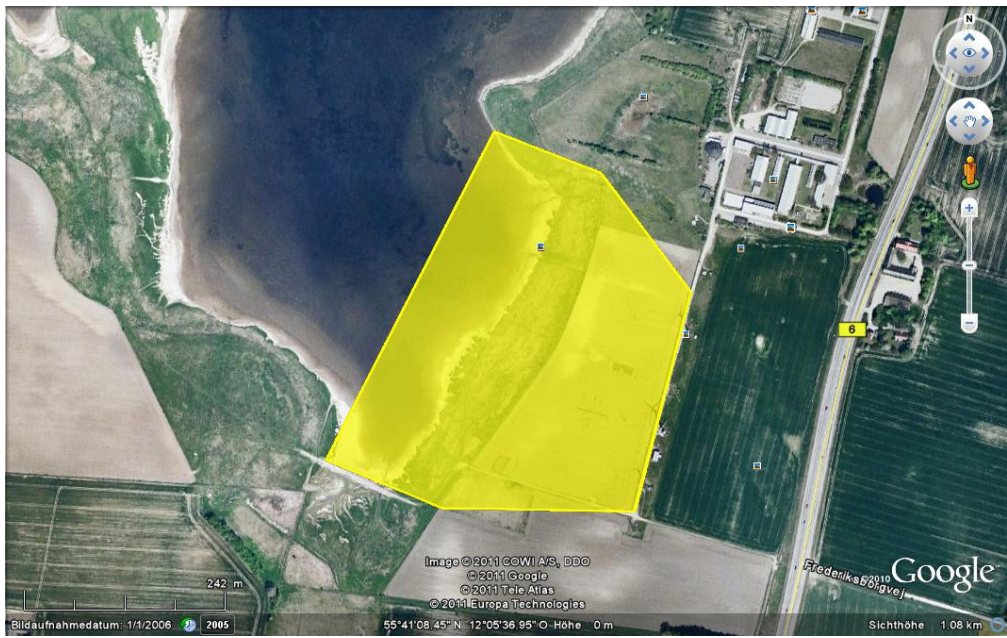


Figure 59: Map of the flight zone requested at Risø. Source: Google Maps.

A hobbyist from the Munich area also had indicated that he wanted to come and fly a kite outfitted with a home-made mounting for a hand-held anemometer, a solution which would have been extremely cheap.

However, the week before the planned flight week the message came from the CAA that they could not dispense from the bird sanctuary in the southern Roskilde Fjord, so we had to again cancel a flight week shortly before it was to happen.

## 5.5 Østerild

A new possibility to measure is the coming test station for very large wind turbines at Østerild. The placement is even windier than the station at Høvsøre. The facility is still being built in 2012, but for future measurement campaigns, it would be a good candidate for trials of the technology. In its final stage, the potential is for 7 turbines of up to 250 m total height, therefore at least one meteorology mast is going to be 250 m. Two of the meteorology masts are already operating, and the first turbines are expected to begin operation this year.

The owner status of Østerild before the expropriations is shown in the image of the environmental study required for the test station. More than half of the area is already owned by a national body, the Danish Nature Agency (*Naturstyrelsen*), which so far has been collaborating with DTU, and is very likely to give overflight rights for a campaign. For preparation and to fulfil the noise limitations, 6 houses were expropriated, but the land stayed with the previous owners.

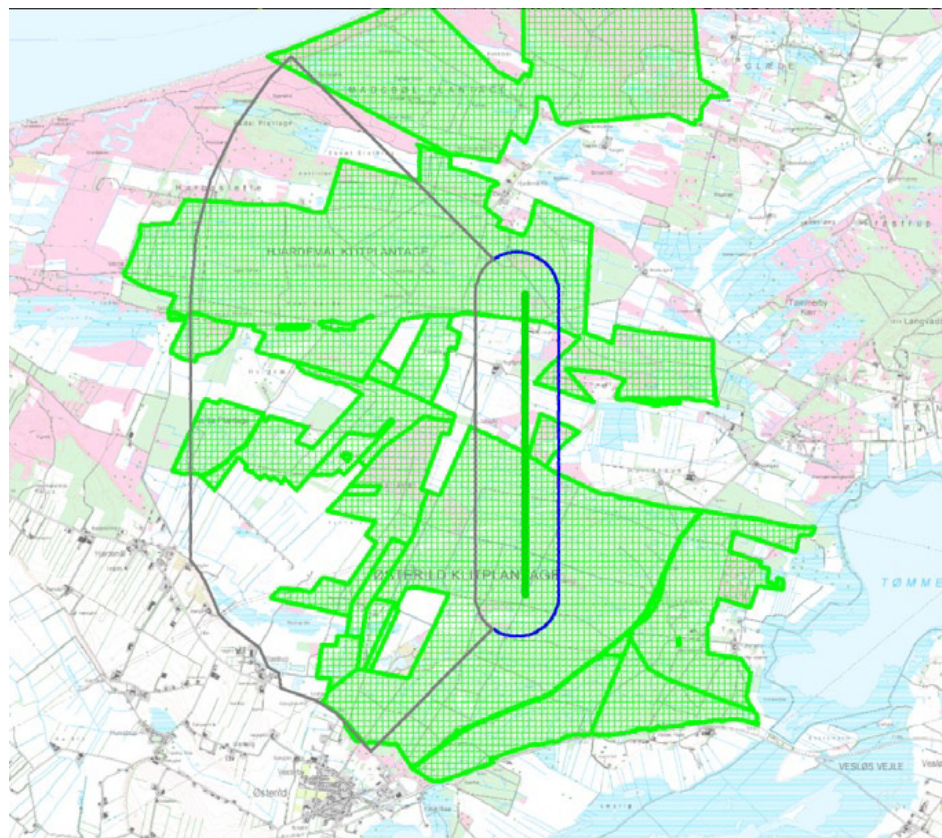


Figure 60: The green land in the vicinity of the Østerild test station is owned by the Danish Nature Agency. Source: Østerild VVM

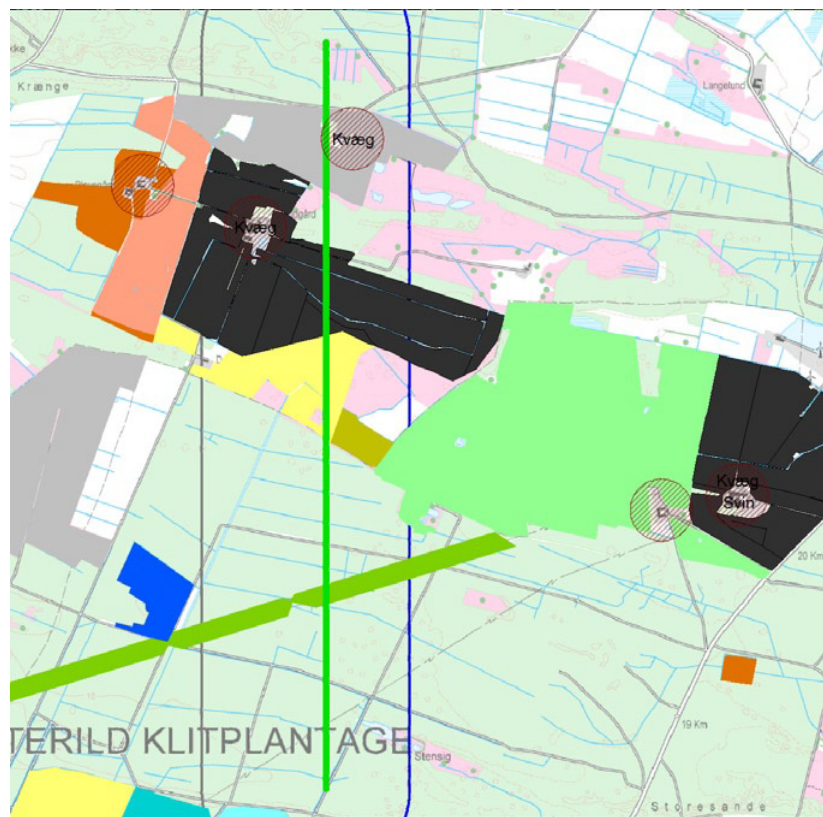


Figure 61: Privately owned land at Østerild. Every owner is denoted in a different colour. Source: Østerild VVM

## 6 Lessons learned

During the course of the project a number of lessons have been learned regarding the use of airborne platforms for wind meteorology. This includes regulatory issues, legal issues, test flights, logistical preparations, coordination with site owners and operators. This chapter reviews the various lessons learned and provide recommendations for future projects and campaigns.

### 6.1 Permits and legal matters

Operation of airborne vehicles is regulated by law in all countries, and it is generally required that operations are safe and occurs in a very controlled manner. For most countries (the regulations are quite varying between nations, in particular for model aircrafts) it is not possible to operate UAS close to wind turbines without some sort of permission from the site owner and/or the national Civil Aviation Agency (CAA). This is certainly the case for Norway, Germany, and Denmark, the nations participating in the present project.

#### 6.1.1 Danish regulation

Since the present project has been carried out solely in Danish territory we briefly review the challenges associated with operating according to the Danish regulation. This description *does not* apply to Norway and Germany.

The general rule in Denmark is that any radio controlled airborne vehicle below 7 kg MTOW can be operated anywhere in Denmark, as long as

1. It is not over protected areas, such as bird sanctuary.
2. It is at least 150 meters from roads and urban areas.
3. It is not over 100 meters altitude over ground.
4. The owner of the land has given permission.
5. The aircraft is within visual line-of-sight (VLOS) at all times.

In addition, if the vehicle is between 7 and 25 kg operations are only allowed from approved airfields (of which there are approximately 70 in Denmark). UAS between 25 and 150 kg cannot legally fly in Denmark. In all cases it is required by law that the pilot is insured, and this is usually done through membership of the Danish modellers union (Modelflyvning Danmark, [www.modelflyvning.dk](http://www.modelflyvning.dk)).

The complete regulation BL 9.4 and associated AICs are available in Danish from the Danish Transport Authority (Transportstyrelsen), and also in an unofficial translation in English at [www.uavlab.org](http://www.uavlab.org) (site maintained by Aalborg University).

#### Permits for the present project

Since some of the above requirements could not be fulfilled in the present project it was necessary to apply for dispensation. This is possible according to §6 in BL 9.4. Generally, dispensation is only given for research purposes, and not for commercial/industrial purposes. It has not been a problem to acquire permits for the present project (except in one case, see below). The three campaign sites 1) Høvsøre, 2) Nøjsomhed, and 3) Risø required individual permits for the individual aircrafts.

The most urgent need for dispensation is for the Vario XLC helicopter since it has a MTOW of 32 kg. Aalborg University has in the beginning of the project acquired a

general permit to operate the helicopter according to BL 9.4 for large model aircrafts (between 7 and 25 kg). On top of this a permit is required to operate the helicopter off-airfield, and therefore permits have been applied for each of the three campaigns planned throughout the project period.

The SUMO aircraft from Bergen and the MAV from Braunschweig/Tübingen only required permission to operate at Høvsøre since the wind turbine are higher than 100 meters, and we needed to fly at least to the upper tip of the turbine blades.

Risø applied successfully a flight permit from the Danish Transport Authority within the regulation BL9-4 stk.6 and BL7-9 stk 5.1.b for the LTA, to be operated at Nøjsomhed, Lolland. In the application filed in 3 weeks before launch, the LTA was described as a 16 m<sup>3</sup> Helium filled vessel, fixed to a winch with 300 m special wire, recommended for this use. The LTA can carry up to 10 kg payload, which consists of a measurement platform. The measurement platform is equipped with a 5-hole pitot tube, temperature and barometer transducers, an INS system and a camera. The measurement platform is controllable by means of remote controlled flaps, though this was not implemented for the campaign in Nøjsomhed. A LIDAR was put in operation at the site close to the measurement position as a reference for wind speed measurements. No light marking of the LTA was applied for in the application.

The permit was given on the basis to launch the LTA from an exact coordinate (54° 56' 14" N 011° 04' 47" E.), and to operate it within a time period (9-13 June 2011, both days included), and to perform elevations over the terrain up to 200 m. The permission was given on the following conditions:

- The helium filled white coloured LTA is identified with an easy identifiable, red band painted around the periphery of the balloon.
- The maximum operational height above ground is 200m.
- The balloon is to be operated within the permitted timeslots between sunrise to sunset.
- During the flight duration, the Danish Transport Authority broadcasted a 'NOTAM' for air-travellers over the flight corridor.

The Høvsøre permit were not applied, because the landowners very early in the project opposed using the land 'below' the aerial flight zone, which were the surrounding land we should operate on.

The Østerild permit is highly affected of the interplay between state, landowners and manufacturers. The project is presently in its initial phases, for site layout and regulations. The regulations are a mix of laws affecting nature and wild life conservation and –maintenance in the surroundings of the turbines, testing of 7 large wind turbines up to 250 m tip heights and a separation distance of 400m. There are currently ongoing negotiations with the landowners, with land up to the vicinity of the turbines. Practically this means a useful small corridor of approximately  $400\text{m} \times 7 = 2800$  m long with a height of 250m. Again launching and operating the LTA practically within this narrow space would be of no practical interest.

For all three campaigns permission from the land owner was necessary to operate the aircrafts and permission from the wind turbine owner/operator is required for flying close to the turbines.

For the third campaign additional dispensation was required since the area close to Risø and thus the wind turbine is a bird sanctuary according to BL 7-16 (on “Naturfølsomme områder”, areas of special interest to nature protection).

A table of all necessary permits and which ones were granted is shown below. The last column shows the not-yet-ready test site at Østerild, and the expected granted permits based on experience with the dispensation process during this project.

| Dispensation for/from     | Høvsøre                           | Nøjsomhed            | Risø               | Østerild   |
|---------------------------|-----------------------------------|----------------------|--------------------|--|
| <b>Vario XLC</b>          | Granted<br>CAA                    | Granted<br>CAA       | Not granted<br>CAA | Would be granted                                     |
| <b>SUMO/MAV</b>           | Not applied<br>CAA                | Not necessary<br>CAA | Not applied<br>CAA | Would be granted                                     |
| <b>LTA</b>                | Granted<br>CAA                    | Granted<br>CAA       | Not granted<br>CAA | Would be granted within 250 m.a.g.l.                 |
| <b>Land owner</b>         | Not granted<br>Farmers            | Granted<br>DONG      | Granted<br>BygSt   | May be granted<br>Farmers,<br>Naturstyrelsen,<br>DTU |
| <b>Wind turbine owner</b> | Not applied<br>Vestas,<br>Siemens | Granted<br>DONG      | Granted<br>DTU     | Would be granted<br>Siemens, Vestas                  |

The reasons for the permits not granted are as follows:

**Vario XLC at Risø:** As stated above the flight zone at Risø is regulated as protected area according to BL 7-16, and the CAA was not willing to dispense from this. An official rejection was issued for the helicopter, and after contacting the CAA for an explanation it became clear that they were not willing to dispense for the somewhat smaller electrical airplanes either. Consequently, no application for dispensation was sent for those aircrafts.

**Land owner at Høvsøre:** As mentioned in section 5.1, since the owners of the land were expropriated to make way for the national test station at Høvsøre, they were not very

cooperative and were not giving overflight rights under reasonable terms. Therefore, flying was not possible at Høvsøre.

### **Dispensation for Vario XLC**

The dispensations given for the Vario XLC are more complex than for the electrical aircraft given the size of the helicopter. Besides BL 9-4 the operations of the helicopter further required that observation posts are stationed at the borders of the flight zone looking for people entering the flight zone. Also, any roads leading into the zone must be surveyed continuously during flight. Further, a member of the flight crew must at all times have a cell phone turned on and the phone number must be submitted to the CAA prior to flight, thus enabling the CAA to immediately contact the flight crew during operations. The dispensation for the Vario XLC at off-airfield sites is typically limited to a few weeks or months.

### **Dispensation for above 100 meters**

For the Høvsøre site permission was given to operate the helicopter above 100 meters (up to 206 meters). This further required that a NOTAM was issued and therefore some days prior to flight operations Airbase Karup was to be notified. Had a dispensation been given to the electrical aircrafts the same requirement would most likely have been included in the dispensation.

## **6.2 Practical considerations for future use**

A range of practical issues have arisen during the project, and this section reviews and comments on these issues. In the least, it tries to raise the questions future users should answer for themselves.

### **Selection of campaign sites**

For our project, the criteria for site selection were easy access, working wind turbines on site, meteorological masts on site (to avoid having to set up a Lidar, and to get a comparison with a bankable technology), sufficient safety distance to roads and buildings, ideally workshops and power in the vicinity or on site, and land and turbine owners willing to cooperate.

### **Campaign planning and logistics**

The level of planning and logistics depends on the site employed. If it is accessible by car, or even better on site with full access to workshops etc., then more can be left to be decided on site. If the transport involves helicopter access, e.g. to an offshore transformer platform, the logistics should be well planned in advance. In any case, it pays off to learn from technicians or other researchers experienced in field measurements.

As for the scientific planning of the campaign, some can be left to be decided according to weather conditions, while some parts of the program should be thought through beforehand.

### **Application for permits**

The practical considerations concerned with LTA flight permits are described in chapter 4.1 and the experience shows the difficulties in the track of permits given (in terms of parties involved). In general following overview can assist in this permit process:

| Vessel       | Permit  |          |       | Constraints   |   |                    |  |
|--------------|---------|----------|-------|---|---|--------------------|--|
|              | Granted | Location | NOTAM | BL Rules  | Landowner                               | Other authorities* | Light marking                            |
| type         |         |          |       |   |   |                    |  |
| Helicopter   | x       | x        |       |   |   |                    |  |
| UAV/<br>SUMO | x       | x        |       |   | x                                       |                    |  |
| LTA          | x       | x        | x     | 1. Deviations of LTA wrt rules in BL 9.4 and BL 7.9<br>2. Flight height below max height<br>3. Duration and period<br>4. Daylight operation | x<br>(comply with dimensions of hangar) | x                  | x<br>(0-24 hour operation, height >200m) |

\* Departments under Danish Nature Ministry (forestry, hunting, countryside, nature)

From experience we strongly recommend to secure permits before booking housing.

### Limits and potentials for flight patterns

What type of flight pattern, altitude, velocity, wind conditions, etc. is possible with the individual platforms. What sensors can be flown and which ones are expected to produce useful outputs?

There were many ideas for flight patterns in the beginning of the project (see also section 3.5). However, realistically for the fixed wing aircraft only straight tracks are of measurement value. This limits the usability of the planes somewhat, but it is not too much of an issue. It also means that the planes should be kept level during the measurement. With the half meter resolution, the planes are able to resolve individual wakes, at least in principle.

For the LTA, the flights are limited by changes in wind direction, and in ranges of recommended wind speeds to operate the balloon under. Under this clause the strength of the wire and the winch to resist wind forces are of importance for operating the LTA safely and controllable. A calculation of a lenticular shaped balloon has shown that the tether angle varies as in Figure 28, and the cable force as in Figure 29. Those results were cast in doubt by the actual flights, which exhibited much more movement than previously calculated, maybe due to the measurement zeppelin. At 20 m/s wind speed the winch system has to resist with a force equivalent more than 237 kg. The lessons showed that the electrical winch was not capable to keep positioning of the measurement platform and in case of wind gusts to prevent the base of the winch from being lifted. Due to these wind direction changes the winch should be mounted on a platform (pick-up or similar) which can be moved according to changes of the wind. Furthermore the design of the winch should include a electrical motor with sufficient power (from a portable generator) to manage the drive train within a safety factor.

Within the permitted altitudes, a roving of the ABL can be carried out. Technically there are no upper limits for the system, considering a safe design of the winch system. With height there can be strong winds from jets which increase cable loads. In any case, cable load and in built safety factor should not exceed the loads.

### **Safety issues**

What are the safety issues for each aircrafts, as well as for a joint campaign? What are the contingencies? How is safety planned and enforced during operations? Who is responsible for what?

The safety about the winch and cable system is essential for the safe operation of a LTA. As described it should be properly designed for environmental conditions during operations and lies within the responsibility of the owner/designer.

### **Aircraft testing and preparations**

Ideally, all equipment should be tuned and ready to measure before coming to a common operation. In some cases this might not be possible, but spending more than half of the time preparing and building the planes has to be seen as wasted time.

The system is prepared before launching. All safety issues (cables, winch, light markers, colouring, drive train power availability) of the balloon are checked, and the measurement system is calibrated and checked for proper operation. Controls (flap system) and camera is checked on the functionality.

### **Data analysis, on-site and off-site**

Careful time synchronisation is needed for later analysis, e.g. through locking onto the GPS time built into most devices. Some data analysis should be begun on-site, to check whether the systems are measuring properly. Having access to the data analysis also makes it possible to react on observations of interesting phenomena.

### **Campaign operation coordination and responsibility**

How is it coordinated? Is there one person responsible? Can more than one UAS fly simultaneously? In case of a crash, who is responsible for what?

## **6.3 Design of an offshore campaign**

The Horns Rev 1 wind farm is about 5 km long by 4.5 km across, so with the range of the SUMO of about 5 km, not even one transect would be possible. However, the MASC range of 120 km would allow for one complete scan between every row of turbines, probably beginning upwind and then gradually flying back. Operationally, the base of operations should be on the transformer platform, where there is also a helicopter deck available. Starting from the heli deck is not a problem for the platforms employed here, but landing might not be so easy. The SUMO has been set down on the heli deck of a Norwegian ice breaker in the Arctic, but it required very good flying skills. Recovery of the plane by a net would not really be an option, as the instruments in the nose might be damaged, and the EPP material is not very well handling an impact like that. InSitu, a subsidiary of Boeing, has an innovative solution to “landing” a plane in confined space

offshore: they fly the ScanEagle, a UAV of 20 kg, to a purpose built crane and dock it automatically there (see [insitu.com/scaneagle](http://insitu.com/scaneagle)). However, a plane of 20 kg could do considerable damage to the wind turbines, so it is doubtful whether the owner would give the permission to fly.

The transformer platform of Horns Rev 2 is about 20 km from the platform of HR1. This distance would be too far for the SUMO, but might be possible for the MASC or Vario XLC.

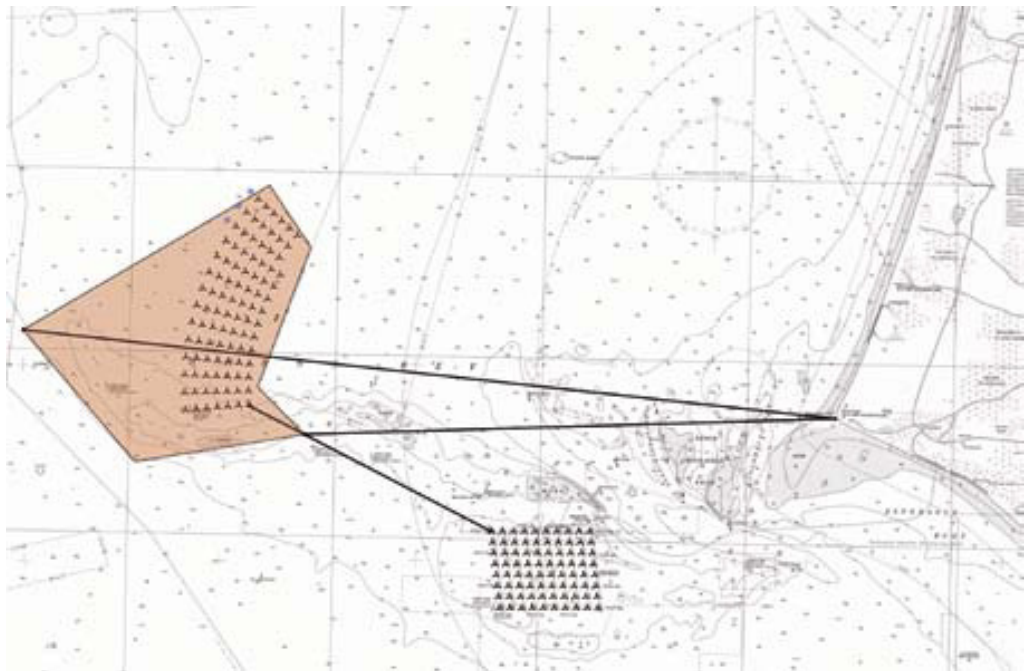


*Figure 62: Map of the wind farms Horns Rev 1 (rectangular, southerly) and 2. Source: [HR2 VVM Report](#), DONG Energy, October 2006*

There are a number of obstacles to the use of UAS in a wind farm like Horns Rev. The owner would have to agree not only to be able to fly there (this permit might be possible to get), one would also have to get access to the transformer platforms. This involves a helicopter set-down with all equipment, which is expensive. The crew performing the flights would probably also have to get an offshore survival course, which also would take some time and would cost. As additional instruments, two radars for rainfall and bird monitoring are installed at the two transformer platforms (the one at HR1 however did not survive the storm in December 2011), which might get additional data on the flights.

Another unknown is the reaction of the CAA to a request like that. Since flying all of Horns Rev would hardly be within visible range (while it might be possible to see the plane, the attitude would be guesswork at best in 5 km distance), so the regulations regarding the safety pilot would have to be relaxed to fly through the whole farm. We tried to get the Danish CAA to speculate about the possibility to get dispensation from the rules in this case, but without a formal request they declined to confirm or deny anything.

## 7 Conclusions

In terms of regulation and permits there are two main lessons learned in this project. The first is that applications for permits should be submitted well in advance, at least 3 months and sometimes even sooner, and the second is that permits are generally granted as long as there is not direct violation of existing law and there is a valid reason for requesting a permit (scientific research qualifies as a valid reason). One reason for submitting permit applications quite some time before the actual flights is that the granting process can take some time, although in our experience the Danish CAA does not take unreasonably long to process an application (typically 2-8 weeks, depending on how close the permit is to previously process permits). Another reason is that some of the requirements in the permit might be difficult and time consuming to fulfill. For instance, if a traffic controller needs to be notified one month prior to the flight, or if permission from land owners needs to be secured. We also learned that permits are temporary and geographically limited, which did not pose a problem in the present project, though, and that permits might be easier to obtain in certain geographical areas, such as remote site like off-shore or when associated with existing flight zones (hobby airfields).

The amount of man-power needed to get an experiment like this going is also not (yet) amenable to automatic operation. Two parts have to be distinguished here: the planes have to be prepped after each flight, and the flight program has to be loaded separately for each flight in a scientific campaign, and there have to be both pilot and safety pilot available (though those two could possibly be combined). While the first is a requirement of the scientific assessment, the latter is a legal requirement and could be a difficulty for repeated operational use. The planes also need some care in handling, which an automated system probably would not supply. It helps to have spare UAS available during a campaign. Therefore we conclude that the systems currently can be support for short-term scientific campaigns, but not replace a long-term resource assessment in an automatic fashion.

The high-resolution RTK GPS (1-2 cm accuracy) is very useful to stabilise the flight, and therefore to make sure the measurements are from the wind and not from the movement of the measurement device. While they are expensive and a bit bulky yet, price and size are going to come down in the near future.

Future R&D should go into longer range UAS, the ability to start and land from a helicopter deck, cheaper and smaller sensors, especially RTK GPS and wind sensors, swarms and staggered flights, and into the regulatory side regarding real autonomous operation including beyond VLOS. For the LTA, a system with a good balance between lift and drag would be very interesting, like a flying wing filled with helium – capable of keeping the payload aloft both without wind and in windy conditions.

Generally, we have developed four different systems with slightly different applications for the investigation of the atmospheric boundary layer in vicinity of wind farms. The technology now needs to be applied for scientific missions.

## 8 Glossary

|                   |   |
|-------------------|---|
| ABL               | Atmospheric Boundary Layer                                    |
| ACONS             | AirCraft OrthoNormal System                                   |
| ADIS              | Analog Devices Inertial System                                |
| BL                | Boundary Layer  |
| BygSt             | Bygningsstyrelsen, the Danish Buildings and Property Agency   |
| CAA               | Civil Aviation Authorities                                    |
| EKUT              | Eberhard Karls Universität Tübingen                           |
| ENAC              | L'Ecole Nationale de l'Aviation Civile, in Toulouse           |
| ETH               | Eidgenössische Technische Hochschule, Zürich                  |
| FHP               | Five-Hole Probe ( <i>also sometimes 5HP</i> )                 |
| FPGA              | Field Programmable Gate Array                                 |
| GCS               | Ground Control Station  |
| GPS               | Global Positioning System                                     |
| IMU               | Inertia Measurement Unit                                      |
| LABL              | Lower Atmospheric Boundary Layer                              |
| M <sup>2</sup> AV | Meteorological Mini Aerial Vehicle                            |
| MASC              | Multi-purpose Autonomous Sensor Carrier                       |
| MONS              | Meteorological OrthoNormal System                             |
| MTOW              | Maximum Take-Off Weight                                       |
| NOTAM             | Notice to Airmen  |
| OBC               | On Board Computer   |
| RTK               | Real Time Kinematics ( <i>a highly accurate type of GPS</i> ) |
| SCADA             | Supervisory Control And Data Acquisition                      |
| SUMO              | Small Unmanned Meteorological Observer                        |
| TDMS              | <i>[the time series format used by DELTA]</i>                 |
| UAS               | Unmanned Aircraft System                                      |
| VLOS              | Visual Line of Sight  |
| WRF               | Weather Research and Forecasting model                        |

## 9 References

- Balsley, B., M. Jensen, and R. Frehlich, The use of state-of-the-art kites for profiling the lower atmosphere, *Boundary-Layer Meteorol.*, 87, 1, 1-25, 1998.
- Bamler,K., Scientific Ballooning And Weather Forecasts, *Mon. Wea. Rev.*, 36, 283–284, 1908.
- Bange, J., Airborne Measurement of Turbulent Energy Exchange Between the Earth Surface and the Atmosphere, Sierke Verlag, 174 pp, ISBN 978-3-86844-221-2, 2009.
- Barth, S., H. Koch, A. Kittel, J. Peinke, J. Burgold, and H. Wurmus, Laser-cantilever anemometer: A new high-resolution sensor for air and liquid flows, *Rev. Sci. Instrum.*, 76, 075110, doi:10.1063/1.1979467, 2005.
- Bisgaard, M., A. la Cour-Harbo, and J. D. Bendtsen, Adaptive Control System for Autonomous Helicopter Slung Load Operations. *Control Engineering Practice*, 18, 7, 07.2010, 800-811, 2010.
- Bisgaard, M., J. D. Bendtsen, and A. la Cour-Harbo, Modeling of Generic Slung Load System. *Journal of Guidance, Control, and Dynamics*, 32, 2, 573-585, 2009.
- BLLAST, Boundary-Layer Late Afternoon and Sunset Turbulence: 2011 Experimental Plans, [http://bllast.sedoo.fr/campaigns/2011/Experimental-plans-document\\_v8.pdf](http://bllast.sedoo.fr/campaigns/2011/Experimental-plans-document_v8.pdf), 2011.
- Boiffier, J.-L., The Dynamics of Flight – the Equations. Wiley, Chichester, UK, 353 pp, 1998.
- de Bort, T., The Franco - Scandinavian Station For Aerial Soundings, *Mon. Wea. Rev.*, 31, 177–178, 1903.
- Brisset, P., A. Drouin, M. Gorraz, P.-S. Huard, and J. Tyler, The Paparazzi solution, [http://www.recherche.enac.fr/paparazzi/papers\\_2006/mav06\\_paparazzi.pdf](http://www.recherche.enac.fr/paparazzi/papers_2006/mav06_paparazzi.pdf), 2006.
- Bryant, L. W., Brown, W S and Sweeting, N E. Collected Researches on the Stability of Kites and Towed Gliders *A.R.C. R & M* 2303, 1942.
- Christensen, L.S. et al. GPS Synchronized high voltage measuring system. Nordic Wind Power Conference, 2007 Symposium held 1-2 November 2007 at Risø DTU
- Christiansen, M.B.: Wind Energy Applications of Synthetic Aperture Radar, *Risø PhD report Risø-PhD-27(EN)*, 2007
- la Cour-Harbo, A., and M. Bisgaard, State-Control Trajectory Generation for Helicopter Slung Load System using Optimal Control. Proceedings of AIAA Guidance, Navigation, and Control 2009. American Institute of Aeronautics & Astronautics, 2009.
- Curry, J. A., J. Maslanik, G. Holland, and J. Pinto, Applications of Aerosondes in the Arctic, *Bull. Amer. Meteor. Soc.*, 85, 12, 1855-1861, 2004.
- DeLaurier, J D. A Stability Analysis of Cable-Body Systems Totally Immersed in a Fluid Stream. Washington D.C. : National Aeronautics and Space Administration, 1972
- Demele, F.A. and Brownson, J.J. Subsonic Longitudinal Aerodynamic Characteristics Of Disks With Elliptic Cross Sections And Thickness-Diameter Ratios From 0.225 To 0.425 National Aeronautics And Space Administration Washington, D. C. April *NASA TN D-788* 25 pp, 1961

Egger, J., S. Bajarachaya, R. Heinrich, P. Kolb, S. Lämmlein, M. Mech, J. Reuder, W. Schäper, P. Shayka, J. Schween, and H. Wendt, Diurnal winds in the Himalayan Kali Gandaki Valley. Part III : Remotely piloted aircraft soundings, *Mon. Wea. Rev.*, 130, 8, 2042-2058, 2002.

Egger, J., L. Blacutt, F. Ghezzi, R. Heinrich, P. Kolb, S. Lämmlein, M. Leeb, S. Meyer, E. Palenque, J. Reuder, W. Schäper, J. Schween, R. Torrez, and F. Zaratti, Diurnal circulation of the Bolivian Altiplano. Part I: Observations, *Mon. Wea. Rev.*, 133, 4, 911-924, 2005.

Ferro, R.S.T. and Hou, E. H.: A Selected Review of Hydrodynamic Force Coefficient Data on Stranded Wires Used in Fishing Gear Marin Lab Aberdeen Electronic version <http://www.scotland.gov.uk/Uploads/Documents/No31.pdf>

Glauert H., The stability of a body towed by a light wire, Aeronautical Research Committee, *R&M No 1312*, pp 28, 1930.

Glauert H. Heavy Flexible Cable for Towing A Heavy Body Below An Aeroplane, Aeronautical Research Committee, *R&M No 1592*, pp 21, 1934.

Guest, P. S., Measuring turbulent heat fluxes over leads using kites, *J. Geophys. Res.*, 112, C05021, doi:10.1029/2006JC003689, 2007.

Gryning, S.-E., E. Batchvarova, B. Brümmer, H. Jørgensen, and S. Larsen, On the extension of the wind profile over homogeneous terrain beyond the surface layer. *Bound.-Layer Meteor.*, 124, 251–268, 2007.

Haering, E. A., Airdata Calibration of a High-Performance Aircraft for Measuring Atmospheric Wind Profiles, *Tech. Mem. 101714*, NASA, 24 pp, 1990.

Heisselmann, H., M. Hölling, M. Wächter, and J. Peinke, Wind velocity measurements using the sphere anemometer, Proceedings of the European Wind Energy Conference, Marseille, 2009.

Hobby, M. J., S. D. Mobbs, and A. M. Blyth, Further development of the Tethersonde instrument, Proceedings of the 18th Symposium on Boundary Layers and Turbulence, 9-13 June 2008, Stockholm, Sweden, [ams.confex.com/ams/pdffiles/139827.pdf](http://ams.confex.com/ams/pdffiles/139827.pdf), 2008.

Hobbs, S E., A Quantitative study of a Kite Performance in Natural Wind with Application to Kite Anemometry. Cranfield Institute of Technology, 1986. (Electronic version 2005, <https://dspace.lib.cranfield.ac.uk/bitstream/1826/918/2/sephd2a.pdf>)

Hoerner, S. F., Fluid Dynamic Drag, Published by the author, New York, 415 pp, pp. 3–11, 1965

Hölling, M., B. Schulte, S. Barth, and J. Peinke, Sphere anemometer - a faster alternative solution to cup anemometry, *Journal of Physics: Conference Series* 75, doi:10.1088/1742-6596/75/1/012064, 2007.

Holland, G. J., P. J. Webster, J. A. Curry, G. Tyrell, D. Gauntlett, G. Brett, J. Becker, R. Hoag, W. Vaglienti, The Aerosonde robotic aircraft: A new paradigm for environmental observations, *Bull. Am. Met. Soc.*, 82, 889, 2001

Inoue, J., and J. A. Curry, Application of Aerosondes to high-resolution observations of sea surface temperature over Barrow Canyon, *Geophys. Res. Lett.*, 31, L14312, doi:10.1029/2004GL020336, 2004.

Keyes, J. W. Aerodynamic Characteristics Of Lenticular And Elliptic Shaped Configurations At A Mach Number Of 6. National Aeronautics And Space Administration Washington, D. C. *NASA TN D-2606*, 29 pp, 1965

Kocer G., Mansour M., Chokani N., Abhari R.S., Müller M., Full-Scale Wind Turbine Near-Wake Measurements Using an Instrumented Uninhabited Aerial Vehicle, *Journal of Solar Energy Engineering*, Vol. 133, No. 4, 2011a

Kocer G., Mansour M., Chokani N., Abhari R.S., Müller M., Full-Scale Wind Turbine Wake Measurements Using an Instrumented UAV, Proceedings of the European Wind Energy Association Annual Event 2011b (see ewec2011proceedings.info)

Koch, G. J., J. Y. Beyon, P. Petzar, M. Petros, J. Yu, B. C. Trieu, M. J. Kavaya, U. N. Singh, E. A. Modlin, B. W. Barnes, and B. B. Demoz, Field testing of a high-energy 2- $\mu\text{m}$  Doppler lidar, *J. Appl. Remote Sens.* 4, 043512, doi:10.1111/1.3368726, 2010.

Konrad, T. G., M. L. Hill, J. R. Rowland, and J. H. Meyer, A small, radio-controlled aircraft as a platform for meteorological sensors, *APL. Tech. Dig.*, 10, 11-19, 1970.

van den Kroonenberg, A. C., Airborne Measurement of Small-Scale Turbulence with special regard to the Polar Boundary Layer. Sierke Verlag, ISBN 13: 978-3-86844-216-8, 136 pp, 2009.

van den Kroonenberg, A., S. Martin, F. Beyrich, and J. Bange, Spatially-Averaged Temperature Structure Parameter Over a Heterogeneous Surface Measured by an Unmanned Aerial Vehicle, *Boundary-Layer Meteorol.*, DOI 10.1007/s10546-011-9662-9, 2011.

van den Kroonenberg, A., T. Martin, M. Buschmann, J. Bange, and P. Vörsmann, Measuring the Wind Vector Using the Autonomous Mini Aerial Vehicle M2AV, *J. Atmos. Oceanic Technol.*, 25, 1969-1981, 2008.

Landwebber, L. and Protter, M. H. The shape and Tension of a Light, Flexible Cable in a Uniform Current, *David Taylor Model Basin, Report 533*. Washington D.C. United States Navy, 1944.

Leise, J. A. and J. M. Masters, Wind Measurements from Aircraft. US Department of Commerce, National Oceanic and Atmospheric Administration, Aircraft Operation Center, Miami, Florida, USA, 166 pp, 1993.

Lenschow, D., V. Savic-Jovcic, and B. Stevens, Divergence and vorticity from aircraft air motion measurements. *J. Atmos. Oceanic Technol.*, 24, 2062—2072, 2007.

Lenschow, D. H., The Measurement of Air Velocity and Temperature Using the NCAR Buffalo Aircraft Measuring System, *Tech. Rep. NCAR-TN/EDD-74*, NCAR, Boulder, Colorado, 1972.

Lenschow, D. H., Aircraft Measurements in the Boundary Layer. In: D. H. Lenschow (editor), *Probing the Atmospheric Boundary Layer*, Amer. Meteorol. Soc., Boston, MA, pp. 39–53, 1986.

Luftfahrtnorm, LN 9300, Blatt 1, Flugmechanik. Normenstelle Luftfahrt, Leinfelden, Germany, 42 pp, 1970.

Ma, S., H. Chen, G. Wang, Y. Pan, and Q. Li, A Miniature Robotic Plane Meteorological Sounding System, *Adv. Atmos. Sci.*, 21, 6, 890-896, 2004

- Mansour M., Kocer G., Lenherr C., Chokani N., Abhari R.S., Seven-Sensor Fast-Response Probe for Full-Scale Wind Turbine Flowfield Measurements, *Journal of Engineering for Gas Turbines and Power*, Vol. 133, 2011
- Martin, S., J. Bange, and F. Beyrich, Profiling the Lower Troposphere Using the Research UAV 'M<sup>2</sup>AV Carolo'. *Atmos. Meas. Tech.*, 4, 705–716, 2011.
- MacLennan, D.N. Hydrodynamic Characteristics of trawl warps, *Marin Labatory Aberdeen RE 70683 750 7/79 TCL*, 10 pp, 1979
- Melbourne, W.H., Predicting the cross-windresponse of masts and structural members, *Journal of Industrial Wind Engineering*, 69-71, 91-103, 1997.
- Neumark, S. Equilibrium Configurations of Flying Cables of Captive Balloons, and Cable Derivatives for Stability Calculations *A.R.C. R&M 3333*, pp 40, 1963.
- O'Connor, Ewan J., Anthony J. Illingworth, Ian M. Brooks, Christopher D. Westbrook, Robin J. Hogan, Fay Davies, Barbara J. Brooks, A Method for Estimating the Turbulent Kinetic Energy Dissipation Rate from a Vertically Pointing Doppler Lidar, and Independent Evaluation from Balloon-Borne In Situ Measurements. *J. Atmos. Oceanic Technol.*, 27, 1652–1664, doi: 10.1175/2010JTECHA1455.1, 2010.
- Peña, A., S.-E. Gryning, J. Mann, J., and C. B. Hasager, Length Scales of the Neutral Wind Profile over Homogeneous Terrain, *J. Appl. Meteorol. Clim.*, 49(4), 792-806, 2010.
- Peters, F., Shape and drag of a bulging rope in uniform cross flow, *Acta Mechanica*, 139, 161-170, 2000.
- Piperas, A.T., Modeling of a lighter than air (LTA) device in free air, DTU special course report, Lyngby, 2010.
- Poulin, S., and A. Larsen, Drag loading of circular cylinders inclined in the along-wind direction, *Journal of Wind Engineering and Industrial Aerodynamics*, 95, 1350–1363, 2007.
- Puczyłowski, J., J. Peinke, and M. Hölling, New anemometer for offshore use, Proceedings of the 9<sup>th</sup> European Turboimachinery Conference, Istanbul, 2011.
- Ramanathan, V., M. V. Ramana, G. Roberts, D. Kim, C. Corrigan, C. Chung, and D. Winker, Warming trends in Asia amplified by brown cloud solar ab-sorption, *Nature*, 448, 575-578, DOI:10.1038/nature06019, 2007.
- Reitebuch, O., Ch. Werner, I. Leike, P. Delville, P. H. Flamant, A. Cress, and D. Engelbart, Experimental validation of wind profiling performed by the airborne 10-μm heterodyne doppler lidar WIND, *J. Atmos. Oceanic Technol.*, 18, 1331–1344, 2001.
- Reuder, J., M. Ablinger, H. Agustsson, P. Brisset, S. Brynjolfsson, M. Garhammer, T. Johannesson, M. O. Jonassen, R. Kühnel, S. Lämmlein, T. de Lange, C. Lindenberg, S. Malardel, S. Mayer, M. Müller, H. Olafsson, O. Rögnvaldsson, W. Schäper, T. Spengler, G. Zängl, and J. Egger, FLOHOF 2007: An overview of the mesoscale meteorological field campaign at Hofsjökull, Central Iceland, *Meteorol. Atmos. Phys.*, DOI: 10.1007/s00703-010-0118-4, 2011.
- Reuder, J., and M. Jonassen, First results of turbulence measurements in a wind park with the Small Unmanned Meteorological Observer SUMO, submitted to Energy Procedia.

Reuder, J., M. Jonassen, and H. Olafsson, The Small Unmanned Meteorological Observer SUMO: Recent developments and applications of a micro-UAS for atmospheric boundary layer research, accepted for publication in *Acta Geophysica*.

Reuder, J., P. Brisset, M. Jonassen, M. Müller, and S. Mayer, The Small Unmanned Meteorological Observer SUMO: A new tool for atmospheric boundary layer research, *Meteorol. Z.*, 18, 2, 141-147, 2009.

Rögnvaldsson, O., [Final report to NORA for project Vejrtjeneste for Søberedskab aka SARWeather](#) Institute for Meteorological Research, Reykjavik, 2011

Schaefer, J.T., and C.A. Doswell III, The inherent position errors in double-theodolite pibal measurements. *J. Appl. Meteor.*, 17, 911-915, 1978.

Spengler, T., M. Ablinger, J. H. Schween, G. Zängl G. and J. Egger, Thermally driven flows at an asymmetric valley exit: Observations and model studies at the Lech Valley exit. *Mon. Wea. Rev.*, 137, 3437-3455, 2009.

Spieß, T., A Contribution to Turbulence Measurements with Autonomous Micro Aerial Vehicles. Ph.D. thesis, Institute for Aerospace Systems, Techn. Univ. Braunschweig, Germany, 137 pp, 2006.

Spiess, T., J. Bange, M. Buschmann, and P. Vörsmann, First application of the meteorological Mini-UAV M2AV, *Meteorol. Z.*, 16, 2, 159–169, 2007.

Stull, R. B., An Introduction to Boundary Layer Meteorology, Kluwer Academic Publishers, Dordrecht, 1997.

Teisserenc de Bort, L. The Franco - Scandinavian Station for Aerial Soundings, Monthly Weather Review, pp 177-178, 1903

Thyer, N, Double Theodolite Pibal Evaluation by Computer, *J. Appl. Met.*, 1,1, 66-68, 1962.

UVS International, UAS - The Global Perspective 2011/2012, 2011-2012 UAS Yearbook, 9th Edition, ed. By P. Blyenburgh, 216 pp., 2011.

Williams, A. and D. Marcotte, Wind Measurements on a Maneuvering Twin-Engine Turboprop Aircraft Accounting for Flow Distortion, *J. Atmos. Oceanic Technol.*, 17(6), 795–810, 2000.

Risø DTU is the National Laboratory for Sustainable Energy. Our research focuses on development of energy technologies and systems with minimal effect on climate, and contributes to innovation, education and policy. Risø has large experimental facilities and interdisciplinary research environments, and includes the national centre for nuclear technologies.

---

**Risø DTU**  
**National Laboratory for Sustainable Energy**  
**Technical University of Denmark**

Frederiksborgvej 399  
PO Box 49  
DK-4000 Roskilde  
Denmark  
Phone +45 4677 4677  
Fax +45 4677 5688

[www.risoe.dtu.dk](http://www.risoe.dtu.dk)